Waveguide Quantum Electrodynamics

Frontiers in the Generation and Scattering of Multiphoton States

Vanessa Paulisch

Ludwig-Maximilians-Universität München

Max-Planck-Institut für Quantenoptik

Waveguide Quantum Electrodynamics

Frontiers in the Generation and Scattering of Multiphoton States

Vanessa Paulisch

Dissertation
an der Fakultät für Physik
der Ludwig-Maximilians-Universität
München

vorgelegt von
Vanessa Paulisch
aus Karlsruhe

München, den 08. Februar 2018

Erstgutachter: Prof. J. I. Cirac

Zweitgutachter: Prof. J. von Delft

Weitere Prüfungskommissionsmitglieder: Prof. H. Weinfurter, Prof. M. Punk

Datum der Abgabe: 08. Februar 2018

Datum der mündlichen Prüfung: 24. April 2018

Abstract

Waveguide quantum electrodynamics (waveguide QED) describes the interaction between an electromagnetic field confined to a one-dimensional waveguide with atom-like quantum emitters close by. The characteristics of these kinds of systems are the possibility for strong and even ultrastrong interactions between the photonic and atom-like systems, and practically infinite range interactions between the emitters. These properties are valuable for a wide range of quantum optical applications, like quantum communication, quantum networks and quantum metrology. In this thesis we focus on two challenges in quantum optics, namely the generation and scattering of multiphoton states.

In the first part of this thesis we demonstrate how waveguide QED systems can be exploited for the generation of multiphoton states, in particular of single-mode Fock states and superpositions thereof as well as multi-mode photonic states with metrological applications. The basic setup for this goal is an ensemble of quantum emitters coupled to a waveguide. In the so-called atomic mirror configuration symmetric Dicke states (or a superposition thereof) decay superradiantly to the ground state and emit the desired multiphoton state, which can be efficiently collected at the ends of the waveguide. We propose various protocols for the preparation of these Dicke states in waveguide QED systems and characterize the emitted photonic state. It turns out that in the low excitation regime, that is, if the number of photons is much lower than the ensemble size, the photonic state is emitted into a single mode. This single-mode structure is fundamental to current proposals for applications in quantum metrology with optical interferometers. Outside the low excitation regime, a multi-mode photonic state is generated, for which the metrological capabilities were unknown. We were able to show that these states still lead to quantum-enhanced optical interferometry.

In the second part of this thesis we demonstrate how the scattering of multiphoton states on a single quantum emitter coupled to the waveguide can be used for testing the limits of the light-matter interaction strength. In particular, we investigate systems in the so-called ultrastrong coupling regime, where the coupling strength between the photonic and atom-like system is of the order of the emitter's transition energy. In this regime, many methods and approximations used in quantum optics, especially the Rotating Wave Approximation, break down and one needs to develop new analytical and numerical methods to study these systems. One approach is the so-called polaron Transformation. We show how this transformation can be applied for predicting the scattering amplitude of few photons scattering on the emitter. The comparison of these results with numerical simulations using matrix product states shows a good agreement for moderate coupling strengths.

Both parts together show that waveguide QED systems are promising candidates for the generation of multiphoton states as well as for the investigation of fundamental limits probed through the scattering of multiphoton states. The latter also finds application in the implementation of photon-photon nonlinearities induced by the interaction with the quantum emitters. Apart from these and many other theoretical predictions, waveguide QED systems are also undergoing rapid progress in experiments. Therefore, we expect these kinds of systems to bring forth several advances in the field of quantum optics.

Zusammenfassung

Die Wellenleiter-Quantenelektrodynamik (Wellenleiter-QED) beschreibt die Wechselwirkung zwischen dem elektromagnetischen Feld eines Wellenleiters und nahe liegenden atomähnlichen Quatenemittern. Charakteristisch für diese Art von Systemen ist die Möglichkeit starker und sogar ultrastarker Wechselwirkungen zwischen den photonischen und atomähnlichen Systemen, sowie Wechselwirkungen zwischen den Emittern mit praktisch unendlicher Reichweite. Diese Eigenschaften sind wertvoll für eine Vielzahl von quantenoptischen Anwendungen, wie die Quantenkommunikation, Quantennetzwerke und Quantenmetrologie. In dieser Arbeit befassen wir uns mit zwei Herausforderungen in der Quantenoptik, nämlich der Erzeugung und der Streuung von Multiphoton-Zuständen.

Im ersten Teil dieser Arbeit zeigen wir, wie Wellenleiter-QED-Systeme für die Erzeugung von Multiphoton-Zuständen, insbesondere von monomodalen Fock-Zuständen und deren Superposition, sowie multimodalen photonischen Zuständen mit Nutzen für die Quantenmetrologie, verwendet werden können. Der grundlegende Aufbau für dieses Ziel ist ein Ensemble von Quantenemittern, die an einen Wellenleiter gekoppelt sind. In der sogenannten Atomspiegelkonfiguration zerfallen symmetrische Dicke-Zustände (oder eine Superposition davon) superradiant in den Grundzustand und emittieren den gewünschten Multiphoton-Zustand, der effizient an den Enden des Wellenleiters entnommen werden kann. Wir schlagen verschiedene Protokolle zur Bereitstellung dieser Dicke-Zustände in Wellenleiter-QED-Systemen vor und charakterisieren den emittierten photonischen Zustand. Es stellt sich heraus, dass im niedrigen Anregungsregime, d.h. wenn die Anzahl der Photonen viel geringer ist als die Größe des Ensembles, der photonische Zustand in eine einzige Mode emittiert wird. Diese monomodale Struktur ist grundlegend für derzeitige Methoden und Ansätze in der Quantenmetrologie mit optischen Interferometern. Außerhalb des niederen Anregungsregimes wird ein multimodaler photonischer Zustand erzeugt, für den die metrologischen Eigenschaften bislang unbekannt waren. Wir konnten zeigen, dass diese Zustände immer noch zu einer durch Quantenmechanik verbesserten optischen Interferometrie führen.

Im zweiten Teil dieser Arbeit zeigen wir, wie die Streuung von Multiphoton-Zuständen an einem einzelnen Quantenemitter, der an den Wellenleiter gekoppelt ist, zum Testen der Grenzen der Licht-Materie-Wechselwirkung genutzt werden kann. Insbesondere untersuchen wir Systeme im Bereich der so genannten ultrastarken Wechselwirkung, bei dem die Kopplungsstärke zwischen dem photonischen und dem atom-ähnlichen System in der Größenordnung der Übergangsenergie des Emitters liegt. In diesem Regime, können viele Methoden und Näherungen, vor allem die Rotating Wave Approximation, nicht mehr angewendet werden und neue analytische und numerische Methoden müssen entwickeln werden,

um diese Systeme zu untersuchen. Ein Ansatz ist die so genannte Polaron-Transformation. Wir zeigen, wie diese Transformation angewendet werden kann, um die Streuamplitude von Photonen, die an dem Emitter streuen, zu berechnen. Der Vergleich dieser Ergebnisse mit numerischen Simulationen zeigt eine gute Übereinstimmung bei moderaten Kopplungsstärken.

Beide Teile zusammen zeigen, dass Wellenleiter-QED-Systeme vielversprechende Kandidaten, einerseits für die Erzeugung von Multiphoton-Zuständen und andererseits für die Untersuchung fundamentaler Grenzen, die durch die Streuung von Multiphoton-Zuständen erforscht werden können, sind. Letzteres findet auch Anwendung in der Erzeugung von Photon-Photon-Interaktionen, die durch die Wechselwirkung mit den Quantenemittern induziert werden. Abgesehen von diesen und vielen anderen theoretischen Vorhersagen, werden Wellenleiter-QED-Systeme auch in Experimenten rapide weiterentwickelt. Daher erwarten wir, dass diese Art von Systemen zahlreiche Fortschritte auf dem Gebiet der Quantenoptik hervorbringen wird.

List of Publications

Publications Related to this Thesis

- [1]: A. González-Tudela, V. Paulisch, D. E. Chang, H. J. Kimble, and J. I. Cirac. "Deterministic Generation of Arbitrary Photonic States Assisted by Dissipation" *Phys. Rev. Lett.* **115** 163603 (2015)
- [2]: V. Paulisch, M. Perarnau-Llobet, A. González-Tudela, and J. I. Cirac. "Quantum Metrology with Multimode Photonic States" *In preparation.* (2018)
- [3]: A. González-Tudela, V. Paulisch, H. J. Kimble, and J. I. Cirac. "Efficient Multiphoton Generation in Waveguide Quantum Electrodynamics" *Phys. Rev. Lett.* **118** 213601 (2017)
- [4]: V. Paulisch, A. González-Tudela, H. J. Kimble, and J. I. Cirac. "Heralded multiphoton states with coherent spin interactions in waveguide QED" *New J. Phys.* **19** 043004 (2017)
- [5]: V. Paulisch, H. J. Kimble, J. I. Cirac, and A. González-Tudela. "Generation of single and two-mode multiphoton states in waveguide QED" *arXiv:1802.00210.* (2018)
- [6]: V. Paulisch, T. Shi, and J. J. García-Ripoll. "Multiphoton Scattering in the Ultrastrong coupling regime" *In preparation.* (2018)

Other Publications

- [7]: V. Paulisch, H. J. Kimble, and A. González-Tudela. "Universal quantum computation in waveguide QED using decoherence free subspaces" *New J. Phys.* **18** 043041 (2016)
- [8]: V. Paulisch, H. Rui, H. K. Ng, and B.-G. Englert. "Beyond adiabatic elimination: A hierarchy of approximations for multi-photon processes" *Eur. Phys. J. Plus* **129** 12 (2014)

Table of Contents

0 Introduction

"[...] the problem of the quantum of action will not cease to inspire research and fructify it, and the greater the difficulties which oppose its solution, the more significant it finally will show itself to be for the broadening and deepening of our whole knowledge in physics."

— Max Planck's Nobel Lecture 1920 for his Nobel Prize 1918

0.1 History and Motivation

By now, 100 years after Max Planck was awarded the Nobel prize "in recognition of the services he rendered to the advancement of Physics by his discovery of energy quanta", quantum mechanics is a widely accepted theory for describing systems at the lowest energy scales. It has been especially fruitful for atomic, molecular and optical physics, where Quantum Optics describes the interaction between light (e.g., the quantized electromagnetic field) and matter (e.g., atoms and other systems with discrete energy levels). Controlling the photonic and atom-like systems individually posed great challenges, but is nowadays a standard task in laboratories and industry. On their own, these quantum systems already show great potential for quantum information processing [9], quantum cryptography [10], quantum metrology [11] and quantum simulation [12]. Interfacing these atom-like and photonic systems remains a challenge, yet one with a great reward: i) By linking different atom-like quantum systems through photonic systems one can build a quantum network [13]. The well controlled atom-like systems then processes quantum information locally, whereas the photonic system (which naturally interacts only weakly with the environment) transfers quantum information from one system to another. ii) Moreover, by using the interaction between the systems one can effectively engineer nonlinear interactions between photons, which otherwise would not interact [14].

The atom-like quantum systems are either natural (e.g., atoms or ions) or artificial (e.g., spins in solids or superconducting circuits), see Section 0.2.1, which can emit single photons, such that we will call them quantum emitters. In the simplest case these emitters are two-level systems (TLS) with a ground state $|g\rangle$ and an excited state $|e\rangle$. Moreover, the system needs to be controllable by external driving fields (e.g., laser beams), but also well enough decoupled from the environment such that quantum properties can emerge.

Although the electromagnetic field of a laser, e.g., for controlling the quantum states of the atom-like systems, can be described semiclassically, there are very many states of light that require a quantum mechanical treatment [15]. One example are squeezed states, which were first observed in the 1980s [16, 17] and will be essential for increasing the sensitivity of next generation gravitational wave detectors [18]. In fact, a large class of nonclassical states can be used to overcome classical limits of optical interferometers [19]. Single photons have also been proposed for photonic quantum computing [20]. However, this either requires large photon-photon nonlinearities [21, 22], which are difficult to realize due to the weak interactions between photons, or rely on efficient photon detectors [23].

A requirement to observe quantum effects in the interaction between an atom-like and a photonic system, is that the time scale of the coupling between these two systems is faster than those of decoherence processes. This was first accomplished in the early 1990s in cavities [24, 25]. Achieving strong coupling at the single photon level has remained of interest ever since. The problem is, that even though single atoms naturally emit single photons, implementing coherent interactions between these two systems requires more work. Two approaches to enhance the interaction between these systems are i) the use of ensembles of N quantum emitters (in which the interaction strength is enhanced by a factor of $\sqrt{N}$) and ii) the use of cavities (in which the electromagnetic field is strongly confined between two mirrors) [13]. We shortly review important concepts and achievements of these two approaches.

When an ensemble of quantum emitters is coupled to the electromagnetic field, its coupling strength scales with the number of quantum emitters in the ensemble. Another advantage is that the ensemble can be controlled globally by one laser-beam and that specific quantum states stored in these ensembles can be robust against particle loss. This system (together with linear optical tools) was proposed for long-distance quantum communication [26] and several advances in this field led to the realization of the basic building blocks for quantum repeaters with atomic ensembles [27]. However, in contrast to the TLS, which has very nonlinear features in its light-matter interaction, large ensembles interact linearly with the electromagnetic field.

In a different approach, namely cavity quantum electrodynamics (cavity QED), one or many quantum emitters are placed inside a cavity. This cavity typically only supports one frequency ω_{cav} that is coupled to the emitter with transition frequency Δ. One was able to reach a regime, in which the coupling g between the emitters and the photonic mode exceeds the decoherence rates of the system. In most state-of-the-art setups one can reach this strong coupling regime with coupling strengths much lower than the frequency of the emitter and cavity, that is, $g \ll \Delta, \omega_{\mathrm{cav}}$. In this regime, only the excitation number conserving interaction terms are relevant, which is the so-called Rotating Wave Approximation (RWA) [28]. Most applications were devised for this regime and we highlight one of them, which is relevant for building quantum networks: the transfer of the quantum state of one TLS in a cavity to another distant TLS-cavity-system [29]. This is important both on a large scale for quantum communication, but also on a small scale for overcoming limitations in the number of coupled TLS in current devices [13]. The experimental real-

ization of this proposal required several advances in cavity QED [30], but was ultimately successful [31]. With superconducting circuits also the ultrastrong coupling regime, in which the coupling is comparable to the other frequencies, $g \sim \Delta, \omega_{\mathrm{cav}}$, was reached [32, 33].

Recently, quantum emitters have been also strongly coupled to one-dimensional waveguides, which support a continuum of propagating photonic modes, to build so-called waveguide QED systems (see Section 0.2.2). Waveguide QED systems offer several assets: the photonic states can be easily coupled into and out of the waveguide at the ends; in contrast to cavity QED, many atoms can couple to a waveguide due to its length without a significant reduction of the coupling strength; for the same reasons one has more freedom in designing the properties of the waveguide and therefore also, e.g., the dispersion relation of the waveguide; the waveguide can support different polarizations of the electromagnetic field; and the decay rate into the waveguide, $\Gamma_{1\mathrm{d}}$, can be of the order of or even surpass the decay rate Γ^* into other modes, e.g., to free space. We will call the ratio between these two rates the Purcell Factor $P_{1\mathrm{d}} = \frac{\Gamma_{1\mathrm{d}}}{\Gamma^*}$. The enhancement of the light-matter interaction stems from confining the electromagnetic field to the one-dimensional waveguide and, for some systems, also from an increased local density of states close to a band edge of the waveguide.

The initial challenges of coupling quantum emitters to the evanescent field of one-dimensional waveguides were further complicated by the fact that results valid in free-space are not directly applicable in the waveguide setup, such that new methods for the loading, cooling and trapping of the quantum emitters needed to be found. Important applications like collective dissipation, which leads to superradiant decay, have been shown both with optical nanofibers [34] and photonic crystal waveguides [35] – the prototypical waveguides in the optical regime. The future directions are set by proposals for single photon transistors based on perfect reflection of a photon scattering on a quantum emitter coupled to a waveguide [36], cavity QED setups with atomic mirrors [37], and new paradigms like chiral interactions (i.e., an interaction depending on the directionality of the photon), atom-photon bound states, band-gap mediated interactions and many more [38].

These recent advances in waveguide QED have opened up new avenues for providing solutions to some fundamental problems and questions of quantum optics. There are many of those challenges [39]: high-fidelity photon sources and photon detectors are required for most quantum technologies, in particular for quantum communication and quantum metrology; quantum memories are needed for storing quantum information for long times; strong single-photon nonlinearities can form the basis of quantum information processing based on photons; and ultrastrong light-matter interactions can significantly accelerate quantum processes. We specifically highlight two open challenges, which are the core topic of this thesis:

- The *generation of multiphoton states* has been a long standing goal in quantum optics. Approaches using spontaneous parametric down conversion, single quantum

emitters and ensembles of quantum emitters (as reviewed in Section 0.2.3) all have their advantages and specific drawbacks, like low collection efficiencies, large bandwidths, or low heralding probabilities for non-deterministic sources. The collective emission from a large ensemble of emitters is probably the best tool for the generation of photonic states of multiple photons [40]. In fact, by coupling such an ensemble to a one-dimensional waveguide we can employ the assets of both systems. The interactions and collective dissipation within the ensemble are then mediated by the waveguide and are practically of infinite range because of the effectively one-dimensional setup. Under certain conditions, the ensemble decays superradiantly and emits a photonic state into the waveguide during the decay, which can be collected efficiently at the ends of the waveguide. The generation of photonic states in this way is the main goal of Chapter 1 and Chapter 2.

- The *scattering of multiphoton states* in the waveguide on a quantum system coupled to it, can be used to study properties of this system. In particular, this approach can give insights into the ultrastrong coupling regime of waveguide QED systems. In this regime, the light-matter coupling is of the order of the TLS's transition energy and usual approximations (like the Rotating Wave Approximation) break down [41, 42]. However, finding new tools for studying ultrastrongly coupled systems is essential for being able to use those interactions for reducing the time of operations [43, 44] or inducing large photon nonlinearities [45]. In particular, photon-photon interactions are of fundamental importance for quantum information processing with photons, because the often used Kerr nonlinearities don't reach the desired interaction strength [46, 47]. Interactions mediated by an ultrastrongly coupled quantum emitter can mediate such nonlinearities. However, one first needs to develop new theoretical tools to understand and approximate processes in the ultrastrong coupling regime, which is the main goal of Chapter 3.

0.2 Experimental Achievements and Considerations

We now introduce some of the basic elements of waveguide QED systems and review experimental achievements relevant to this thesis. The aim is to present the main ideas and concepts and provide references to reviews where possible. The basic elements we cover are the quantum emitters themselves (Section 0.2.1), the one-dimensional waveguides (Section 0.2.2), the generation of photonic states (Section 0.2.3) and the detectors for the state of quantum emitters and photons (Section 0.2.4).

0.2.1 Quantum Emitters

Quantum emitters are typically classified either as natural (e.g., atoms or ions) or artificial (e.g., spins in solids or superconducting circuits) [48, 49]. The former have an internal level structure determined by nature and therefore they have the same characteristics, e.g., the same transition energies. Typically, they have many optically excited and metastable

states, and therefore many optical/microwave transitions to choose from. Furthermore, these systems show long coherence times in the metastable states. On the other hand, one requires initial cooling and trapping, e.g., in ion traps or with optical tweezers or lattices, before the atom-like systems can be coherently manipulated by driving, e.g., an optical transition of the atom or ion with a laser-beam [50, 51]. In contrast, artificial systems are typically fixed on a substrate, such that there is no need for trapping. Furthermore, their level structure, transition energies, position and so forth can be engineered to fit the desired properties. These systems can be manipulated through their optical and microwave transitions, but often also by applying voltages and currents. On the other hand, experimental imperfections when creating these systems lead to deviations from the exact transition energies and positions. Furthermore, due to the contact to the substrate, they couple more strongly to the environment, which limits their coherence time. Examples of artificial systems with optical and microwave transitions are quantum dots [52], e.g., grown from gallium arsenide (GaAs), and point defects in the diamond lattice, like nitrogen-vacancy centers [53]. A different approach are superconducting artificial atoms [54], which are superconducting quantum circuits with a Josephson Junction inducing a nonlinearity in the energy spectrum. These systems can be addressed electronically or via coupling them to waveguides in the microwave regime [55].

0.2.2 Photonic Waveguides

Let us shortly review some of the experimental implementations of waveguide QED systems. The common desired characteristics are that the emitters can be positioned close to the waveguide to facilitate strong coupling, that the transition frequency of the emitters matches one of the guided modes of the waveguide, and that the emitters can be controlled by additional laser-beams either through the waveguide or from other directions. Furthermore, it is desirable that the propagating mode of the waveguide can be efficiently coupled into a regular optical fiber for further propagation and use in quantum optical applications. The most common waveguides are optical nanofibers and photonic crystal waveguides in the optical regime and transmission lines for superconducting circuits in the microwave regime. For full reviews of the current waveguide technologies, see References [56], [57], and [58], respectively. A common property of all these waveguides is that long propagation lengths can be achieved, such that we can neglect losses of the propagating waveguide mode.[1]

Optical Nanofibers Optical nanofibers are tapered optical fibers, that is, optical fibers that are stretched and thinned to a subwavelength radius (see Figure 0.1a). Close to the waveguide, where the exponentially decreasing evanescent field is still large, quantum emitters can interact strongly with the guided mode of the nanofiber. Due to the tapered structure, the light within the tapered part is naturally mode matched to the one in the

[1] The description of systems with a finite propagation length L is nontrivial, but we note that, e.g., absorption in the material leads to a trade-off with the Purcell factor and introduces small corrections to the dynamics of the system of the order of d/L, where d is the distance between emitters. As this correction is typically very small, we neglect it in the remainder of this thesis.

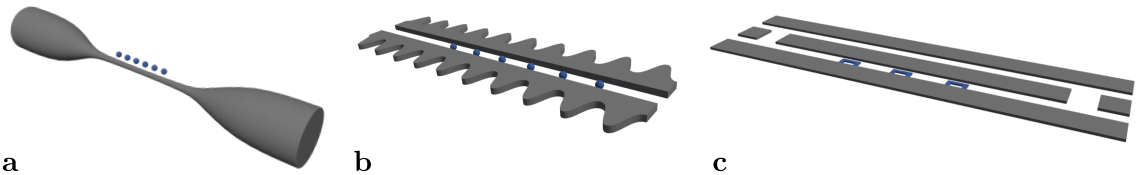

a **b** **c**

Figure 0.1: The three most common platforms of waveguide QED systems are **a** optical nanofibers, which are stretched and thinned optical fibers, **b** photonic crystal waveguides, which have a periodicity in their dielectric coefficient, and **c** transmission lines for superconducting qubits. The figures are inspired by the References [59], [60] and [55], respectively.

untapered part of the optical fiber. The first experiments involved a cloud of atoms surrounding the nanofiber [61], but soon atoms were controllably coupled to the waveguide by using optical traps [59]. Further experiments showed single atoms emitting single photons [62], nondestructive dispersive readout of the atom number [63, 64], the theoretically predicted [65, 36] full reflection of resonant photons [66, 67] and superradiant emission [34]. In these state-of-the-art experiments the value of the Purcell factor is on the order of $P_{1\mathrm{d}} \sim 0.01 - 0.1$ and the number of atoms that have been trapped is on the order of $N \sim 10^2 - 10^3$.

Photonic Crystal Waveguides The coupling to the waveguide can be increased by designing appropriate photonic crystal waveguides. These are dielectric structures with a periodic dielectric coefficient giving rise to a band structure for the electromagnetic field of the waveguide (see Figure 0.1b). At the band edge, the group velocity v_{g} is strongly reduced with respect to the speed of light c, which leads to an enhancement in addition to the one from mode confinement.[2] In particular, the decay rate into the waveguide $\Gamma_{1\mathrm{d}} \propto n_g$ is proportional to the group index $n_g = c/v_g$ around the frequency of the TLS, $\omega \approx \Delta$. The group index $n_g \propto D(\omega)$ in turn is proportional to the local density of states $D(\omega)$. Both natural and artificial quantum emitters have been coupled to photonic crystal waveguides, and one has been able to observe photon emission [68], implement basic building blocks towards a quantum phase switch [69, 70], induce interactions at the band-edge [71], and show superradiant emission from few atoms [35]. The Purcell factor of state-of-the-art systems is on the order of $P_{1\mathrm{d}} \sim 1 - 60$. Note, that the group velocity cannot be decreased too far because with very slow light also negative effects of defects in the waveguides are enhanced and non-markovian effects can emerge [72, 73]. Currently trapping many atoms or growing many quantum dots close to the waveguide is challenging and the number of emitters coupled is on the order of $N \sim 1 - 10$. Recent progress in atom-by-atom assembly of atomic one and two-dimensional arrays [74, 75] and positioning of quantum dots [76] indicates that the number of coupled emitters can be significantly improved.

Superconducting Circuits A different route to implementing waveguide QED systems are superconducting circuits which work in the microwave regime. Here, atoms are

[2] Intuitively one can understand this behavior by comparison to the enhancement in a cavity. In a cavity the interaction time between the emitters and the photons is increased because the electromagnetic field is reflected many times at the cavity mirrors such that it interacts many times with the emitter. When the photons are traveling slowly in the waveguide also the interaction time with the emitter is increased.

replaced by superconducting artificial atoms, which are superconducting quantum circuits with a Josephson Junction inducing a nonlinearity in the energy spectrum. The waveguide is replaced by a so-called transmission line, that is, a microwave LC circuit (see Figure 0.1c). Depending on the engineered behavior for the microwave photons at the ends of the transmission line, it behaves either like a cavity or a waveguide. The superconducting artificial atoms can be coupled to the transmission line either inductively or capacitatively, but when a device has been constructed, the distance between different emitters is fixed. However, due to the control over the transition energies, the ratio of distance and wavelength can be modified. Furthermore, level structures that would not be possible in other systems (like atoms) can be designed. The first observation of strong coupling [77] could still be explained classically. Soon thereafter, the first non-classical state of the microwave field was generated by close to full reflection of a single photon from a coherent input state [78]. In the following years, first experiments demonstrated photon mediated interactions and superradiance [79, 80] and bound states near a photonic bandgap [81]. Recently, also propagating shaped single photons were generated in experiments [82]. A broad variety of level structures and couplings can be fabricated with the current techniques. In contrast to other waveguide QED systems, the decay rate to other modes outside the waveguide is very low by construction. Therefore, Purcell factors on the order of $P_{1\mathrm{d}} \sim 10 - 100$ have been achieved. Furthermore, the coupling to the waveguide can be of the same order as the transition energy of the artificial atom, that is, one has reached the ultrastrong coupling regime [83]. However, in recent experiments only on the order of $N \sim 1 - 10$ artificial atoms have been coupled to a single transmission line.

0.2.3 Generation of Photonic States

There are a variety of photonic states of theoretical and experimental interest. In this thesis we are concerned with the generation of multiphoton states, in particular, superpositions of Fock states. For quantum metrology in the optical regime especially NOON-states, Yurke states and twin-Fock states are important [19]. However, the generation of these states can be very challenging [84]. In principle, multiphoton states can be generated by adding single identical photons, e.g. with linear optical tools [85, 86]. In particular, photonic states can be added by interfering them at a beamsplitter and heralding on no detection event in one of the output ports of the beamsplitter. The problem of this approach is that the probability of generating the desired multiphoton state is the product of the probability for a successful heralding at every step and is therefore exponentially low in the number of photons [85]. Nonetheless, let us review the three main approaches to the generation of (mostly single-photon) photonic states [87, 88]:

- By pumping a nonlinear crystal with a laser, photon pairs can be generated through *Spontaneous Parametric Down Conversion* [89]. Even though these photon pairs are created at random times, this process is widely used because by heralding on measuring one photon of the pair (the signal photon) one can determine that the other photon of the pair (the idler photon) is present. In addition to the photon pair of a single photon, also pairs of two (and more) photons in the signal and idler channel

each are generated. For generating single photons, one thus has to choose the pump power small enough such that these higher order processes can be neglected, which also implies that there are only few events with a single photon in each channel. On the other hand, one can use the higher photon numbers to generate multiphoton states directly, but this is also limited due to the low probability of heralding the correct multiphoton signal state [90, 91, 92, 93].

- One can generate photons deterministically by triggering *single quantum emitters* to emit one photon. By placing these emitters in cavities or close to one-dimensional waveguides, their light-matter coupling and the collection efficiency of emitted photons can be enhanced. The generation of single photons has been observed from atoms or ions [94, 95, 96, 97, 98], solid state emitters [99, 100, 101] and superconducting qubits [102, 103, 82]. Even though one can only generate a single photon at a time, photons generated by different emitters or from the same emitter at different times, can be combined as long as their mode profile is the same. This limits the generation of multiphoton states by artificial quantum emitters because the emitted photons don't necessarily have the same mode profile as the emitters themselves differ slightly.

- To generate a state of more than one photon directly, one can use *ensembles of quantum emitters* in which one stores multiple collective excitations and later triggers the emission of a multiphoton state [26]. This was experimentally realized for single photons [104, 105, 106, 107, 108], but is limited due to a low retrieval efficiency of the stored collective excitations. The emitters can be the same as the ones used for the emission from a single quantum emitter as long as their characteristics are almost identical. The emission can be enhanced by exciting superradiant states of the collection of emitters, but the difficulty in this approach typically lies in the preparation of this collective, superradiant state with a given excitation number. This is due to the fact that large ensembles of emitters behave like a linear system.

0.2.4 Detectors

In order to verify theoretical predictions, one has to be able to measure properties of the system, that is, on one side the state of the quantum emitters and on the other side the photonic state, which couples out of the waveguide at the ends.

Quantum Emitter State When quantum emitters can be addressed electronically (like quantum dots and superconducting circuits), the state of individual emitters can often be read out with the same methods. An alternative approach is to excite the emitter and look into its fluorescence. If the emitters are coupled to a waveguide, part of the fluorescence is emitted into the waveguide and can be detected efficiently at the ends [61]. One then typically drives a cyclic transition, in which the emitter is driven from a metastable state to an optically excited state, from which it decays back only to the same metastable state, to produce many photons. The emitted photonic state is then measured by a photon detector.

Photonic State A photonic state of many photons in the optical regime can be detected by a regular avalanche photodiode. This is sufficient for the detection of the state of a quantum emitter as described above. However, the detection of photonic states at the single photon level and in a number-resolved fashion is more challenging. One of the most promising approaches [87, 88] are transition-edge sensors. These work at a temperature around the transition from the superconducting to normal resistance phase. The absorbed photons and their energy increase the temperature, which can then be detected as a change of the resistance. These detectors already show a large detection efficiency of around $\eta \sim 98\%$ [109], but still suffer from a slow response and low counting rates. On the other hand, some applications do not require a number resolving measurement of the photons, but work with a parity measurement of the number of photons [110]. Even though this has fewer requirements, it doesn't imply that one can build such parity detectors more easily because they typically require a photonic nonlinearity [111]. In contrast, in the microwave regime, different methods for photon detection are necessary because the energy of microwave photons is around five orders of magnitude lower than that of optical photons. This was a long-standing challenge in the community [112, 113], but recent achievements of single photon detection efficiencies of $\eta \sim 70\%$ [114] suggest that this won't be a major limitation in the future. Furthermore, parity measurements in microwave cavities, have already been implemented [115].

0.3 Light-Matter Interaction in One Dimension

We now introduce the basic theoretical tools for treating waveguide QED systems. We start with the basic setup of an ensemble of N TLSs coupled to a one-dimensional waveguide as depicted in Figure 0.2. We introduce a toy model Hamiltonian to describe the system (Section 0.3.1), derive a master equation for the ensemble of TLSs (Section 0.3.2) and introduce the notion of sub- and superradiance in the so-called atomic mirror configuration (Section 0.3.3).

0.3.1 Light-Matter Hamiltonian

We use a toy model for the light-matter interaction in one dimension, which is sufficient for the description throughout this thesis. The results can be rigorously derived using an approach based on the electromagnetic Green's functions of the material [116, 117, 118]. We start by discretizing the waveguide of length L into $2n+1$ segments of length δx and thus also the photonic field confined to it. The possible wavevectors in one dimension (say the x-direction) are then $k \in \frac{\pi}{L}\{0, \pm 1, \cdots \pm n\}$. In this discretized version, one can canonically quantize the electromagnetic field $\vec{E}(x) = \hat{e}_3 \sum_k \sqrt{\frac{\hbar\omega_k}{2\epsilon_0 L}} \left(a_k^\dagger \mathrm{e}^{-\mathrm{i}kx} + a_k \mathrm{e}^{\mathrm{i}kx}\right)$, where we have picked the polarization to be in the z-direction with unit vector $\hat{e}_3$, and where the photonic creation and annihilation operators $a_k^\dagger$ and a_k satisfy the usual bosonic commutation relations [28]. The j-th TLS can be fully described by the Pauli matrices $\sigma^j_{x/y/z}$ in the basis of the excited state $|e\rangle$ and the ground state $|g\rangle$. The two systems are

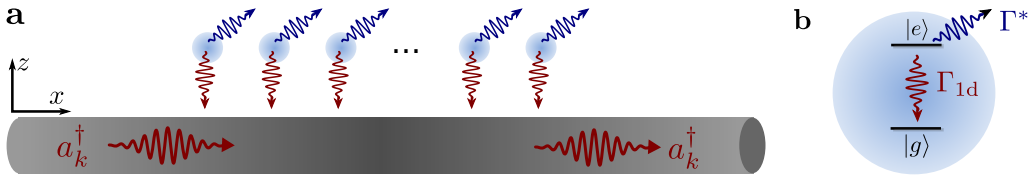

Figure 0.2: **a** Quantum emitters are coupled to a one-dimensional waveguide. The photonic field of the waveguide consists of a continuum of different wavevectors described by the bosonic creation operators $a_k^\dagger$. **b** The simplest level structure of the emitters are two-level systems, where the transition between the excited state $|e\rangle$ and the ground state $|g\rangle$ couples to the waveguide modes with a decay rate Γ_{1d}. Furthermore, individual spontaneous emission into other modes is embedded into a rate Γ^*.

typically coupled primarily through a dipole transition described by $H_I = -\sum_j \vec{d}_j \cdot \vec{E}(x_j)$, where $\vec{d}_j$ is the dipole operator of emitter j, and H_I is then proportional, e.g., to σ_x^j.

Then, the light-matter interactions is described by a Hamiltonian of the form

$$H = \frac{1}{2}\Delta \sum_j \sigma_z^j + \sum_k \omega_k a_k^\dagger a_k + \sum_{k,j} g_k \sigma_x^j (a_k^\dagger \mathrm{e}^{-\mathrm{i}kx_j} + a_k \mathrm{e}^{\mathrm{i}kx_j}), \tag{0.1}$$

where we assume $g_k \in \mathbb{R}$ and where we have set $\hbar = 1$ and the speed of light in the medium $c = 1$, which we use throughout this thesis. The sums run over all emitters j and wavevectors k. In this toy model the coupling has the form $g_k = \sqrt{\frac{\pi\alpha\omega_k}{2L}}$, where we collected all system parameters into a constant α which quantifies the strength of interaction. Note, that we have assumed all emitters to have the same transition energy Δ, and that the phase factors $\mathrm{e}^{\pm\mathrm{i}kx_j}$ correspond to the phase that the photons acquire when propagating through the waveguide to the emitter's position x_j. The dispersion relation ω_k is typically assumed to be approximately linear around the emitter energy Δ, but this depends on the specific microscopic model of the waveguide.

The continuum model of the waveguide is then obtained by taking $n \to \infty$ and therefore the mode spacing $\delta k = \frac{2\pi}{L} \to 0$. The sums are then replaced as $\sum_k = \frac{1}{\delta k}\sum_k \delta k \to \frac{2\pi}{\delta k}\int \frac{\mathrm{d}k}{2\pi}$, where the integral runs from $-L/2$ to $L/2$. The prefactor $\frac{2\pi}{\delta k} = L$ is then incorporated in the operators $a_k^\dagger \to \sqrt{L}a_k^\dagger$ and in the couplings $g_k \to \sqrt{L}g_k \equiv g(k)$. Note, that the dispersion relation is unchanged when we go to the continuum, $\omega_k \to \omega_k \equiv \omega(k)$. We use both the discrete and continuum version throughout this thesis and typically also work in the limit of very long waveguides, so that we can extend the integrals to the range $(-\infty, \infty)$. In addition, we often make a change of variables to frequency space, that is $\int_{-\infty}^{\infty} \frac{\mathrm{d}k}{2\pi} = 2\int_0^\infty \frac{\mathrm{d}\omega}{2\pi}(\partial_k\omega)^{-1}$ if the argument and the dispersion relation are symmetric under interchange $k \leftrightarrow -k$.

We note that other microscopic models for the waveguide may lead to a different form of the coupling g_k. Furthermore, this model can be mapped to a few-impurity spin-boson model in a rotated spin basis [119]. In that setting it was shown that the dynamics don't depend on g_k itself but rather on the spectral density, which turns out to be ohmic for the

coupling we considered above,

$$J(\omega) = 2\pi \sum_k |g_k|^2 \delta(\omega - \omega_k) \approx 2\pi \int \frac{\mathrm{d}k}{2\pi} |g(k)|^2 \, \delta(\omega - \omega_k) = \pi\alpha\omega. \tag{0.2}$$

This intimate relation to the spin-boson model also transfers some features of the spin-boson model, like a phase transition at a critical α_c depending on the form of the spectral density, over to the light-matter interface.[3] However, these effects are not relevant for the ohmic case with the values for the coupling strength considered throughout this thesis ($\alpha \leq 0.5$), such that there is no need to discuss them here.

Let us now get a sense of the quantity α by comparing the system of the one-dimensional waveguide to a cavity QED system, which has been studied thoroughly both experimentally and theoretically [30]. In fact, the waveguide behaves like a cavity when its length is equal to half the wavelength corresponding to the emitter transition, that is $L = \lambda/2 \approx \pi/\Delta$. The effective coupling to the cavity is then $g_{\mathrm{cav}} = \Delta\sqrt{\alpha/2}$ [120]. If the coupling to the cavity is weaker than the decay to other modes, $g_{\mathrm{cav}} \lesssim \Gamma^*$, one cannot observe coherent processes in the emitters. This is the so-called weak coupling regime. Most cavity QED systems nowadays reach the strong coupling regime at coupling strengths exceeding the decoherence rates, but still much smaller than the transition energy of the TLSs, $g_{\mathrm{cav}} \ll \Delta$ (or $\alpha \ll 0.01$). In this regime, the relevant interaction terms are only $\sigma_+^j a_k + \sigma_-^j a_k^\dagger$, which is called the Rotating Wave Approximation (RWA) [28]. In this case, the total excitation number in the TLSs and the cavity is conserved. If the coupling strength is increased to $g_{\mathrm{cav}} \lesssim \Delta$ (or $\alpha \lesssim 0.5$), the processes in the TLS are very fast, but also pair creation and annihilation processes, $\sigma_+^j a_k^\dagger + \sigma_-^j a_k$, become relevant. This regime is known as the ultrastrong coupling regime.

0.3.2 Master Equation of the System

One of the main motivations to study the interaction of TLSs with the electromagnetic field (also referred to as bath B) is to understand decoherence, and especially, dissipation in the TLSs. The model introduced above describes a specific type of interaction between the TLSs and the bath – the origin of the decoherence in the TLSs. The full TLS-bath-system undergoes unitary evolution, but the state ρ of the full system is quite difficult to obtain. If one is only interested in observables of the TLSs, it suffices to look at the reduced state of this system, $\rho_{\mathrm{S}} = \mathrm{Tr}_{\mathrm{B}}\rho$. The evolution of the TLSs simplifies considerably if the Born-Markov Approximation is valid, that is if the interactions aren't too strong such that $\rho(t) = \rho_{\mathrm{S}}(t) \otimes \rho_{\mathrm{B}}$ over a coarse grained time scale (Born) and the correlation times of the environment are short compared to the time scales of the TLSs (Markov). Typically, these approximations are only valid when $g \ll \Delta$, where one can apply the RWA. Under this approximation terms rotating with $\mathrm{e}^{\pm \mathrm{i}\Delta t}$ average out quickly over the timescales of the system $g^{-1}_{\omega_k \approx \Delta}$. The density matrix of the TLSs then evolves under a

[3] For the ohmic case, the critical coupling strength is $\alpha_c = 1$.

Master equation in Lindblad form [121],

$$\partial_t \rho_{\mathrm{S}}(t) = -\mathrm{i}\left[\left(H_{\mathrm{S}} + \sum_{ij} J_{ij}\sigma_{eg}^{i}\sigma_{ge}^{j}\right), \rho_{\mathrm{S}}(t)\right] + \sum_{ij}\gamma_{ij}\left(\sigma_{ge}^{j}\rho_{\mathrm{S}}\sigma_{eg}^{i} - \sigma_{eg}^{i}\sigma_{ge}^{j}\rho_{\mathrm{S}} + \mathrm{h.c.}\right), \quad (0.3)$$

where the sums run over all emitters j with the TLS operator given by $\sigma_{\alpha\beta}^{j} = |\alpha\rangle_j\langle\beta|$, or equivalently $\sigma_{eg/ge}^{j} = \sigma_{\pm}^{j}$. The coefficients γ_{ij} and J_{ij} are given by the real and imaginary parts of the coupling matrix $\Gamma_{ij} = \gamma_{ij} + \mathrm{i}J_{ij} = \int_0^\infty \mathrm{d}\tau\ (\mathrm{e}^{\mathrm{i}\Delta\tau} + \mathrm{e}^{-\mathrm{i}\Delta\tau})\langle \mathrm{vac}|B_i^\dagger(\tau)B_j(0)|\mathrm{vac}\rangle$ with the bath operators $B_j = \sum_k g_k(a_k^\dagger \mathrm{e}^{-\mathrm{i}kx_j} + a_k \mathrm{e}^{\mathrm{i}kx_j})$.

In our one-dimensional system, this matrix evaluates to $\Gamma_{ij} = \frac{\Gamma_{1\mathrm{d}}}{2}\mathrm{e}^{\mathrm{i}k_0|x_{ij}|}$ with $\Gamma_{1\mathrm{D}} = 2|g_{k_0}|^2/|\partial_k\omega_k(k_0)|$ [37, 122]. In particular, the interactions don't decay with the distance between emitters, $|x_{ij}| = |x_i - x_j|$, and only depend on the wavevector k_0 corresponding to the TLS transition energy, $\omega_{k_0} = \Delta$. On the one hand, the imaginary part of the matrix Γ_{ij} gives rise to coherent flip-flop interactions between emitters i and j,

$$H_{\mathrm{coll}} = \frac{\Gamma_{1\mathrm{d}}}{2}\sum_{ij}\sin\left(k_0|x_{ij}|\right)\sigma_{eg}^{i}\sigma_{ge}^{j}. \quad (0.4)$$

On the other hand, the real part of the matrix Γ_{ij} gives rise to collective dissipation of the form

$$\mathcal{L}_{\mathrm{coll}}\left[\rho_{\mathrm{S}}\right] = \frac{\Gamma_{1\mathrm{d}}}{2}\sum_{ij}\cos\left(k_0|x_{ij}|\right)\left(\sigma_{ge}^{j}\rho_{\mathrm{S}}\sigma_{eg}^{i} - \sigma_{eg}^{i}\sigma_{ge}^{j}\rho_{\mathrm{S}} + \mathrm{h.c.}\right). \quad (0.5)$$

In addition to the coupling to the waveguide, there is a coupling to free-space modes in realistic systems. The decay rate Γ^* into these modes is typically of the order of the natural decay rate in free space. Because the photons are emitted into the 4π solid angle, it is highly unlikely that emitted photons interact with another TLS, such that we can assume the decay into these modes to be individual. These individual baths are then described by an additional Lindblad term in the master equation, which reads

$$\mathcal{L}_{\mathrm{ind}}\left[\rho_{\mathrm{S}}\right] = \frac{\Gamma^*}{2}\sum_{j}\left(2\sigma_{ge}^{j}\rho_{\mathrm{S}}\sigma_{eg}^{j} - \sigma_{eg}^{j}\sigma_{ge}^{j}\rho_{\mathrm{S}} + \mathrm{h.c.}\right). \quad (0.6)$$

The decay rate Γ^* into these free-space modes has to be taken in relation to the decay rate into waveguide modes with rate $\Gamma_{1\mathrm{d}}$, so recall, that we call this ratio the Purcell factor $P_{1\mathrm{d}} = \frac{\Gamma_{1\mathrm{d}}}{\Gamma^*}$.

We point out, that the parameters of the TLSs can be tuned by replacing them by three-level systems in a Λ-configuration and driving one of the transitions with a Rabi coupling Ω off-resonantly with detuning δ. The excited state can then be adiabatically eliminated, such that the system behaves like a TLS [28]. The renormalized parameters are then $\Gamma_{1\mathrm{d}} \to \Gamma_{1\mathrm{d}}\frac{\Omega^2}{4\delta^2}$ and $\Gamma^* \to \Gamma^*\frac{\Omega^2}{4\delta^2}$. Thus, the Purcell factor $P_{1\mathrm{d}}$ is unchanged, but we have gained freedom in the collective decay rate $\Gamma_{1\mathrm{d}}$.

0.3.3 The Atomic Mirror Configuration

The coherent flip-flop interactions of Equation 0.4 can be made to vanish by placing the TLSs such that the distance d between the emitters is commensurate with the wavelength corresponding to the transition energy Δ, i.e. $d = 2\pi/k_0 \cdot n$, where k_0 is the wavevector satisfying $\omega_{k_0} = \Delta$ and $n \in \mathbb{N}$.[4] The dynamics of the emitters are then only undergoing collective decay with $S_{ge} = \sum_j \sigma^j_{ge}$. This configuration is also known as the atomic mirror configuration because the emitters act as a mirror for a resonant photon [36, 67, 66]. The master equation without external driving is then

$$\partial_t \rho_{\mathrm{S}} = -\mathrm{i}\left[\Delta S_{ee}, \rho_{\mathrm{S}}\right] + \frac{\Gamma_{1\mathrm{d}}}{2}\left(S_{ge}\rho_{\mathrm{S}}S_{eg} - S_{eg}S_{ge}\rho_{\mathrm{S}} + \mathrm{h.c.}\right) + \frac{\Gamma^*}{2}\sum_j \left(\sigma^j_{ge}\rho_{\mathrm{S}}\sigma^j_{eg} - \sigma^j_{ee}\rho_{\mathrm{S}} + \mathrm{h.c.}\right),$$

where we have moved the zero-point energy by $\Delta/2$ up to be able to write $\Delta S_{ee} = \Delta \sum_j \sigma^j_{ee}$ instead of $\frac{1}{2}\Delta S_z$. In this configuration, it is generally useful to describe the dynamics in terms of the collective operators $S_{\alpha\beta} = \sum_j \sigma^j_{\alpha\beta}$.

One can unravel master equations of Lindblad form as above into a non-hermitian evolution $S(t, t_0)\rho = e^{-iH_{\mathrm{eff}}t}\rho e^{iH^\dagger_{\mathrm{eff}}t}$ given by an effective Hamiltonian H_{eff} and quantum jumps J as

$$\rho(t) = S(t, t_0)\rho(t_0) + \sum_{n=1}^{\infty}\int_{t_0}^{t} \mathrm{d}t_n \cdots \int_{t_0}^{t_2} \mathrm{d}t_1 S(t, t_n) J \cdots J S(t_1, t_0)\rho(t_0). \tag{0.7}$$

Then, the n-th order of the sum corresponds to the evolution where n quantum jumps have occurred. In the atomic mirror configuration, the effective non-hermitian Hamiltonian is

$$H_{\mathrm{eff}} = (\Delta - \mathrm{i}\frac{\Gamma^*}{2})S_{ee} - \mathrm{i}\frac{\Gamma_{1\mathrm{d}}}{2}S_{eg}S_{ge}, \tag{0.8}$$

and the quantum jumps $J\rho = J_{\mathrm{coll}}\rho + J_{\mathrm{ind}}\rho$ are either collective, $J_{\mathrm{coll}}\rho = \Gamma_{1\mathrm{d}}S_{ge}\rho S_{eg}$, or individual, $J_{\mathrm{ind}}\rho = \Gamma^* \sum_j \sigma^j_{ge}\rho\sigma^j_{eg}$.

The arising collective operators are sums of spin operators, e.g., $S_{eg} \equiv S_+$, and therefore one can use the theory of addition of angular momenta to simplify the description. When spins are added, the tensor product of the Hilbert space $\mathcal{H}$ of a single spin ($\mathcal{H} = \mathbb{C}^2$ for a TLS) splits up into the direct sum [123]

$$\mathcal{H}^{\otimes N} \cong \bigoplus_{s=\frac{N}{2},\frac{N}{2}-1,\ldots} \mathcal{H}_s^{\otimes d_s}, \tag{0.9}$$

where $\mathcal{H}_s$ is a Hilbert space that carries the irreducible spin-s representation of $su(2)$ and has a multiplicity $d_s = \binom{N}{\frac{N}{2}-s} - \binom{N}{\frac{N}{2}-s-1}$ with $d_{N/2} = 1$.

[4] The coherent flip-flop interactions actually also vanish for half this distance, that is $d = \pi/k_0 \cdot n$ with n odd. In this case, additional factors of $(-1)^j$ are introduced, but the physics remain unchanged. For simplicity, we focus on the distance $d = 2\pi/k_0 \cdot n$ for the remainder of this thesis.

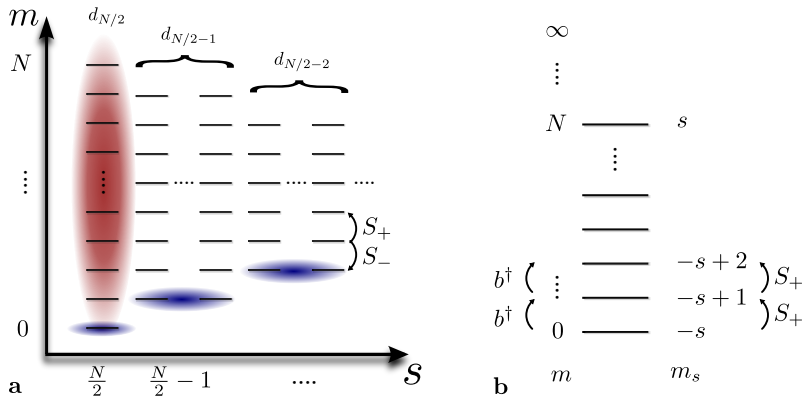

Figure 0.3: **a** The basis states $|s, m_s, \alpha\rangle$ of the Dicke basis can be arranged in orthogonal ladders, within which the states are connected through the ladder operators $S_\pm$. The number of excitations in the state e is $m = m_s + \frac{N}{2}$. The subspace for a specific total spin s has a degeneracy d_s. The states $|s, -s\rangle$ are subradiant (blue) and the states $|\frac{N}{2}, m_s\rangle$ with $m_s > -N/2$ are superradiant (red). **b** The Holstein-Primakoff Approximation replaces the collective spin operators S_+ by approximately bosonic operators $b^\dagger$ in the low excitation regime $m \ll N$. Here, we visualize this behavior for the maximal spin $s = \frac{N}{2}$ for which the states are fully symmetric.

The new basis states $|s, m_s, \alpha\rangle$ are then characterized as the eigenstates of the collective spin operator, $S^2 = (S_x + S_y + S_z)^2$, and the projection onto the z-axis, S_z, as

$$S^2|s, m_s, \alpha\rangle = s(s+1)|s, m_s, \alpha\rangle, \tag{0.10a}$$
$$S_z|s, m_s, \alpha\rangle = m_s|s, m_s, \alpha\rangle. \tag{0.10b}$$

For $s < N/2$ the states are degenerate, such that we have introduced the parameter $\alpha = 1, \dots d_s$ in the basis states $|s, m_s, \alpha\rangle$. The ladder operators $S_\pm = S_x \pm \mathrm{i}S_y = S_{eg/ge}$ raise or lower the spin quantum number m_s by one and leave s unchanged. This splitting into distinct ladders can be visualized as in Figure 0.3a. Instead of the quantum number m_s, one can use the number of excitations $m = m_s + N/2$ in the excited state e.

There are two types of states in the Dicke basis with very particular features that manifest themselves in their decay rate and therefore in the coupling to the waveguide photons. On the one hand, there are the *subradiant* states, which are zero eigenstates of the collective decay operator, i.e., $S_-|\psi\rangle = S_{ge}|\psi\rangle = 0$. In the Dicke basis these can be easily found to be $|\psi\rangle = |s, -s, \alpha\rangle$. They are called subradiant because the collective decay vanishes and only individual decay processes with rate Γ^* occur. If $\Gamma^* = 0$ one often uses the term "Decoherence-Free Subspace" to describe this set of states [124, 125, 126]. On the other hand, the states $|\frac{N}{2}, m_s\rangle$ show a strongly enhanced decay rate for $m_s > -N/2$ and are thus coined *superradiant*.[5] These states have a very strong coupling to the waveguide and turn out to be essential for the generation of photonic states in the waveguide. One also uses the term symmetric Dicke state for these states because they

[5]The decay in the low excitation regime $m \ll N$ is often only referred to as "collective decay", to reserve the term "superradiant decay" for the region of $m \sim N/2$, where the decay rate scales quadratically with the ensemble size, $\sim \frac{1}{4}N^2$. We use both expressions equivalently throughout this thesis.

can be written as

$$|\psi_m\rangle = |\frac{N}{2}, m - \frac{N}{2}\rangle = \binom{N}{m}^{-1/2} \mathrm{sym}\Big\{|e\rangle^{\otimes m} \otimes |g\rangle^{\otimes N-m}\Big\}, \tag{0.11}$$

where m is the excitation number, i.e., $S_{ee}|\psi_m\rangle = m|\psi_m\rangle$ and "sym" denotes the symmetrization operator. As an example, take

$$|\psi_0\rangle = |gggg\cdots\rangle, \tag{0.12a}$$

$$|\psi_1\rangle = \binom{N}{1}^{-1/2} \left(|eggg\cdots\rangle + |gegg\cdots\rangle + |ggeg\cdots\rangle + \cdots\right), \tag{0.12b}$$

$$|\psi_2\rangle = \binom{N}{2}^{-1/2} \left(|eegg\cdots\rangle + |egeg\cdots\rangle + \cdots + |geeg\cdots\rangle + \cdots\right). \tag{0.12c}$$

From an historical perspective, superradiance is a term coined by R. H. Dicke and describes the collective spontaneous emission from a cloud of N excited emitters [127, 128, 129]. In these days it was realized that correlations between the emitters can be induced by the interaction with a common radiation field, leading to super- and subradiant decay. For superradiance, the emitters have to be in the same phase, which occurs if all emitters are in a region that is much smaller than the wavelength of the emitted light. The observation of sub- and superradiance in this regime is very difficult due to the low optical thickness [130] and due to propagation effects if they are placed farther apart (while retaining the phase correlation) [131]. Furthermore, the collective decay rate needs to be larger than the individual decay rate. Fortunately, all of these requirements can be satisfied in waveguide QED setups in the optical regime [34, 35].

Coming back to the effective Hamiltonian, we note that if we start in the set of superradiant states, we remain in this set until the ground state $|\psi_0\rangle = |g\rangle^{\otimes N}$ is reached. In particular, the effective Hamiltonian of Equation 0.8 is diagonal in the symmetric Dicke state basis,

$$H_{\mathrm{eff}} = \sum_m (m\Delta - \mathrm{i}\frac{\gamma_m + m\Gamma^*}{2})|\psi_m\rangle\langle\psi_m|. \tag{0.13}$$

The decay rate γ_m is defined by $\Gamma_{1\mathrm{d}} S_{eg} S_{ge}|\psi_m\rangle = \gamma_m|\psi_m\rangle$ and can be calculated to be $\gamma_m = m(N - m + 1)\Gamma_{1\mathrm{d}}$.

To simplify the description, the collective spin operators can be expressed in terms of bosonic operators by using the Holstein-Primakoff transformation [132, 133, 134],

$$S_+ = b^\dagger \sqrt{2s - b^\dagger b}, \tag{0.14a}$$

$$S_z = b^\dagger b - s. \tag{0.14b}$$

One can check that the spin commutation relations $[S_+, S_-] = 2S_z$ and $[S_z, S_\pm] = \pm S_\pm$ imply the correct bosonic commutation relations $\left[b, b^\dagger\right] = 1$ and $[b, b] = \left[b^\dagger, b^\dagger\right]$. The

operator inside the square root ensures, that the bosonic system is finite and it is impossible to put arbitrarily many excitations in the system (see Figure 0.3b). This transformation can be useful to study spin systems in general, but we are interested here in the low excitation regime $m \ll N$. For the symmetric Dicke states ($s = N/2$) the square root can be expanded in the low excitation regime $\langle b^\dagger b\rangle = m \ll 2s = N$.[6] Thus, the collective operators S_+ are approximated by bosonic operators as

$$S_+ \approx \sqrt{2s}\; b^\dagger = \sqrt{N} b^\dagger. \tag{0.15}$$

While the transformation of Equation 0.14 is exact, the Holstein-Primakoff Approximation (HPA) of Equation 0.15 is only valid in the low excitation regime $m \ll N$. In this case, we find $|\psi_m\rangle \approx \frac{1}{\sqrt{m!}} b^{\dagger m}|g\rangle^{\otimes N}$ and a decay rate linear in the excitation number, $\gamma_m \approx mN\Gamma_{1\mathrm{d}} = m\gamma_1$.

As a final point, we emphasize that the collective dissipation in the atomic mirror configuration not only induces sub- and superradiance, but can also lead to collective coherent couplings induced by the Quantum Zeno Dynamics (QZD) [135]. This is a generalization of the Quantum Zeno Effect (QZE) [136], in which frequent measurements on a specific state (QZE) or on a subspace (QZD) of the system restrict the evolution to this state or subspace. Both the QZE [137] and the QZD [138, 139] have been observed experimentally. In our case the strong collective decay wit rate $\sim N\Gamma_{1\mathrm{d}}$ acts as a measurement on whether the state is in a subradiant state or not. In particular, if one starts in the subspace of subradiant states and weakly drives a transition on a single emitter with strength Ω to a state outside this subspace, then the coupling to this state is reduced to $\frac{\Omega^2}{N\Gamma_{1\mathrm{d}}}$. Thus, through the QZD the collective dissipation together with weak local drivings $\Omega \ll N\Gamma_{1\mathrm{d}}$ can lead to collective dynamics within the subspace of subradiant states. These dynamics can also be used to implement a set of universal quantum gates in this subspace [140, 7].

0.4 Outline of this Thesis

The motivation of our work was the development of novel methods for solving two of the current challenges in quantum optics. On the one hand, we investigated how waveguide QED tools can be exploited for the generation of propagating photonic states in the well understood strong coupling regime under the RWA. This problem in itself is twofold: First, we have to determine which states of an ensemble of emitters generate the desired photonic states and from what limitations these states suffer. Second, we need to find methods how to generate said collective emitter states. On the other hand, we propose to use multiphoton scattering to study the behavior of waveguide QED systems in the ultrastrong coupling regime. In particular, we look at the scattering of few photons on a single quantum emitter because the scattering matrix is experimentally accessible [141] and provide a new method for analytically studying this process. The remainder of this thesis is split into the following three chapters:

[6] In fact, this approximation works in the lower part ($m_s \gtrsim -s$) of every ladder s where $\langle b^\dagger b\rangle = (m_s + s) \ll 2s$, but clearly best for the maximal $s = N/2$.

Chapter 1 – Generation of Photonic States As we have motivated, the light-matter interaction is enhanced both in waveguide QED systems as well as by using many emitters. In particular, the superradiant decay of emitters in the atomic mirror configuration suggests that this system is a promising candidate for the generation of photonic states. In fact, symmetric Dicke states over an ensemble of N emitters can be used to trigger the generation of photonic states in the waveguide. The emitted wavepacket can be shaped to be time symmetric such that a different ensemble can absorb the photonic state. In the low excitation regime the outgoing photonic state is a single-mode state. However, when, e.g., all emitters are excited, the emitted N photon state has a multi-mode structure. Nevertheless, these states are still useful for quantum-enhanced optical interferometry. In Chapter 1 we aim to answer the following main questions: For what parameters is a single-mode photonic state generated? What are the characteristics of the emission? Are multi-mode photonic states useful for quantum metrology – in general and in the specific waveguide QED setting?

Chapter 2 – Preparation of Dicke States The generation of arbitrary single-mode photonic states as described in Chapter 1 requires the preparation of arbitrary symmetric Dicke states of a specific excitation number and superpositions thereof. These symmetric states are also of fundamental interest due to their robustness against particle loss and for atomic interferometry. We investigate how waveguide QED tools can be exploited to prepare these highly entangled states. We provide various protocols for their preparation, which favor one or the other experimental platform with their characteristic Purcell factor $P_{1\mathrm{d}}$ and number of coupled emitters N. In particular, there is a simple protocol, which only requires coherent driving, and others with an increased fidelity, which use either the collective dissipation or the coherent flip-flop interactions induced by the waveguide. In Chapter 2 we aim to answer the following main questions: Which waveguide QED resources are necessary for the preparation of symmetric Dicke states? Can we find protocols for the efficient and high-fidelity preparation of these states? How can these protocols be extended to Dicke states over multiple metastable states?

Chapter 3 – Ultrastrong Coupling Regime One of the goals of increasing the light-matter coupling strength is to decrease the necessary interaction times for specific processes and enhance nonlinearities of the system. However, when the coupling strength becomes comparable to the emitter's transition energy, standard tools (like the Rotating Wave Approximation) for understanding and analytically studying the interaction between emitters and photons break down [41, 42]. One alternative approach is the so-called polaron transformation, which is a variational approach to finding the ground state of an ultrastrongly coupled system. The results obtained from this new approximation can then be compared to experimental results. We derive the scattering matrix (e.g., reflection and transmission coefficients for a single photon) for these scattering processes, which can be compared to numerical results. In Chapter 3 we aim to answer the following main questions: What is a polaron transformation and why is it expected to aid in describing ultrastrongly coupled systems? How are the scattering properties in the original picture and the polaron transformed picture related? Is it possible to obtain analytical or numerical results for the scattering in the polaron transformed picture?

1 Generation of Photonic States

Abstract

Many methods to use quantum optics for advancing current technologies rely on high fidelity photonic states. Examples of such applications are quantum communication [10] and quantum metrology [11]. However, the efficient and on demand generation of (arbitrary) photonic states remains elusive. Single photons can be generated trough spontaneous parametric down conversion, from single quantum emitters coupled to cavities or waveguides or from an ensemble of such emitters [88]. States containing multiple photons are generally obtained by combining single photons with linear optical devices and heralding measurements. This approach is however inherently limited due to a low heralding probability with increasing photon number [86].

By using an ensemble of quantum emitters, one can prepare specific states that directly emit multiple photons. We show in this chapter that (superpositions of) symmetric Dicke states of a chain of quantum emitters coupled to a one-dimensional waveguide efficiently generate high fidelity multiphoton states. The preparation of these Dicke states will be covered in Chapter 2. Moreover, we show that the wavepacket of the emitted photonic state can be shaped to be, e.g., symmetric in time, such that the process is reversible. Another feature of these photonic states is that they can be emitted into a single mode, which is a basic requirement for many applications. However, even if the photonic state has an intricate multi-mode structure, it can still be useful for quantum optical applications, as we show on the example of quantum metrology.

In this chapter, we first motivate the importance of the generation of photonic states and introduce some of their applications (Section 1.1). Then we derive the structure of the emitted photonic state through an input-output formalism (Section 1.2). Finally, we discuss one of the most important applications of photonic states – quantum metrology (Section 1.3). After introducing some basic concepts of quantum metrology, we show that multi-mode photonic states generated by exciting all emitters of the waveguide QED system are useful for quantum-enhanced optical interferometry. Finally, we summarize the results (Section 1.4).

This chapter is based on and uses parts of References

- [1]: A. González-Tudela, V. Paulisch, D. E. Chang, H. J. Kimble, and J. I. Cirac. "Deterministic Generation of Arbitrary Photonic States Assisted by Dissipation" *Phys. Rev. Lett.* **115** 163603 (2015),
- [2]: V. Paulisch, M. Perarnau-Llobet, A. González-Tudela, and J. I. Cirac. "Quantum Metrology with Multimode Photonic States" *In preparation.* (2018).

1.1 Motivation and Basic Concepts

Photonic states play a key role in a variety of quantum technologies [39]. Because photons interact only weakly with the environment, they are a prime candidate for secure transmission of quantum information over long distances [142] and thus an essential building block for quantum networks [13]. Quantum states of light can also enhance the performance of optical interferometers by using non-classical initial states or by special measurements, e.g. photon number resolving or parity measurements [19]. Other applications for single photons include the KLM scheme for quantum computation with linear optics [23], and for many photons, quantum lithography for imaging features below the wavelength of the light [143].

For most of these applications, one considers single-mode photonic states, where all photons are in a specific photonic mode, which can have some modal structure, $\int \frac{\mathrm{d}k}{2\pi} A_k a_k^\dagger$. The structure of the mode is determined by the coefficient A_k of the superposition of the propagating photons (with the creation operator $a_k^\dagger$ for the wavevector k). Entangled photonic states are a superposition of photonic states between two orthogonal modes, e.g., in different polarization degrees of freedom, different legs of an interferometer or in different time bins. However, in some setups one might generate multi-mode photonic states, $\int \left\{\frac{\mathrm{d}k_j}{2\pi}\right\} A_{k_1\cdots k_m} a_{k_1}^\dagger \cdots a_{k_m}^\dagger |\mathrm{vac}\rangle$, instead of single-mode states, $\frac{1}{\sqrt{m!}}\left(\int \frac{\mathrm{d}k}{2\pi} A_k a_k^\dagger\right)^m |\mathrm{vac}\rangle$. Note, that if one photon from the single-mode state is measured, one cannot infer any information about the remaining photons, whereas one can for multi-mode states. It was unclear whether these multi-mode states are as useful for quantum applications (like quantum metrology) as the single-mode ones. But at least for certain multi-mode states we show that the classical limit for the phase resolution of an optical interferometer can still be overcome.

There are a variety of photonic states of theoretical and experimental interest. However, the generation of these states can be very challenging [84]. As reviewed in Section 0.2.3, there are three main approaches to the generation of photonic states, namely the use of spontaneous parametric down conversion, the emission from single quantum emitters and from ensembles of quantum emitters. The first two naturally suffer from an exponentially low heralding probability for generating photonic states with many photons. On the other hand, in the latter, one can prepare collective states of the ensemble with m excitations, that can then be triggered to emit m photons, in the ideal case, superradiantly.

In waveguide QED systems, a chain of symmetrically excited quantum emitters in the atomic mirror configuration undergoes such superradiant decay (see Section 0.3.3) and emits a photonic state into the waveguide. This photonic state can be efficiently collected at the ends of the waveguide. In the following sections we study these photonic states and investigate their usefulness for quantum metrology. The main losses we consider here are due to spontaneous emission processes from the quantum emitters, whereas we neglect losses within the waveguide due to the typically large propagation lengths.

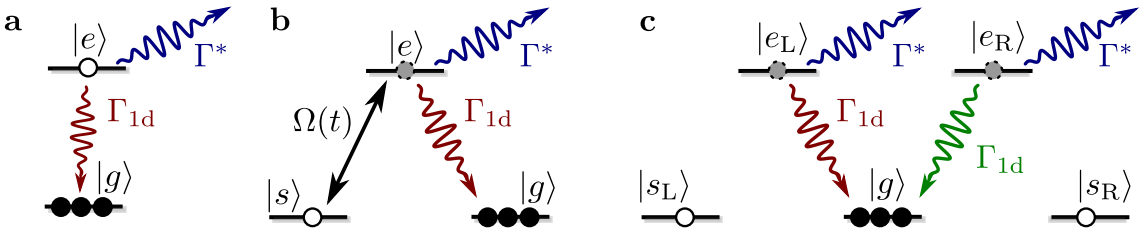

Figure 1.1: The level structures considered within this chapter. **a** The simplest level structure is a two-level system, where the $g-e$ transition is coupled to the waveguide. **b** With a three-level system and a time-dependent Rabi coupling on the $s-e$ transition, one can trigger the emission and shape the emitted wavepacket. **c** If two orthogonal guided modes, which couple the ground state with two optical excited states $e_{\mathrm{L/R}}$, are available, one can generate two-mode photonic states. The decay rates $e_{\mathrm{L}}-g$ and $e_{\mathrm{R}}-g$ are depicted in different colors to highlight that they are related to two orthogonal guided modes.

1.2 Generation of Photonic States

First of all, we need to understand the structure of the photonic states that are emitted by a chain of quantum emitters in the atomic mirror configuration. Let us therefore assume that we can prepare a symmetric Dicke state with m excitations in the excited state, that is

$$|\psi_m\rangle = \frac{1}{m!}\binom{N}{m}^{-\frac{1}{2}} S_{eg}^m |g\rangle^{\otimes N}, \tag{1.1}$$

where N is the number of emitters in the chain and $S_{eg} = \sum_j \sigma_{eg}^j$. We assume the transition between the ground state g and the optically excited state e to be coupled to the waveguide modes (see Figure 1.1a). We emphasize, that in three-level systems this state can be obtained from a symmetric Dicke state in the metastable state s by applying a π-pulse on the transition $s-e$ (see Figure 1.1b). We propose various protocols for the preparation of these states in Chapter 2. This excited symmetric Dicke state then decays to the ground state $|\psi_0\rangle$ after a time of at most $T \gg (N\Gamma_{1d})^{-1}$, so that no TLS-photon entanglement remains. If we neglect spontaneous emission into other modes and assume linear dispersion, the emitted photonic state in the waveguide after this time T is in general of the form

$$|\phi_m\rangle = \int_{-\infty}^{\infty} \frac{\mathrm{d}k_1}{2\pi} \cdots \int_{-\infty}^{\infty} \frac{\mathrm{d}k_m}{2\pi} \frac{A_{\{k\}} \mathrm{e}^{-\mathrm{i}\sum \omega_{k_j} t}}{m!} a_{k_1}^\dagger a_{k_2}^\dagger \dots a_{k_m}^\dagger |\mathrm{vac}\rangle. \tag{1.2}$$

The coefficient $A_{\{k\}} = A_{k_1 \cdots k_m}$ is symmetric under all interchanges $k_i \leftrightarrow k_j$ and satisfies the normalization condition $\int \left\{\frac{\mathrm{d}k_j}{2\pi}\right\} \frac{1}{m!} |A_{\{k\}}|^2 = 1$, where we write $\int \left\{\frac{\mathrm{d}k_j}{2\pi}\right\}$ as a shorthand notation for the m momentum integrals. Note, that we require the factor of $m!$ because the wavevectors are not ordered. If the emission into other modes cannot be neglected, the emitted state is $|\Phi_m\rangle = |\phi_m\rangle + |\phi_m^*\rangle$, where all parts of the state where a spontaneous emission event has taken place have been collected into $|\phi_m^*\rangle$, which is orthogonal to $|\phi_m\rangle$. Note, that in this case $|\langle\phi_m|\phi_m\rangle| < 1$.

We assume the dispersion to be linear around the energy of the emitter, $\omega_k \approx |k|$, so that we can apply the input-output formalism (e.g., see Reference [144] and Appendix 1.A)

to obtain the coefficient

$$A_{\{k\}} = (-i)^m \int_0^\infty ds_1 \cdots \int_0^\infty ds_m \, \mathrm{e}^{\mathrm{i}\sum_{j=1}^m k_j s_j} \langle \psi_0 | \mathcal{T} O_{k_1}(s_1) O_{k_2}(s_2) \cdots O_{k_m}(s_m) | \psi_m \rangle, \quad (1.3)$$

where $\mathcal{T}$ denotes the time ordering operator[7] and the decay operators $O_k = g_k \sum_j \sigma_{ge}^j \mathrm{e}^{-\mathrm{i}kx_j}$ are taken in the interaction picture of the effective Hamiltonian of Equation 0.8, $H_{\mathrm{eff}} = (\Delta - \mathrm{i}\frac{\Gamma^*}{2}) S_{ee} - \mathrm{i}\frac{\Gamma_{1\mathrm{d}}}{2} S_{eg} S_{ge}$. Under the Markov approximation, the decay operators can be taken as independent of the wavevectors,

$$O_k(s) \approx \sqrt{\Gamma_{1\mathrm{d}}} \mathrm{e}^{\mathrm{i}H_{\mathrm{eff}} s} S_{ge} \mathrm{e}^{-\mathrm{i}H_{\mathrm{eff}} s} \equiv O(s). \quad (1.4)$$

Notice that under this approximation, the different time orderings lead to different $\{k\}$-permutations and that therefore, it suffices to calculate one time ordering, e.g., $s_1 > s_2 > \cdots > s_m$ and symmetrize the coefficient with respect to the momenta k_j. The coefficient of the emitted photonic state is then

$$A_{\{k\}} \approx \prod_{n=1}^m \frac{\sqrt{\gamma_n}}{(n\Delta - \sum_{j=1}^n k_j) - \frac{\mathrm{i}}{2}(\gamma_n + n\Gamma^*)} + \{k - \text{permutations}\}, \quad (1.5)$$

where we have introduced the decay rate of state $|\psi_n\rangle \to |\psi_{n-1}\rangle$ as $\gamma_n = n(N-n+1)\Gamma_{1\mathrm{d}}$ (see Section 0.3.3). Here, we have also assumed a vanishing Lamb shift $\delta_{\mathrm{L}} = 0$. If this is not the case, we simply need to replace $\Delta \to \Delta - \delta_{\mathrm{L}}$. The normalization can be calculated to be

$$|\langle \phi_m | \phi_m \rangle|^2 = \int \frac{\mathrm{d}k_1}{2\pi} \cdots \int \frac{\mathrm{d}k_m}{2\pi} \frac{1}{m!} |A_{\{k\}}|^2 = \prod_{n=1}^m \frac{\gamma_n}{\gamma_n + n\Gamma^*} \leq 1. \quad (1.6)$$

In the case $\Gamma^* = 0$, we recover $|\langle \phi_m | \phi_m \rangle|^2 = 1$. In the low excitation regime $m \ll N$ we find $|\langle \phi_m | \phi_m \rangle|^2 \approx 1 - \frac{m}{NP_{1\mathrm{d}}}$, that is, the probability of emitting all excitations into the waveguide is close to 1. Similarly, we can approximate the fidelity of the emitted photonic state in the low excitation regime as

$$F_{\mathrm{ph}} = |\langle \Phi_m | \phi_m \rangle| \approx 1 - \frac{m}{2NP_{1\mathrm{d}}}, \quad (1.7)$$

where $P_{1\mathrm{d}} = \Gamma_{1\mathrm{d}}/\Gamma^*$ is the Purcell factor of the system. This is also an upper bound for the fidelity when we map superpositions of symmetric Dicke states to superpositions of Fock states. In particular, the state $|\psi\rangle = \sum_{n=0}^m c_n |\psi_n\rangle$ with $\sum |c_n|^2 = 1$ generates the waveguide state $|\phi\rangle = \sum_{n=0}^m c_n |\phi_n\rangle$. In that case, the fidelity of the atom-photon mapping can be lower bounded by $1 - \sum_{n=0}^m \frac{|c_n|^2 n}{2NP_{1\mathrm{d}}} \geq F_{\mathrm{ph}}$.

To study the form of the wavepacket further, we consider the emission of one and two photons from a symmetric Dicke state. For $m = 1$, the output wavepacket is a Lorentzian peaked at the resonance frequency Δ and with linewidth $\gamma_1 = N\Gamma_{1\mathrm{d}}$,

$$A_k = \frac{\sqrt{\gamma_1}}{(\Delta - k) - \mathrm{i}\gamma_1/2}. \quad (1.8)$$

[7] The time ordered product of two commuting operators is defined as $\mathcal{T}O(s_1)O(s_2) = \Theta(s_1 - s_2)O(s_1)O(s_2) + \Theta(s_2 - s_1)O(s_2)O(s_1)$ with Θ the Heaviside step function.

For $m = 2$ the emitted state can be separated into a linear and a nonlinear part as

$$A_{k_1,k_2} = \sqrt{\frac{\gamma_2}{\gamma_1}} \frac{(2\Delta - k_1 - k_2) - \frac{\mathrm{i}}{2}(2\gamma_1 + 2\Gamma^*)}{(2\Delta - k_1 - k_2) - \frac{\mathrm{i}}{2}(\gamma_2 + 2\Gamma^*)} A_{k_1} A_{k_2}. \tag{1.9}$$

From this expression we observe that the output coefficient is a product of the single-mode functions, $A_{k_1 k_2} = \sqrt{2} A_{k_1} A_{k_2}$, if $\gamma_2 = 2\gamma_1$. In this case, the two photons are emitted into the same mode. This linear relation between the decay rates, $\gamma_n = n\gamma_1$, is approximately true in the low excitation regime $n \ll N$, where the Holstein-Primakoff Approximation is valid (see Section 0.3.3). This result can be extended to higher excitations to obtain $A_{\{k\}} \approx \sqrt{m!} A_{k_1} \cdots A_{k_m}$ for $m \ll N$. The photonic state of the waveguide in the low excitation regime is therefore approximately a single-mode state,

$$|\phi_m\rangle \approx |\phi_m^{\mathrm{SM}}\rangle = \frac{1}{\sqrt{m!}} \left(\int \frac{\mathrm{d}k}{2\pi} \mathrm{e}^{-\mathrm{i}\omega_k t} A_k a_k^\dagger \right)^m |\mathrm{vac}\rangle, \tag{1.10}$$

that is, the state is emitted into a single mode with modal structure $\int \frac{\mathrm{d}k}{2\pi} A_k a_k^\dagger$. Outside this regime or even for the emission from a fully excited state $m = N$, a multi-mode state is emitted. The overlap with the single-mode state (neglecting Γ^*),

$$\langle \phi_m | \phi_m^{\mathrm{SM}} \rangle = \prod_{n=1}^{m} \frac{2\sqrt{\gamma_n \cdot n\gamma_1}}{\gamma_n + n\gamma_1} = \prod_{n=1}^{m} \frac{\sqrt{N(N-n+1)}}{N - (n-1)/2} \approx 1 - \frac{m^3}{24N^2} + \mathcal{O}(\frac{m^4}{N^2}, \frac{1}{N^3}), \tag{1.11}$$

shows that the emitted state is well approximated by a product state in the low excitation regime.

One important feature of this mapping to photonic states is that the wavepacket can be shaped as first proposed in Reference [145]. In particular, one requires the wavepacket to be symmetric in time for quantum communication applications and to build quantum networks, such that the photonic state can be mapped back to the corresponding emitter state with high fidelity at another node of the quantum network. If the emitters simply decay from an excited symmetric Dicke state $S_{eg}^m |g\rangle^{\otimes N}$ the wavepacket in time follows the exponential decay. However, if one uses a three-level system and starts with a symmetric Dicke state in the metastable levels, $S_{sg}^m |g\rangle^{\otimes N}$, the decay can be modified by driving the $s - e$ transition with an external driving field and an appropriately chosen time-dependent Rabi coupling $\Omega(t)$ (see Figure 1.1b).

We also point out, that the mapping between symmetric Dicke states and photonic states can be generalized to orthogonal modes, e.g., different polarization modes. For this, we require a more complex level scheme of the emitters and two orthogonal guided modes of the waveguide, e.g., left and right polarized photonic modes $a_{\mathrm{L(R)}k}$ which couple to the optical transitions $g - e_{\mathrm{L(R)}}$ (see Figure 1.1c). Because these modes are orthogonal, a symmetric Dicke state over two modes in the low excitation regime $m, n \ll N$ maps to a product of photonic states in the different polarizations,

$$|\psi_{m,n}\rangle \propto S_{e_{\mathrm{L}}g}^m S_{e_{\mathrm{R}}g}^n |g\rangle^{\otimes N} \longrightarrow |\phi_m^{\mathrm{L}}\rangle |\phi_n^{\mathrm{R}}\rangle \tag{1.12a}$$

$$|\phi_m^{\mathrm{L/R}}\rangle = \int \frac{\mathrm{d}k_1}{2\pi} \cdots \int \frac{\mathrm{d}k_m}{2\pi} \frac{A_{\{k\}} \mathrm{e}^{-\mathrm{i}\sum \omega_{k_j} t}}{m!} a_{\mathrm{L/R}k_1}^\dagger a_{\mathrm{L/R}k_2}^\dagger \cdots a_{\mathrm{L/R}k_m}^\dagger |\mathrm{vac}\rangle, \tag{1.12b}$$

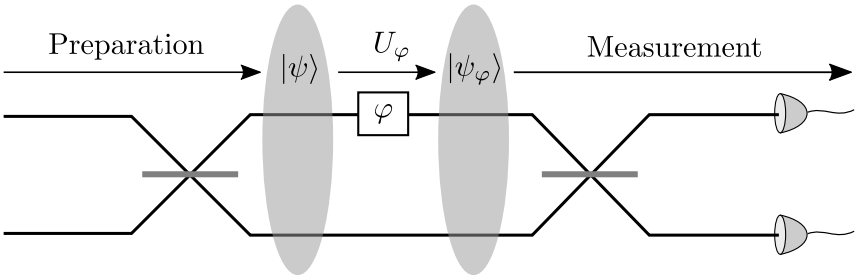

Figure 1.2: In general an optical interferometer has a preparation step before the phase φ is acquired. With an appropriate measurement on $|\psi_\varphi\rangle$ one can then measure the phase shift φ. In a Mach-Zehnder Interferometer, the preparation step is a beamsplitter transformation and the measurement e.g., an intensity measurement after passing through another beamsplitter.

To prove this, we use the fact that the collective operators $O_{\mathrm{R/L}} = \sqrt{\Gamma_{1\mathrm{d}}} S_{ge_{\mathrm{R/L}}}$ satisfy $O_{\mathrm{R}} O_{\mathrm{L}} |\psi_m\rangle \approx O_{\mathrm{L}} O_{\mathrm{R}} |\psi_m\rangle$ in the low excitation regime. Therefore, the correlation function and consequently the final state factorizes,

$$\langle \psi_{0,0} | O_{\mathrm{L}}(s_1) O_{\mathrm{R}}(s_2) O_{\mathrm{L}}(s_3) \cdots | \psi_{m,n} \rangle \approx \langle \psi_0 | O_{\mathrm{L}}(s_1) O_{\mathrm{L}}(s_3) \cdots | \psi_m \rangle \langle \psi_0 | O_{\mathrm{R}}(s_2) \cdots | \psi_n \rangle .$$

This type of mapping can be useful to generate entangled photon states in two orthogonal modes like NOON-states and Yurke states.

1.3 Multi-Mode States for Quantum Metrology

One reason why photonic states are of interest is their value for quantum metrology [11] in optical setups [19]. In most cases, the quantity to be estimated can be mapped to a phase φ, that the photons acquire during some interaction time. Often one considers a Mach-Zehnder-Interferometer (MZI) as depicted in Figure 1.2. The phase sensitivity of the classical MZI is limited by the shot-noise limit (SL), also known as the Standard Quantum Limit, $(\Delta\varphi)_{\mathrm{SL}} = 1/\sqrt{M}$, where M are the number of resources, e.g., the number of photons. Nonclassical input states can overcome this limit and even reach the Heisenberg limit (HL) of $(\Delta\varphi)_{\mathrm{HL}} = 1/M$.

In this section we first discuss some basic concepts of quantum optical interferometry (Section 1.3.1). Then, we derive a lower bound for the phase sensitivity $\Delta\varphi$ for general multi-mode states (Section 1.3.2), and show that with a parity measurement one can reach this bound (Section 1.3.3). Moreover, we use our particular multi-mode states to show that these can beat the SL and perform only slightly worse than the single-mode states (Section 1.3.4). Finally, we discuss the effect of decoherence during the emission process on the phase sensitivity (Section 1.3.5).

1.3.1 Basic Concepts in Quantum Metrology

The variance of the phase measurement depends on the quantum state ρ used as a resource and the measurement scheme that is chosen. The Quantum Cramér-Rao Bound (QCRB) [146, 147] gives a lower bound for the variance for all choices of measurements and only depends on the quantum state $\rho_\varphi = U_\varphi \rho U_\varphi^\dagger$ after the phase has been acquired, which is described by the unitary U_φ. The QCRB states

$$(\Delta\varphi)^2 \geq \frac{1}{\nu F_Q[\rho_\varphi]}, \tag{1.13}$$

where ν denotes the number of repetitions and $F_Q[\rho_\varphi]$ is the Fisher Information of the state ρ_φ. One can always construct a measurement scheme to attain this bound [148], but it might not be realizable easily in an experimental setup. The Fisher Information for pure states $\rho_\varphi = |\psi_\varphi\rangle\langle\psi_\varphi|$ is given by [19]

$$F_Q[|\psi_\varphi\rangle\langle\psi_\varphi|] = 4\left(\langle\dot{\psi}_\varphi|\dot{\psi}_\varphi\rangle - |\langle\dot{\psi}_\varphi|\psi_\varphi\rangle|^2\right), \tag{1.14}$$

where $|\dot{\psi}_\varphi\rangle = \partial_\varphi|\psi_\varphi\rangle$.

For single-mode states the phase variance has been thoroughly studied [19]. In this case, the interferometer can be described with the help of the group SU(2) and group theoretical arguments can be used to calculate the Fisher Information and find optimal states [149]. Single-mode NOON-states $|\psi\rangle = \frac{1}{\sqrt{2}}\left(|\phi_M^{\mathrm{SM}}, 0\rangle + |0, \phi_M^{\mathrm{SM}}\rangle\right)$ reach the HL as their Fisher Information can be calculated to be $F_Q = M^2$. However, these states are difficult to prepare. An alternative are the so-called twin-Fock states that have passed through a 50:50-beamsplitter, i.e. $|\psi\rangle = U_{\mathrm{BS}}|\phi_m^{\mathrm{SM}}, \phi_m^{\mathrm{SM}}\rangle$, where now the number of resources is $M = 2m$. These states have a Fisher Information of $F_Q = 2m(m+1) = M(M+2)/2$ which shows the same scaling as the HL for large photon numbers $m \gg 1$.

The experimentally observed phase variance also depends on the measurement that is performed on the state $|\psi_\varphi\rangle$. Typical measurement schemes include intensity measurements at the output ports of the MZI, photon number resolving measurements and parity measurements. A measurement scheme, that reaches the QCRB, for these two states (and an even wider class of so-called path-symmetric states) is a photon number resolving measurement [150]. For this measurement scheme the QCRB is attained for any phase φ, but it may be difficult to implement such a photon number resolving detector. Parity measurements of the photon number are a simpler measurement scheme, even though they too are difficult to implement experimentally. We refer to Section 0.2.4 for a short overview over current photon detection techniques. With parity measurements one can also attain the QCRB for the NOON-state and twin-Fock state (and an even wider class of states) around particular values of the phase φ [110]. Even though the phase can only be approximated very well locally (with HL-scaling), the simpler measurement scheme can yield an advantage.

1.3.2 Quantum Fisher Information of Multi-Mode States

The open question is how these results change when we consider multi-mode states as one obtains, e.g., from the emission of a chain of atoms as described in Section 1.2. On the one hand, we have shown that in the low excitation regime $m \ll N$ the emitted photonic state behaves like a single-mode state and we provide protocols for the preparation of collective states that can generate Fock states and NOON-states in Chapter 2. On the other hand, by exciting all emitters of the chain and letting them decay, a multi-mode state of N photons is generated. We now study the phase variance of arbitrary multi-mode twin-Fock states at the QCRB.

For this purpose, we assume the phase to be independent of the momenta k over the relevant range, such that $U_\varphi = \exp\left[-\mathrm{i}\varphi \int \frac{\mathrm{d}k}{2\pi} a_k^\dagger a_k\right]$. We also assume that the two Fock states arrive at the beamsplitter at the same time, so that we can ignore the time-dependence in the input states of the form

$$|\phi_m\rangle = \int \frac{\mathrm{d}k_1}{2\pi} \cdots \int \frac{\mathrm{d}k_m}{2\pi} \frac{A_{\{k\}}}{m!} a_{k_1}^\dagger a_{k_2}^\dagger \dots a_{k_m}^\dagger |\mathrm{vac}\rangle. \tag{1.15}$$

Furthermore, we assume here that spontaneous emission processes can be neglected, i.e. $\Gamma^* = 0$, such that $|\phi_m\rangle$ is normalized. We discuss the effect of decoherence during the emission process in Section 1.3.5.

The states after the first beamsplitter and the phase operation, $|\psi_\varphi\rangle = U_\varphi U_{\mathrm{BS}} |\phi_m, \phi_m\rangle$, with operators a_k (b_k) in the first (second) arm of the interferometer, can be expressed in terms of the operators

$$c_k^\dagger(\varphi) = U_\varphi U_{\mathrm{BS}} a_k U_{\mathrm{BS}}^\dagger U_\varphi^\dagger = \frac{1}{\sqrt{2}} \left(a_k^\dagger + \mathrm{e}^{-\mathrm{i}\varphi} b_k^\dagger\right), \tag{1.16a}$$

$$d_k^\dagger(\varphi) = U_\varphi U_{\mathrm{BS}} b_k U_{\mathrm{BS}}^\dagger U_\varphi^\dagger = \frac{1}{\sqrt{2}} \left(-a_k^\dagger + \mathrm{e}^{-\mathrm{i}\varphi} b_k^\dagger\right). \tag{1.16b}$$

To separate the original a_k and b_k modes we give the former odd indices and the latter even indices and introduce the shorthand notation $A_{k,13\cdots 2m-1} = A_{k_1 k_3 \cdots k_{2m-1}}$. With these definitions,

$$\begin{aligned} |\psi_\varphi\rangle = \int \frac{\mathrm{d}k_1}{2\pi} \cdots \int \frac{\mathrm{d}k_{2m}}{2\pi} A_{k,13\cdots 2m-1} A_{k,24\cdots 2m} \frac{1}{m!^2} \\ \times c_{k_1}^\dagger(\varphi) \cdots c_{k_{2m-1}}^\dagger(\varphi) d_{k_2}^\dagger(\varphi) \cdots d_{k_{2m}}^\dagger(\varphi) |\mathrm{vac}\rangle. \end{aligned} \tag{1.17}$$

Before we go on to the evaluation of the Fisher Information, let us first check the normalization of the state to introduce some methods used later. The main tool is Wick's theorem [151] with which we can reduce a correlation function of many bosonic operators to a product of commutators. As a small example take

$$\begin{aligned} \langle \mathrm{vac}| c_{p_1} d_{p_2} c_{k_1}^\dagger d_{k_2}^\dagger |\mathrm{vac}\rangle &= \langle \mathrm{vac}| \overbrace{c_{p_1} d_{p_2} c_{k_1}^\dagger} d_{k_2}^\dagger |\mathrm{vac}\rangle + \langle \mathrm{vac}| \overbrace{c_{p_1} d_{p_2} c_{k_1}^\dagger} d_{k_2}^\dagger |\mathrm{vac}\rangle \\ &= \left[c_{p_1}, c_{k_1}^\dagger\right] \left[d_{p_2}, d_{k_2}^\dagger\right] + \left[c_{p_1}, d_{k_2}^\dagger\right] \left[d_{p_2}, c_{k_1}^\dagger\right]. \end{aligned} \tag{1.18}$$

The brackets above the operators (similar to Wick's contractions) depict the different ways in which the annihilation and creation operators can be connected in a nonvanishing manner. Because the commutator between to bosonic annihilation and creation operators commute with all other operators, the correlation function reduces to a product of all these commutators. This motivates the importance of the commutators between the $c_k(\varphi)$ and $d_k(\varphi)$, for which we find

$$\left[c_p(\varphi), c_k^\dagger(\varphi)\right] = \left[d_p(\varphi), d_k^\dagger(\varphi)\right] = 2\pi\delta(p-k), \tag{1.19a}$$

$$\left[c_p(\varphi), d_k^\dagger(\varphi)\right] = \left[d_p(\varphi), c_k^\dagger(\varphi)\right] = 0. \tag{1.19b}$$

The normalization of the state is then (omitting the phase dependence and writing $c_k(\varphi) = c_k$ for a more compact notation)

$$\begin{aligned}\langle\psi_\varphi|\psi_\varphi\rangle = &\int \frac{\mathrm{d}p_1}{2\pi}\cdots\int\frac{\mathrm{d}p_{2m}}{2\pi}\int\frac{\mathrm{d}k_1}{2\pi}\cdots\int\frac{\mathrm{d}k_{2m}}{2\pi}A^*_{p,13\cdots}A^*_{p,24\cdots}A_{k,13\cdots}A_{k,24\cdots}\frac{1}{m!^4}\\ &\times\langle\mathrm{vac}|\overbrace{d_{p_{2m}}\cdots\overbrace{d_{p_2}\overbrace{c_{p_{2m-1}}\cdots\overbrace{c_{p_1}c^\dagger_{k_1}}\cdots c^\dagger_{k_{2m-1}}}d^\dagger_{k_2}}\cdots d^\dagger_{k_{2m}}}^{}|\mathrm{vac}\rangle,\end{aligned} \tag{1.20}$$

where we can just take the commutator between p_i and k_i without loss of generality because of the symmetry of $A_{\{k\}}$ under exchange of indices. This yields a factor of $m!$ within the c's and d's each. Thus, the state is normalized,

$$\langle\psi_\varphi|\psi_\varphi\rangle = \int\frac{\mathrm{d}k_1}{2\pi}\cdots\int\frac{\mathrm{d}k_{2m}}{2\pi}|A_{k,13\cdots}|^2|A_{k,24\cdots}|^2\frac{1}{m!^2} = |\langle\phi_m|\phi_m\rangle|^4 = 1. \tag{1.21}$$

Returning to the evaluation of the Fisher Information, one needs to take the derivative of the state with respect to the phase,

$$\begin{aligned}|\dot\psi_\varphi\rangle = \frac{-\mathrm{i}\mathrm{e}^{-\mathrm{i}\varphi}}{\sqrt{2}}&\int\frac{\mathrm{d}k_1}{2\pi}\cdots\int\frac{\mathrm{d}k_{2m}}{2\pi}A_{k,13\cdots2m-1}A_{k,24\cdots2m}\frac{m}{m!^2}\\ &\times\left(b^\dagger_{k_1}c^\dagger_{k_3}\cdots c^\dagger_{k_{2m-1}}d^\dagger_{k_2}\cdots d^\dagger_{k_{2m}} + c^\dagger_{k_1}\cdots c^\dagger_{k_{2m-1}}b^\dagger_{k_2}d^\dagger_{k_4}\cdots d^\dagger_{k_{2m}}\right)|\mathrm{vac}\rangle,\end{aligned} \tag{1.22}$$

where we have not explicitly written the phase dependence of the operators c_k and d_k. Due to the symmetry of $A_{\{k\}}$ we have taken the derivative only in c_{k_1} and d_{k_2} together with a factor of m. The Fisher Information can then be evaluated in analogy to the calculation of the norm, where the main difference is that due to the b operators the even and odd modes can mix because $\left[b_p, c_k^\dagger\right] = \left[b_p, d_k^\dagger\right] = 2\pi\delta(p-k)\frac{1}{\sqrt{2}}\mathrm{e}^{-\mathrm{i}\varphi}$. The calculation yields (see Appendix 1.B)

$$\langle\dot\psi_\varphi|\dot\psi_\varphi\rangle = \frac{1}{2}\left((2m^2+m)I_m^{(0)} + m^2 I_m^{(1)}\right), \tag{1.23a}$$

$$|\langle\dot\psi_\varphi|\psi_\varphi\rangle| = mI_m^{(0)}, \tag{1.23b}$$

where we have introduced the integrals $I_m^{(l)}$ in which l indices of $A_{k,1\cdots}$ have been exchanged with the ones from $A_{k,2\cdots}$, i.e. in particular

$$I_m^{(0)} = \int \frac{\mathrm{d}k_1}{2\pi} \cdots \int \frac{\mathrm{d}k_{2m}}{2\pi} |A_{k,13\cdots 2m-1}|^2 |A_{k,24\cdots 2m}|^2 \frac{1}{m!^2} = 1, \tag{1.24a}$$

$$I_m^{(1)} = \int \frac{\mathrm{d}k_1}{2\pi} \cdots \int \frac{\mathrm{d}k_{2m}}{2\pi} A^*_{k,13\cdots 2m-1} A^*_{k,24\cdots 2m} A_{k,23\cdots 2m-1} A_{k,14\cdots 2m} \frac{1}{m!^2}. \tag{1.24b}$$

These quantities can be shown to be real by complex conjugating and exchanging of integration variables.

The Fisher Information of the multi-mode states,

$$F_Q[|\psi_\varphi\rangle\langle\psi_\varphi|] = 4\left(\langle\dot{\psi}_\varphi|\dot{\psi}_\varphi\rangle - |\langle\dot{\psi}_\varphi|\psi_\varphi\rangle|^2\right) = 2m(mI_m^{(1)} + 1), \tag{1.25}$$

then shows a Heisenberg-like scaling if $I_m^{(1)}$ is approaching a constant for large m. As we show in Section 1.3.4 this is true for the emitted state from a fully excited chain of atoms. We point out, that the single-mode result with $I_m^{(1)} = 1$ is recovered straightforwardly because of the product structure of the coefficient, $A_{k,13\cdots} = \sqrt{m!} A_{k_1} A_{k_3} \cdots$.

1.3.3 Phase Variance for a Parity Measurement

We now show that a parity measurement after the second beamsplitter transformation of the MZI locally resolves the phase at the Heisenberg limit. The measurement operator can be written as $O = U_{\mathrm{BS}}^\dagger (-1)^{\int \frac{\mathrm{d}k}{2\pi} a_k^\dagger a_k} U_{\mathrm{BS}}$, where the beamsplitter transformation is generated by $\int \frac{\mathrm{d}k}{2\pi} \mathrm{i}(a_k^\dagger b_k - b_k^\dagger a_k)\pi/4$, such that

$$O = \prod_k \mathrm{e}^{-(a_k^\dagger b_k - b_k^\dagger a_k)\pi/4} \mathrm{e}^{\mathrm{i}\pi a_k^\dagger a_k} \mathrm{e}^{(a_k^\dagger b_k - b_k^\dagger a_k)\pi/4} = \prod_k \mathrm{e}^{\mathrm{i}(a_k^\dagger - b_k^\dagger)(a_k - b_k)\pi/2}. \tag{1.26}$$

We used the transformation $U_{\mathrm{BS}}^\dagger a_k^\dagger U_{\mathrm{BS}} = \frac{1}{\sqrt{2}}\left(a_k^\dagger - b_k^\dagger\right)$. Because $O^2 = 1$ and the variance of the measurement $\Delta O^2 = \langle O^2\rangle - \langle O\rangle^2$, the phase variance around $\varphi \approx 0$,

$$\Delta\varphi^2 = \lim_{\varphi\to 0} \frac{\Delta O^2}{(\partial_\varphi \langle O\rangle)^2} = \lim_{\varphi\to 0} \frac{1 - \langle O\rangle^2}{(\partial_\varphi \langle O\rangle)^2}, \tag{1.27}$$

only depends on the expectation value $\langle O\rangle = \langle\psi_\varphi|O|\psi_\varphi\rangle$.

This expectation value can be evaluated by using the transformations $O(a^\dagger \pm b^\dagger)O^\dagger = \pm(a^\dagger \pm b^\dagger)$, and therefore $O c_k^\dagger(\varphi) O^\dagger = \mathrm{e}^{-\mathrm{i}\varphi} c_k^\dagger(-\varphi)$ and $O d_k^\dagger(\varphi) O^\dagger = -\mathrm{e}^{-\mathrm{i}\varphi} d_k^\dagger(-\varphi)$. The expectation value

$$\begin{aligned}\langle O\rangle = &\int \frac{\mathrm{d}p_1}{2\pi} \cdots \int \frac{\mathrm{d}p_{2m}}{2\pi} \int \frac{\mathrm{d}k_1}{2\pi} \cdots \int \frac{\mathrm{d}k_{2m}}{2\pi} A^*_{p,1\cdots} A^*_{p,2\cdots} A_{k,1\cdots} A_{k,2\cdots} \frac{1}{m!^4} \mathrm{e}^{-\mathrm{i}2m\varphi} \\ &\times \langle \mathrm{vac}| d_{p_{2m}}(\varphi) \cdots c_{p_1}(\varphi) c_{k_1}^\dagger(-\varphi) \cdots d_{k_{2m}}^\dagger(-\varphi)|\mathrm{vac}\rangle,\end{aligned} \tag{1.28}$$

can then be further evaluated by using the commutation relations

$$\left[c_p(\varphi), c_k^\dagger(-\varphi)\right] = \left[d_p(\varphi), d_k^\dagger(-\varphi)\right] = 2\pi\delta(p-k)\mathrm{e}^{\mathrm{i}\varphi}\cos\varphi, \tag{1.29a}$$

$$\left[c_p(\varphi), d_k^\dagger(-\varphi)\right] = \left[d_p(\varphi), c_k^\dagger(-\varphi)\right] = 2\pi\delta(p-k)(-\mathrm{i})\mathrm{e}^{\mathrm{i}\varphi}\sin\varphi. \tag{1.29b}$$

Because the commutators between c_k and d_k don't vanish, all indices can become mixed and the expectation value yields

$$\langle O\rangle = \sum_{l=0}^{m}(-1)^l \sin^{2l}(\varphi)\cos^{2(m-l)}(\varphi)\binom{m}{l}^2 I_m^{(l)}, \tag{1.30}$$

where the integrals $I_m^{(l)}$ are the natural extension of Equation 1.24. We note, that $I_j^{(l)} = I_{m-j}^{(l)}$ such that one can reduce the number of calculations if they are necessary.

By observing that $\partial_\varphi\langle O\rangle\big|_{\varphi=0} = 0$ and $\langle O\rangle_{\varphi=0} = I_m^{(0)} = 1$, the variance of the measured phase can be calculated from the second derivative $\partial_\varphi^2\langle O\rangle$ as

$$\Delta\varphi^2 = \lim_{\varphi\to 0}\frac{1-\langle O\rangle^2}{(\partial_\varphi\langle O\rangle)^2} = \lim_{\varphi\to 0}\frac{-2\langle O\rangle\partial_\varphi\langle O\rangle}{2\partial_\varphi\langle O\rangle\partial_\varphi^2\langle O\rangle} = \left(-\partial_\varphi^2\langle O\rangle\big|_0\right)^{-1}. \tag{1.31}$$

The second derivative around $\varphi \approx 0$ only depends on the first two terms of Equation 1.30 because all sine-terms vanish when taking the limit $\varphi \to 0$. We find $-\partial_\varphi^2\langle O\rangle\big|_0 = 2m(mI_m^{(1)} + I_m^{(0)})$ and therefore, we reach the QCRB locally around $\varphi \approx 0$,

$$\Delta\varphi^2\big|_{\varphi\approx 0} = \frac{1}{2m(mI_m^{(1)}+1)} = \frac{1}{F_Q[|\psi_\varphi\rangle\langle\psi_\varphi|]}. \tag{1.32}$$

We note, that for single-mode states $I_m^{(l)} = 1$ holds, which leads to the result derived in Reference [152]. In that case, the expectation value $\langle O\rangle = P_m[\cos 2\varphi]$ can be expressed in terms of Legendre Polynomials P_m and the second derivative $-\partial_\varphi^2\langle O\rangle\big|_0 = 4P'_m[1]$ is calculated with the help of the well-known result $P'_m[1] = m(m+1)/2$.

1.3.4 Evaluation for the Maximal Symmetric Dicke State

For specific coefficients $A_{\{k\}}$ one can evaluate the integrals $I_m^{(l)}$ efficiently. For single-mode states, that is, when the coefficients can be written as a product $A_{k,13\ldots} = \sqrt{m!}A_{k_1}A_{k_2}\cdots$, one can show $I_m^{(l)} = 1$ for all l. In the following we focus on the calculation of $I_m^{(1)}$ as this determines the scaling of the Fisher Information and therefore the minimal phase variance.

The evaluation of the integral $I_m^{(1)}$ for arbitrary multi-mode states may be difficult. However, due to the origin of the coefficients from exponential decay of a chain of emitters, one can evaluate the integral through a recurrence relation. To obtain this recurrence

relation, we substitute the coefficients $A_{\{k\}}$ in $I_m^{(1)}$ by their expression as time ordered correlation functions as in Equation 1.3. The integral over the wavevectors is then replaced by a time integral,

$$I_m^{(1)} = \frac{1}{m!^2}\int_0^\infty \mathrm{d}t_1 \cdots \int_0^\infty \mathrm{d}t_{2m} \mathcal{T}\langle \mathrm{vac}|O_1 O_3 \cdots O_{2m-1}|\psi_m\rangle^* \langle \mathrm{vac}|O_2 O_4 \cdots O_{2m}|\psi_m\rangle^* \\ \times \langle \mathrm{vac}|O_2 O_3 \cdots O_{2m-1}|\psi_m\rangle \langle \mathrm{vac}|O_1 O_4 \cdots O_{2m}|\psi_m\rangle. \quad (1.33)$$

For a more compact notation, we have defined $O_i \equiv O(t_i) = \sqrt{\Gamma_{1\mathrm{d}}}\mathrm{e}^{\mathrm{i}H_{\mathrm{eff}}t_i} S_{ge} \mathrm{e}^{-\mathrm{i}H_{\mathrm{eff}}t_i}$ with H_{eff} as defined in Equation 0.8. Notice, that in the correlation functions two indices (1 and 2) are exchanged, in analogy with the expressions in momentum space, and that the integral is symmetric with respect to the remaining even (odd) indices.

The integral can be evaluated recursively by picking a time ordering and integrating over the latest time $t_i \geq \max_{j\neq i} t_j \equiv T$, and repeating this step on the next integral. The exponential decay then gives rise to the simple form of $\int_T^\infty \mathrm{d}t_i\ \mathrm{e}^{-ct_i} = \frac{1}{c}\mathrm{e}^{-cT}$ if $\mathrm{Re}(c) > 0$. Using these results, we can define three structurally different integrals, depending on whether one has already integrated over one or both of the special (i.e., exchanged) indices t_1 and t_2,

$$F_{ij}^{(2)} = \int \Big\{\mathrm{d}t_n\Big\} \mathcal{T}\mathrm{e}^{-c_{ij}^{(2)} \max t_n} \langle \psi_{m-1-i}|O_1 \cdots O_{2i+1}|\psi_m\rangle^* \langle \psi_{m-1-j}|O_2 \cdots O_{2j+2}|\psi_m\rangle^* \\ \times \langle \psi_{m-1-i}|O_2 O_3 \cdots O_{2i+1}|\psi_m\rangle \langle \psi_{m-1-j}|O_1 O_4 \cdots O_{2j+2}|\psi_m\rangle, \quad (1.34a)$$

$$F_{ij}^{(1)} = \int \Big\{\mathrm{d}t_n\Big\} \mathcal{T}\mathrm{e}^{-c_{ij}^{(1)} \max t_n} \langle \psi_{m-1-i}|O_1 O_3 \cdots O_{2i+1}|\psi_m\rangle^* \langle \psi_{m-j}|O_4 \cdots O_{2j+2}|\psi_m\rangle^* \\ \times \langle \psi_{m-i}|O_3 \cdots O_{2i+1}|\psi_m\rangle \langle \psi_{m-1-j}|O_1 O_4 \cdots O_{2j+2}|\psi_m\rangle, \quad (1.34b)$$

$$F_{ij}^{(0)} = \int \Big\{\mathrm{d}t_n\Big\} \mathcal{T}\mathrm{e}^{-c_{ij}^{(0)} \max t_n} \langle \psi_{m-i}|O_3 \cdots O_{2i+1}|\psi_m\rangle^* \langle \psi_{m-j}|O_4 \cdots O_{2j+2}|\psi_m\rangle^* \\ \times \langle \psi_{m-i}|O_3 \cdots O_{2i+1}|\psi_m\rangle \langle \psi_{m-j}|O_4 \cdots O_{2j+2}|\psi_m\rangle. \quad (1.34c)$$

The integrals only run over the remaining time variables $\{t_n\}$ and we have introduced the exponents $c_{ij}^{(2)} = \gamma_{m-1-i} + \gamma_{m-1-j}$, $c_{ij}^{(0)} = \gamma_{m-i} + \gamma_{m-j}$, and $c_{ij}^{(1)} = (c_{ij}^{(2)} + c_{ij}^{(0)})/2$. Recall that the decay rates are given by $\gamma_j = j(N-j+1)\Gamma_{1\mathrm{d}}$. Note that these integrals always converge because $c_{ij}^{(2/1/0)} > 0$.

By integrating over the latest time, one can remove one operator O_i from the above expressions until one ends up with $F_{00}^{(0)} = 1$. This motivates the fact that the integral

$$I_m^{(1)} = \frac{1}{m!^2} F_{m-1,m-1}^{(2)} \quad (1.35)$$

can be evaluated by a recurrence relation (see also Figure 1.3). Let us understand the structure of the recurrence relation on the example of $F_{ij}^{(2)}$. If the largest time is one with a regular odd index (for which there are i possibilities), we take without loss of generality t_{2i+1} and use the fact that

$$\langle \psi_{m-1-i}|O_{2i+1} = \sqrt{\gamma_{m-i}}\mathrm{e}^{-(\gamma_{m-i}-\gamma_{m-i-1})t_{2i+1}/2} \langle \psi_{m-1-i}|. \quad (1.36)$$

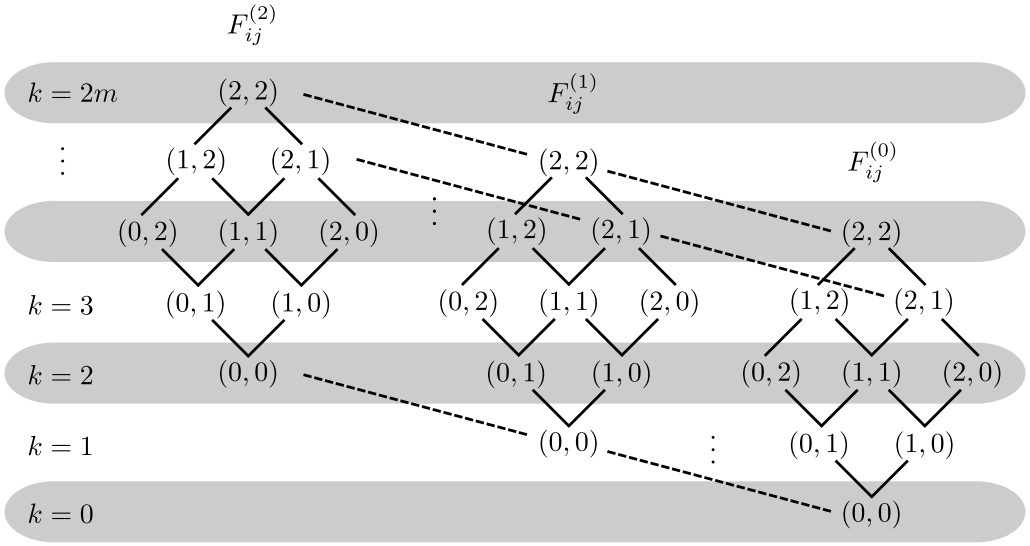

Figure 1.3: The recurrence relation of $F_{ij}^{(2/1/0)}$ to calculate $I_m^{(1)}$ can be represented pictorially, here on the example of $m = 3$. The solid lines represent the terms of the recurrence relation in between every group $F^{(n)} \to F^{(n)}$, whereas the dashed lines correspond to the terms $F^{(2)} \to F^{(1)}$ and $F^{(1)} \to F^{(0)}$. By grouping the elements in terms of the number of excitations, or equivalently the number of remaining time integrals, one can evaluate the recurrence relation efficiently.

This term appears twice such that the integral gives a prefactor $\frac{\gamma_{m-i}}{c_{ij}^{(2)}+(\gamma_{m-i}-\gamma_{m-i-1})} = \frac{\gamma_{m-i}}{c_{i-1,j}^{(2)}}$. The remaining integral is then of the form $F_{i-1,j}^{(2)}$. The same considerations apply if the largest time is one with a regular even index. In contrast, if the largest time is t_2 (or equivalently t_1), then after the integration over this variable, the remaining integral is of the form $F_{ij}^{(1)}$. By carefully calculating all these steps, we find the recurrence relation

$$F_{ij}^{(2)} = i\frac{\gamma_{m-i}}{c_{i-1,j}^{(2)}} F_{i-1,j}^{(2)} + j\frac{\gamma_{m-j}}{c_{i,j-1}^{(2)}} F_{i,j-1}^{(2)} + 2\frac{\sqrt{\gamma_{m-i}\gamma_{m-j}}}{c_{i,j}^{(1)}} F_{i,j}^{(1)}, \tag{1.37a}$$

$$F_{ij}^{(1)} = i\frac{\sqrt{\gamma_{m-i}\gamma_{m-i+1}}}{c_{i-1,j}^{(1)}} F_{i-1,j}^{(1)} + j\frac{\sqrt{\gamma_{m-j}\gamma_{m-j+1}}}{c_{i,j-1}^{(1)}} F_{i,j-1}^{(1)} + \frac{\sqrt{\gamma_{m-i}\gamma_{m-j}}}{c_{i,j}^{(0)}} F_{i,j}^{(0)}, \tag{1.37b}$$

$$F_{ij}^{(0)} = i\frac{\gamma_{m-i+1}}{c_{i-1,j}^{(0)}} F_{i-1,j}^{(0)} + j\frac{\gamma_{m-j+1}}{c_{i,j-1}^{(0)}} F_{i,j-1}^{(0)}, \tag{1.37c}$$

$$F_{00}^{(0)} = 1. \tag{1.37d}$$

The trick to evaluating this recurrence relation efficiently is to group elements of the same excitation subspace $0 \leq k \leq 2m$ as in Figure 1.3. Elements of this subspace are, for example, $F_{ij}^{(2)}$ satisfying $i + j + 2 = k$ and $0 \leq i, j \leq m - 1$. By applying one recursive step starting from $k = 0$, in which only $F_{00}^{(0)} = 1$ lies, one moves to a subspace with one excitation more $k \to k + 1$ until $k = 2m$ is reached. This subspace only contains the desired term $F_{m-1,m-1}^{(2)}$. For better numerical results it is also recommendable to remove the factors of i and j by substituting $F_{ij}^{(n)} = i!j!\tilde{F}_{ij}^{(n)}$.

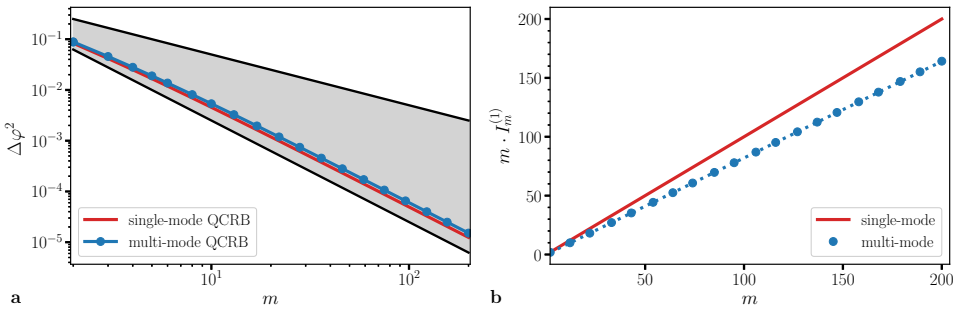

Figure 1.4: **a** The QCRB bound for single-mode twin-Fock states (red line) has the same scaling with m^{-2} in the number of photons used as the Heisenberg limit (lower black line). The bound for the multi-mode twin-Fock states generated by a chain of quantum emitters in the atomic mirror configuration has a larger variance in the measured phase (blue dots) but still beats the Standard Quantum Limit (upper black line). **b** This behavior relies on the fact that the integral $mI_m^{(1)}$ (blue dots) is not a constant in m but is approximated by a linear function $0.82m$ (blue dashed line). For the single-mode case one obtains $mI_m^{(1)} = m$ (red line).

Let us first look at the expression for two photons. Through the recurrence relation (alternatively by direct evaluation of the integrals) we find

$$I_{m=2}^{(1)} = \frac{\gamma_2(10\gamma_1 + \gamma_2)}{2(\gamma_1 + \gamma_2)(2\gamma_1 + \gamma_2)}. \tag{1.38}$$

If the number of atoms in the chain is very large $N \gg m = 2$, one finds $I_2^{(1)} = 1 - \frac{1}{6N^2} + \mathcal{O}(N^{-3})$ as expected for states close to a single-mode state. If the chain only contains two emitters, which are both excited and left to decay to a two photon multi-mode state ($N = m = 2$), we obtain $I_2^{(1)} = 11/12 < 1$. Even though this is smaller than one, it leads to a scaling better than the SL.

We now focus on the scaling of $I_m^{(1)}$ when the number of emitters equals the number of excitations, i.e. $N = m$. On the one hand, we consider this state because exciting all emitters to $|e\rangle^{\otimes N}$ is conceptually straightforward to implement by transferring the population from g to e in every emitter independently. During the decay, this state generates the photonic state $|\phi_m\rangle$. On the other hand, the emitted state is far away from being in a single mode, so that we expect the largest deviations from the single-mode result $I_m^{(1)} = 1$. We calculated $I_m^{(1)}$ by evaluating the recurrence relation of Equation 1.34 numerically and found that the QCRB for this multi-mode state is very close to the bound for single-mode states (see Figure 1.4a). This is due to the fact the integral is approximately constant, $I_m^{(1)} \approx 0.82$, for the photon numbers $m \lesssim 2 \cdot 10^3$ for which we were able to calculate the integral numerically.

One can prove that these multi-mode states perform at least as good as the SL. This originates in the fact that the integrals are strictly positive, in particular $F_{m-1,m-1}^{(2)} > 0$. However, this does not imply that the scaling with m is necessarily better than the SL. For claiming a better scaling than the SL, one needs to show that $mI_m^{(1)}$ does not approach

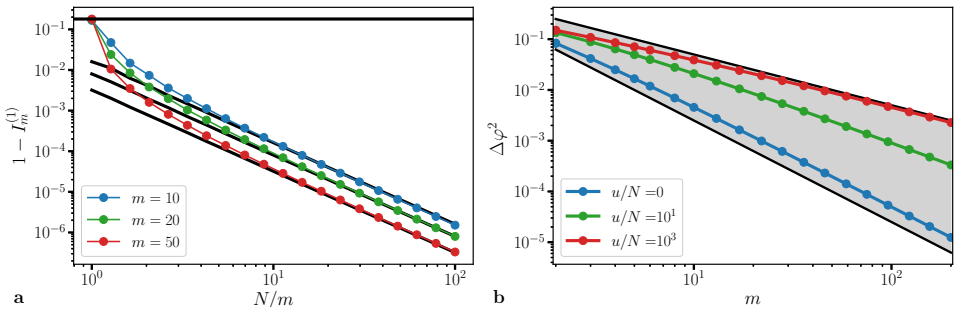

Figure 1.5: **a** $I_m^{(1)}$ approaches the single-mode value of $I_m^{(1)} = 1$ when the number of emitters N with respect to the excitation number m in the Dicke states $|\psi_m\rangle$ is increased. For $N/m = 1$ the value of approximately 0.82 (black horizontal line) is attained and for large ratios, the deviations from the single-mode result vanish as in Equation 1.39 (black lines). **b** When a nonlinearity u is introduced in the system, the phase resolution changes from a HL-scaling for vanishing nonlinearity u to the SL-scaling when the nonlinearity u is large, that is when the photons become distinguishable.

a constant. The fact that we found that $I_m^{(1)}$ approaches a constant, and therefore, $mI_m^{(1)}$ scales linearly (see Figure 1.4b), leads to the conclusion that one can reach a scaling similar to the HL with multi-mode states. It is still an open question whether an analytical proof of this behavior can be found.

We emphasize, that we have checked numerically that the integral approaches the single-mode value when the number of atoms is much larger than the number of excitations (see Figure 1.5a). In particular, the deviations for large atom numbers N scale as

$$I_m^{(1)} \sim 1 - 0.16\frac{m}{N^2}. \tag{1.39}$$

Furthermore, the recurrence relation can be generalized to any effective Hamiltonian diagonal in the Dicke basis, i.e., satisfying $H_{\text{eff}}|\psi_m\rangle = \lambda_m|\psi_m\rangle$ with $\text{Im}(\lambda_m) < 0$. The decay operators then typically satisfy $O|\psi_j\rangle = \sqrt{\gamma_j}|\psi_{j-1}\rangle$, where $\gamma_j = -\text{Im}(\lambda_m)$. The recurrence relation is then slightly modified (see Appendix 1.C). This generalization is useful to show certain limits. For example, a large nonlinearity u in the frequency, $\text{Re}(\lambda_m) = m\Delta + um(m-1)$ implies that the emitted photons become distinguishable. Therefore, the quantum enhancement will be lost and the phase can only be measured at SL precision, which we also see numerically in Figure 1.5b.

1.3.5 Effect of Decoherence during Emission

We close the discussion on the capabilities of multi-mode states in quantum metrology with some results on the effect of decoherence. Here, we consider only decoherence during the emission process because the effect of decoherence processes inside the interferometer has been covered in many prior works [19] – although not necessarily for multi-mode states.

In general, the state that is emitted by a chain of emitters in the atomic mirror con-

figuration, $|\Phi_m\rangle = |\phi_m\rangle + |\phi_m^*\rangle$, has a part with m guided photons in the waveguide and a part where some of the excitations have decayed spontaneously and emitted a photon into free space. The photonic state at each of the input ports of the MZI is therefore described by a mixed state

$$\sigma = \mathrm{Tr}_*|\Phi_m\rangle\langle\Phi_m| = |\phi_m\rangle\langle\phi_m| + \sigma_\perp, \tag{1.40}$$

where Tr_* denotes the trace over the photonic states in free space. Note that $\sigma_\perp = \mathrm{Tr}_*|\phi_m^*\rangle\langle\phi_m^*|$ and $|\phi_m\rangle\langle\phi_m|$ are states in orthogonal subspaces of the Hilbert space of the photonic states because they have a different number of photons in the waveguide.

The input state $\sigma \otimes \sigma$ is then passed trough the beamsplitter and undergoes a phase shift in one arm of the interferometer. Because these transformations are all described by a unitary and $\sigma_\perp$ has strictly less than m photons, the state on which the measurement is performed,

$$\rho_\varphi = \mathcal{N}^4|\psi_\varphi\rangle\langle\psi_\varphi| + \rho_\perp, \tag{1.41}$$

can be written as the desired term and an orthogonal term. We have used $|\psi_\varphi\rangle = \mathcal{N}^{-2}U_\varphi U_{\mathrm{BS}}|\phi_m\rangle|\phi_m\rangle$ with the normalization $\mathcal{N}^2 = \prod_n \frac{\gamma_n}{\gamma_n + n\Gamma^*} \leq 1$ (see Equation 1.6). Because $|\psi_\varphi\rangle$ is normalized the density matrix ρ_φ is normalized when $\mathcal{N}^4 + \mathrm{Tr}\rho_\perp = 1$.

Due to the orthogonality of $\rho_\perp$ to the desired state, the density matrix can be written as a direct sum $\rho_\varphi = \oplus_k p_k\rho_k$. Furthermore, the Fisher information is additive under the direct sum [153], so that it is lower bounded by

$$F_Q\left[\rho_\varphi\right] = \sum_k p_k F_Q\left[\rho_k\right] \geq \mathcal{N}^4 F_Q\left[|\psi_\varphi\rangle\langle\psi_\varphi|\right] = \mathcal{N}^4 \cdot 2m\left[mI_m^{(1)} + 1\right]. \tag{1.42}$$

The integral $I_m^{(1)}$ does not change when spontaneous emission events take place and the state is only renormalized. This renormalization factor of $\mathcal{N}^4$ is responsible for the reduction of the phase resolution. Fortunately, this factor,

$$\mathcal{N}^2 = \prod_{n=1}^{m} \frac{\gamma_n}{\gamma_n + n\Gamma^*} = 1 - \frac{1}{P_{1\mathrm{d}}}\sum_{n=1}^{m}\frac{1}{N-n+1} + \mathcal{O}\left(P_{1\mathrm{d}}^{-2}\right) \tag{1.43}$$

scales favorably with m for large Purcell factors $P_{1\mathrm{d}}$. In particular, in the low excitation regime $m \ll N$ we find $\mathcal{N}^2 \approx 1 - \frac{m}{NP_{1\mathrm{d}}}$. And even for the fully excited state, we still observe a quantum-enhanced phase sensitivity because of the scaling $\mathcal{N}^2 \sim 1 - \frac{1}{P_{1\mathrm{d}}}\ln(2m)$.

The exact Fisher Information is actually better than this bound because elements of $\rho_\perp$ can still lead to a good scaling with a slightly reduced effective photon number, e.g., $m-1$. But even with the crude approximation we used above, we have shown that decoherence processes can reduce the phase sensitivity, but one can still beat the classical limit.

1.4 Conclusion and Outlook

The generation of photonic states is an essential resource for building quantum networks [13] and for quantum-enhanced optical interferometry [19]. Existing methods efficiently generate single photons, but often suffer from an exponentially low probability of generation with increasing photon number. We have proposed here a novel method for the generation of multiphoton states. The features of the process are that i) the photonic state is emitted on-demand, such that one knows that the photons are in a specific time interval, ii) the wavepacket of the emitted field can be shaped to be e.g., time symmetric, such that the mapping between the ensemble state and the photonic state is reversible and iii) the emitted state has a broad bandwidth so that it is localized in position space.

In the first part of this chapter we focused on the mapping between the state of an ensemble of N quantum emitters to a photonic state. These ensembles are a natural candidate for generating multiphoton states because many excitations $m \leq N$ can be stored as a collective state in a metastable state s of the quantum emitters. By coupling this ensemble to a one-dimensional waveguide one can enhance the light-matter coupling and collect an emitted photonic state efficiently at the ends of the waveguide. In particular, the (superpositions of) symmetric Dicke states with a specific excitation number m of an ensemble in the atomic mirror configuration are suitable for the generation of (superpositions) of single-mode Fock states in the waveguide in the low excitation regime $m \ll N$. The emission can be triggered by exciting a symmetric Dicke state in the metastable state s to the excited state e by a fast laser pulse with Rabi coupling Ω. By choosing an appropriate time-dependent coupling $\Omega(t)$ one can even shape the form of the emitted wavepacket to be symmetric in time such that the mapping from the ensemble state to the photonic state can be made reversible. The broad bandwidth stems from the fact, that the symmetric Dicke states decay superradiantly with rate $\gamma_m \sim mN\Gamma_{1\mathrm{d}}$. The difficulty in this approach lies in the preparation of the symmetric Dicke state, for which we propose protocols in Chapter 2.

This difficulty can be alternatively overcome by noting that the symmetric Dicke state with excitation number $m = N$, has a conceptually straightforward preparation: transfer the population from g to e in every emitter independently. The photonic state generated from this Dicke state has an intricate multi-mode structure, which motivated us to look into the quantum applications, in particular quantum-enhanced optical interferometry, with multi-mode states in the second part of this chapter. The usefulness of a state for quantum metrological applications is quantified by the Quantum Fisher Information. In this context, we showed that the photonic states prepared in the low excitation regime $m \ll N$ yield the same Quantum Fisher Information as single-mode states up to a correction of order $\mathcal{O}(\frac{m}{N^2})$, which is related to the fact that the overlap of these states with the single mode state is perfect with a correction of order of $\mathcal{O}\left(\frac{m^3}{N^2}\right)$. Furthermore, we showed that also the truly multi-mode states emitted by the fully excited Dicke state $|\psi_{m=N}\rangle$ overcome the classical limit of phase sensitivity.

Even though the use of waveguide QED systems for the generation of single-mode photonic states is experimentally challenging because of the state preparation of the ensemble (see Chapter 2), the generation of multi-mode photonic states through emission from the maximally excited symmetric Dicke state $|\psi_N\rangle$ is conceptually realistic. As we showed in Section 1.3, these multi-mode states still achieve quantum-enhanced optical interferometry. This opens up future perspectives for the use of multi-mode photonic states in quantum applications. On the one hand, these can be further improvements in the area of quantum metrology, e.g., by shaping the wavepacket of the multi-mode photonic state, or using measurements other than the parity operator. Furthermore, we stress that the expression for the Quantum Fisher Information of Equation 1.25 is valid for any multi-mode photonic state, which opens up the field of quantum-enhanced optical metrology to many new photonic states. On the other hand, the usefulness of multi-mode photonic states has to be investigated for other quantum applications, e.g., for quantum communication or quantum teleportation.

Appendix

1.A Input-Output Formalism

Let us review the ideas behind the input-output formalism of Reference [144]. We assume a light-matter coupling of the system (with Hamiltonian H_S) and the bath (with Hamiltonian $H_\mathrm{B} = \sum_k \omega_k a_k^\dagger a_k$) of the form

$$H = H_\mathrm{S} + H_\mathrm{B} + \sum_k \left(O_k a_k^\dagger + \mathrm{h.c.} \right), \tag{1.44}$$

$$O_k = g_k \sum_j O^j \mathrm{e}^{-\mathrm{i}kx_j}. \tag{1.45}$$

Note, that this is the same Hamiltonian as introduced in Equation 0.1 with $O^j = \sigma_{ge}^j$; the only difference being, that we have embedded the phase due to the propagation of the photonic state, $\mathrm{e}^{-\mathrm{i}kx_j}$, in the operators O_k. We are then interested in how an initial state evolves to a final state under this Hamiltonian. This is captured in the scattering amplitude

$$A(T) = \langle \psi_\mathrm{f} | \langle B_\mathrm{f} | \mathrm{e}^{-\mathrm{i}H(t_\mathrm{f}-t_\mathrm{i})} | B_\mathrm{i} \rangle | \psi_\mathrm{i} \rangle, \tag{1.46}$$

where $|\psi_{\mathrm{i/f}}\rangle$ denotes the initial (final) system state and $|B_{\mathrm{i/f}}\rangle$ the initial (final) state of the bath, that is, e.g., the electromagnetic field inside the waveguide. We note, that the expression only depends on the time difference $T = t_\mathrm{f} - t_\mathrm{i}$. This scattering amplitude contains all the necessary information for the calculation of the various correlation functions. In order to evaluate the scattering amplitude $A(T)$, we take the bath states $|B\rangle = |\{n_k\}\rangle$ to be Fock states, which we can express through (unnormalized) coherent bath states $|\{J_k\}\rangle$,

$$|B_\mathrm{f}\rangle = |\{n_k\}\rangle = \lim_{J_k \to 0} \prod_k \frac{1}{\sqrt{n_k!}} \frac{\delta^{n_k}}{\delta J_k^{n_k}} |\{J_k\}\rangle. \tag{1.47}$$

The scattering amplitude is then $A(T) = \mathcal{F}_\mathrm{out}^* \mathcal{F}_\mathrm{in} A_J(T)$ with $\mathcal{F} = \lim_{J_k \to 0} \prod_k \frac{1}{\sqrt{n_k!}} \frac{\delta^{n_k}}{\delta J_k^{n_k}}$. In particular, this reduced the task to the evaluation of

$$A_J(T) = \langle \psi_\mathrm{f} | \langle \{J_k\} | \mathrm{e}^{-\mathrm{i}HT} | \{J_k\} \rangle | \psi_\mathrm{i} \rangle. \tag{1.48}$$

This expression can be further simplified by transforming into an interaction picture rotating with the bath Hamiltonian $H_\mathrm{B} = \sum_k \omega_k a_k^\dagger a_k$ and expressing the coherent states

in terms of a generalized displacement D operator,

$$|\{J_k(t_\mathrm{i})\}\rangle = |\{J_k e^{\mathrm{i}\omega_k t_\mathrm{i}}\}\rangle = D\mathrm{e}^{\sum_k |J_k|^2 e^{\mathrm{i}\omega_k t_\mathrm{i}}/2}|\{0_k\}\rangle, \tag{1.49a}$$

$$D = \exp\left[\sum_k \left(J_k(t_\mathrm{i})a_k^\dagger - J_k^*(t_\mathrm{f})a_k\right)\right]. \tag{1.49b}$$

By noting that $D^\dagger D = 1$, the scattering amplitude can then be written as

$$A_J(T) = \mathrm{e}^{\sum_k |J_k|^2 e^{-\mathrm{i}\omega_k T}}\langle\psi_\mathrm{f}|\langle\{0_k\}|U(T)|\psi_\mathrm{i}\rangle|\{0_k\}\rangle, \tag{1.50a}$$

$$U(T) = D^\dagger \mathrm{e}^{\mathrm{i}H_\mathrm{B}t_\mathrm{f}}\mathrm{e}^{-\mathrm{i}HT}\mathrm{e}^{-\mathrm{i}H_\mathrm{B}t_\mathrm{i}}D. \tag{1.50b}$$

To obtain analytical expressions for the scattering amplitude, we use the transformations

$$D^\dagger b_k^\dagger D = b_k^\dagger + J_k^* e^{-i\omega_k t_\mathrm{f}}, \tag{1.51a}$$

$$D^\dagger b_k D = b_k + J_k e^{i\omega_k t_\mathrm{i}}. \tag{1.51b}$$

This introduces an additional summand $H_D(t) = \exp\left[J_k^* O_k \mathrm{e}^{-\mathrm{i}\omega_k(t_\mathrm{f}-t)} + J_k O_k^\dagger \mathrm{e}^{-\mathrm{i}\omega_k(t-t_\mathrm{i})}\right]$ in the time evolution (denoting the time ordering operator by $\mathcal{T}$),

$$U(T) = \mathcal{T}\exp\left[-\mathrm{i}\int_{t_\mathrm{i}}^{t_\mathrm{f}} \mathrm{d}t\,(H(t) + H_D(t))\right]. \tag{1.52}$$

When the functional derivatives with respect to J_k are performed to calculate $A(T)$, this brings integrals containing the jump operators O_k down. When the initial photonic state is in the vacuum, one obtains correlation functions of the form

$$\langle\psi_\mathrm{f}|\langle\{0_k\}|\mathcal{T}O_{k_1}(t_1)\cdots O_{k_m}(t_m)|\psi_\mathrm{i}\rangle|\{0_k\}\rangle \tag{1.53}$$

where the operators are taken in an interaction picture with respect to H. Note that the part from H_D vanishes when the limit $J_k \to 0$ is taken.

In a final step, the quantum regression theorem [154] is applied, with which one can trace out the bath degrees of freedom. This replaces the evolution under the full Hamiltonian H by the effective non-hermitian evolution of the system H_eff (like the one from Equation 0.8) because only system operators O_k appear in the correlation function. The correlation functions are then of the form

$$\langle\psi_\mathrm{f}|\langle\{0_k\}|\mathcal{T}\tilde{O}_{k_1}(t_1)\cdots\tilde{O}_{k_m}(t_m)|\psi_\mathrm{i}\rangle|\{0_k\}\rangle \tag{1.54}$$

where the exact form depends on the initial and final system states and the operators are $\tilde{O}_k(t) = \mathrm{e}^{\mathrm{i}H_\mathrm{eff}t}O_k\mathrm{e}^{-\mathrm{i}H_\mathrm{eff}t}$ taken in the interaction picture with respect to H_eff.

1.B Details on the Calculation of the Fisher Information

When evaluating the Fisher Information, we need to calculate $\langle\dot{\psi}_\varphi|\dot{\psi}_\varphi\rangle$ and $\langle\psi_\varphi|\dot{\psi}_\varphi\rangle$ with the states as defined in Equation 1.17 and 1.22. In the latter term correlation functions of the form

$$\begin{aligned}&\langle \mathrm{vac}|d_{p_{2m}}\cdots d_{p_2}c_{p_{2m-1}}\cdots c_{p_1}b^\dagger_{k_1}c^\dagger_{k_3}\cdots c^\dagger_{k_{2m-1}}d^\dagger_{k_2}\cdots d^\dagger_{k_{2m}}|\mathrm{vac}\rangle\\ &\quad=\frac{1}{\sqrt{2}}m(m-1)!m!\prod_j 2\pi\delta(p_j-k_j)\end{aligned}\tag{1.55}$$

appear. When performing the integral this leads to a factor $|\langle\psi_\varphi|\dot{\psi}_\varphi\rangle| = mI_m^{(0)}$.

In the term $\langle\dot{\psi}_\varphi|\dot{\psi}_\varphi\rangle$ there are more terms emerging in the correlation function, e.g.,

$$\begin{aligned}&\langle \mathrm{vac}|d_{p_{2m}}\cdots d_{p_2}c_{p_{2m-1}}\cdots c_{p_3}b_{p_1}b^\dagger_{k_1}c^\dagger_{k_3}\cdots c^\dagger_{k_{2m-1}}d^\dagger_{k_2}\cdots d^\dagger_{k_{2m}}|\mathrm{vac}\rangle\\ &\quad=\langle \mathrm{vac}|d_{p_{2m}}\cdots d_{p_2}c_{p_{2m-1}}\cdots c_{p_3}b_{p_1}b^\dagger_{k_1}c^\dagger_{k_3}\cdots c^\dagger_{k_{2m-1}}d^\dagger_{k_2}\cdots d^\dagger_{k_{2m}}|\mathrm{vac}\rangle\\ &\qquad+\langle \mathrm{vac}|d_{p_{2m}}\cdots d_{p_2}c_{p_{2m-1}}\cdots c_{p_3}b_{p_1}b^\dagger_{k_1}c^\dagger_{k_3}\cdots c^\dagger_{k_{2m-1}}d^\dagger_{k_2}\cdots d^\dagger_{k_{2m}}|\mathrm{vac}\rangle\\ &\qquad+\langle \mathrm{vac}|d_{p_{2m}}\cdots d_{p_2}c_{p_{2m-1}}\cdots c_{p_3}b_{p_1}b^\dagger_{k_1}c^\dagger_{k_3}\cdots c^\dagger_{k_{2m-1}}d^\dagger_{k_2}\cdots d^\dagger_{k_{2m}}|\mathrm{vac}\rangle\\ &\quad=\frac{1}{2}(m-1)!^2\prod_{j>2}2\pi\delta(p_j-k_j)\\ &\qquad\times(2\pi)^2\Big(m(m+1)\delta(p_1-k_1)\delta(p_2-k_2)+m^2\delta(p_1-k_2)\delta(p_2-k_1)\Big).\end{aligned}\tag{1.56}$$

The remaining correlation function has a simpler form again

$$\begin{aligned}&\langle \mathrm{vac}|d_{p_{2m}}\cdots d_{p_4}b_{p_2}c_{p_{2m-1}}\cdots c_{p_1}b^\dagger_{k_1}c^\dagger_{k_3}\cdots c^\dagger_{k_{2m-1}}d^\dagger_{k_2}\cdots d^\dagger_{k_{2m}}|\mathrm{vac}\rangle\\ &\quad=\frac{1}{2}m^2(m-1)!^2\prod_j 2\pi\delta(p_j-k_j).\end{aligned}\tag{1.57}$$

Taking both results together and performing the integration, we obtain a factor $\langle\dot{\psi}_\varphi|\dot{\psi}_\varphi\rangle = \frac{1}{2}\left[(2m^2+m)I_m^{(0)}+m^2I_m^{(1)}\right]$.

1.C Generalization of the Recurrence Relation

The recurrence relation for a general Hamiltonian diagonal with respect to the symmetric Dicke states $|\psi_m\rangle$ with eigenvalues $\lambda_m = \omega_m - \mathrm{i}\gamma_m$ is the same as in Equation 1.34 with

the only exception in $F_{ij}^{(2)}$, which changes to

$$F_{ij}^{(2)} = i\frac{\gamma_{m-i}}{c_{i-1,j}^{(2)}}F_{i-1,j}^{(2)} + j\frac{\gamma_{m-j}}{c_{i,j-1}^{(2)}}F_{i,j-1}^{(2)} + 2\mathrm{Re}\left[\frac{\sqrt{\gamma_{m-i}\gamma_{m-j}}}{c_{i,j}^{(1)}}F_{i,j}^{(1)}\right], \tag{1.58}$$

and where the factors $c_{ij}^{(2/1/0)}$ are now given by the differences $\delta\lambda_k = \lambda_k - \lambda_{k-1}$ with $\lambda_0 = 0$. In particular,

$$\begin{aligned}
c_{ij}^{(2)} =& -\mathrm{i}\left(\sum_n^{m-1-i}\delta\lambda_n^* + \sum_n^{m-1-j}\delta\lambda_n^* + \sum_n^{m-1-i}\delta\lambda_n + \sum_n^{m-1-j}\delta\lambda_n\right) \\
=& 2\gamma_{m-1-i} + 2\gamma_{m-1-j}, && (1.59a)\\
c_{ij}^{(1)} =& -\mathrm{i}\left(\sum_n^{m-1-i}\delta\lambda_n^* + \sum_n^{m-j}\delta\lambda_n^* + \sum_n^{m-i}\delta\lambda_n + \sum_n^{m-1-j}\delta\lambda_n\right) \\
=& \gamma_{m-1-i} + \gamma_{m-1-j} + \gamma_{m-i} + \gamma_{m-j} - \mathrm{i}\left(\delta\omega_{m-i} - \delta\omega_{m-j}\right), && (1.59b)\\
c_{ij}^{(2)} =& -\mathrm{i}\left(\sum_n^{m-i}\delta\lambda_n^* + \sum_n^{m-j}\delta\lambda_n^* + \sum_n^{m-i}\delta\lambda_n + \sum_n^{m-j}\delta\lambda_n\right) \\
=& 2\gamma_{m-i} + 2\gamma_{m-j}. && (1.59c)
\end{aligned}$$

Note, that $c_{ij}^{(2/1/0)} \in \mathbb{R}$ if the frequencies are linear functions of the excitation number, e.g., $\omega_n = n\Delta$ such that $\delta\omega_n = \omega_n - \omega_{n-1} = \Delta$. Then also $F_{ij}^{(2/1/0)} \in \mathbb{R}$ and the recurrence relation simplifies to the one given in Equation 1.37.

2 Preparation of Dicke States

Abstract

The generation of multiphoton states by exploiting the superradiant decay of ensembles of quantum emitters coupled to a one-dimensional waveguide as explored in Chapter 1 is very promising for applications in quantum metrology and quantum communication. To take advantage of the mapping of superradiant quantum emitter states to photonic states, one requires the high fidelity preparation of symmetric Dicke states. These states are interesting in themselves as they are highly entangled and robust to particle loss [155, 156, 157]. In particular, they are also useful for building quantum memories and for atomic interferometry [158, 159, 160, 161].

This chapter is concerned with the preparation of symmetric Dicke states with a specific excitation number using collective effects arising in waveguide QED systems. We propose four different protocols exploiting various tools, in particular coherent driving, Quantum Zeno Dynamics or coherent flip-flop interactions mediated through the waveguide. For a specific experimental setup with given resources (i.e., the number of coupled emitters N and the Purcell factor $P_{1\mathrm{d}}$), one can pick the protocol scaling the most favorable with the available resources. Furthermore, our protocols can be extended to the preparation of Dicke states over multiple metastable states, which can be used to generate entangled single-mode photonic states.

In this chapter we first motivate the importance of symmetric Dicke states and introduce the basic concepts (Section 2.1). Then, we shortly present our protocols and motivate the fundamental principles behind each one, identify possible problems and how these problems can be overcome (Section 2.2), before we discuss the protocols in detail (Section 2.3). Because the different protocols exploit the characteristic resources of various experimental platforms currently available, we examine which protocols are suitable for each one (Section 2.4). Finally, we show how our protocols can be extended to prepare Dicke states over two or even more metastable states (Section 2.5) and summarize the results (Section 2.6).

This chapter is based on and uses parts of References

- [1]: A. González-Tudela, V. Paulisch, D. E. Chang, H. J. Kimble, and J. I. Cirac. "Deterministic Generation of Arbitrary Photonic States Assisted by Dissipation" *Phys. Rev. Lett.* **115** 163603 (2015),
- [3]: A. González-Tudela, V. Paulisch, H. J. Kimble, and J. I. Cirac. "Efficient Multiphoton Generation in Waveguide Quantum Electrodynamics" *Phys. Rev. Lett.* **118** 213601 (2017),
- [4]: V. Paulisch, A. González-Tudela, H. J. Kimble, and J. I. Cirac. "Heralded multiphoton states with coherent spin interactions in waveguide QED" *New J. Phys.* **19** 043004 (2017),
- [5]: V. Paulisch, H. J. Kimble, J. I. Cirac, and A. González-Tudela. "Generation of single and two-mode multiphoton states in waveguide QED" *arXiv:1802.00210*. (2018).

2.1 Motivation and Basic Concepts

In this section, we first motivate the importance of preparing Dicke states and then discuss the atom and waveguide QED tools, on which our protocols are based.

2.1.1 Motivation

Our main motivation for preparing (superpositions of) symmetric Dicke states is their importance for the generation of arbitrary photonic states of a single mode as illustrated in Chapter 1. Beyond their efficient mapping to multiphoton states, they are of fundamental interest due to their robustness against particle loss [155] and their entanglement properties [156, 157]. One asset of the symmetric Dicke states is that they can be characterized and experimentally studied more easily due to their symmetry [158, 159]. Finally, regarding applications, they are useful for building quantum memories [160] and for atomic interferometry [161].

As our main motivation is the generation of photonic states, our goal is the preparation of specific states in a chain of N quantum emitters, where we assume the emitters to be three-level systems so that a quantum state can be stored in the metastable ground states s and g (see Figure 2.1). In particular, we are interested in preparing Dicke states with m excitations in a metastable state s,

$$|\psi_m\rangle = \frac{1}{\mathcal{N}_{N,m}}\mathrm{sym}\left(|s\rangle^{\otimes m}|g\rangle^{\otimes N-m}\right) = \frac{1}{m!}\binom{N}{m}^{-\frac{1}{2}} S_{sg}^m|g\rangle^{\otimes N}, \tag{2.1}$$

or superpositions thereof, $|\psi\rangle = \sum c_n|\psi_n\rangle$, where we define the collective operator as $S_{\alpha\beta} = \sum_j |\alpha\rangle_j\langle\beta|$. The normalization of the state is $\mathcal{N}_{N,m}^2 = \binom{N}{m}$ and the symmetrization operator is denoted as "sym". By applying the collective operator S_{sg} on the state $|\psi_m\rangle$, an additional excitation is generated, $|\psi_{m+1}\rangle = \frac{1}{\sqrt{(m+1)N_m}}S_{sg}|\psi_m\rangle$, where we have introduced the effective atom number remaining in the state g as $N_m = N - m$.

There are several protocols for the preparation of symmetric Dicke states in the literature, e.g., using adiabatic transitions [162, 163], coherent driving of ensembles [164], measurement and feedback [165], linear optical tools [166], trapped ion setups [167, 168], or cavity QED systems [169]. However, only few of these proposals can be extended to the high fidelity preparation of arbitrary superpositions of symmetric Dicke states with a specific excitation number, and even fewer for symmetric Dicke states over several metastable states.

In particular, we look for protocols, with which one can prepare symmetric Dicke states and superpositions thereof, $|\psi\rangle$, with a fidelity of at least

$$F_{\mathrm{em}} = \sqrt{\langle\psi|\rho_{\mathrm{S}}|\psi\rangle} \geq 1 - \frac{m}{2NP_{\mathrm{1d}}} = F_{\mathrm{ph}} \tag{2.2}$$

where ρ_{S} denotes the density matrix of the emitter state at the end of the protocol and F_{ph} is the fidelity of the photon generation of Equation 1.7. We emphasize, that we are mainly

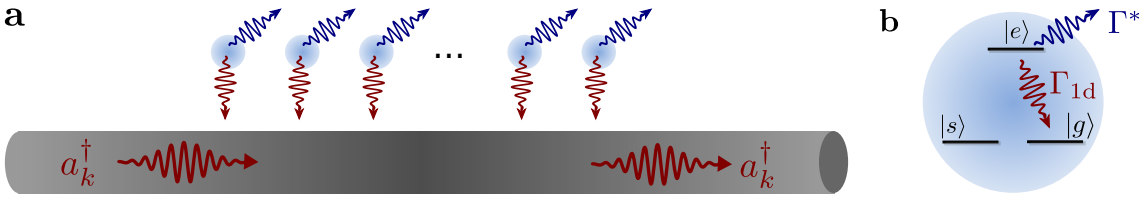

Figure 2.1: **a** The goal is to prepare Dicke states in a one-dimensional chain of emitters. **b** These states can be stored in metastable ground states $|s\rangle$ and $|g\rangle$. Furthermore, the emitters are required to have an optically excited state $|e\rangle$.

interested in the scaling with the resources in waveguide QED systems, that is the number of emitters N and the Purcell factor P_{1d} and not the exact proportionality factors. We distinguish between two types of protocols, namely deterministic and probabilistic ones. In the latter, one has to perform a heralding measurement on measuring a state $|\phi_{aux}\rangle$. Therefore, in addition to the figure of merit of the fidelity, for probabilistic protocols one has to consider the probability p_{her} of successful heralding (and thus projecting on the state $|\phi_{aux}\rangle$),

$$p_{her} = \mathrm{Tr}\left[\langle\phi_{aux}|\rho_S|\phi_{aux}\rangle\right]. \tag{2.3}$$

2.1.2 Atom and Waveguide QED Tools

We focus on protocols which exploit several properties typical for waveguide QED systems (see Section 0.2), i.e.,

i) the quantum emitters, e.g., atoms, have a rich level structure with several metastable ground states, which can be used as quantum memories, as well as several optically excited and metastable states, which can be addressed by an external driving field or are coupled to a guided mode of the waveguide;

ii) due to the confinement of the guided photons to the one-dimensional waveguide, the decay rate to the waveguide, Γ_{1d}, can be of the order of or even surpass the decay into all other modes, Γ^*, leading to a large Purcell factor $P_{1d} = \Gamma_{1d}/\Gamma^*$;

iii) the waveguide mediates a practically infinite ranged and collectively enhanced interaction between the emitters because it is an effective one-dimensional system.

In particular, recall that the master equation for the ensemble is given by (see Section 0.3.2)

$$\partial_t \rho = -\mathrm{i}\left[H_{ext} + H_{coll}, \rho\right] + \mathcal{L}_{coll}\left[\rho\right] + \mathcal{L}_{ind}\left[\rho\right], \tag{2.4}$$

where all external, coherent, resonant driving terms (e.g., laser or microwave fields) are contained in H_{ext}. We assume that we already work in an interaction picture rotating with

$H_S = \Delta S_{ee}$. The interaction with the waveguide induces coherent, H_{coll}, and dissipative terms, $\mathcal{L}_{\text{coll}}$, depending on the distance between emitters in the chain, $x_{ij} = x_i - x_j$. In particular, if the transition $g - e$ couples to the waveguide they take the form [37]

$$H_{\text{coll}} = \frac{\Gamma_{1d}}{2} \sum_{ij} \sin\left(k_0 |x_{ij}|\right) \sigma_{eg}^i \sigma_{ge}^j, \tag{2.5a}$$

$$\mathcal{L}_{\text{coll}}[\rho] = \frac{\Gamma_{1d}}{2} \sum_{ij} \cos\left(k_0 |x_{ij}|\right) \left(\sigma_{ge}^j \rho \sigma_{eg}^i - \sigma_{eg}^i \sigma_{ge}^j \rho + \text{h.c.}\right), \tag{2.5b}$$

where k_0 is the wavevector corresponding to the emitter energy, that is $\omega_{k_0} = \Delta$. In particular, the interactions only depend on the phase between emitters $\phi_{ij} = k_0 |x_{ij}| \pmod{2\pi}$. We can distinguish two regimes depending on the distance between the emitters:

- A **purely dissipative** regime arises in the atomic mirror configuration, where the distance between emitters is commensurate with the wavelength, that is $\phi_{ij} = 0$ (see Section 0.3.3). In this case the coherent part of the interaction vanishes, $H_{\text{coll}} = 0$, and the decay is collective, that is

$$\mathcal{L}_{\text{coll}}[\rho] = \frac{\Gamma_{1d}}{2} \left(S_{ge} \rho S_{eg} - S_{eg} S_{ge} \rho + \text{h.c.}\right). \tag{2.6}$$

- When the distance between emitters satisfies $\phi_{ij} = \pi/2$ an excitation from one emitter can be **coherently transferred** to a second one through a type of flip-flop interaction. For two emitters this would lead to $H_{\text{coll}} = \frac{\Gamma_{1d}}{2} \left(\sigma_{eg}^1 \sigma_{ge}^2 + \text{h.c.}\right)$. However, it is not possible to cancel all dissipative terms, such that for the two emitters there are additional individual decay terms, $\mathcal{L}_{\text{coll}}[\rho] = \frac{\Gamma_{1d}}{2} \sum_{j=1,2} \left(\sigma_{ge}^j \rho \sigma_{eg}^j - \sigma_{eg}^j \sigma_{ge}^j \rho + \text{h.c.}\right)$. Nonetheless, this interaction can be used to couple ensembles of emitters of size N coherently with an enhanced coupling of $\sqrt{N}\Gamma_{1d}$.

Furthermore, recall that the spontaneous emission into other modes is assumed to appear as individual decay, that is

$$\mathcal{L}_{\text{ind}}[\rho] = \frac{\Gamma^*}{2} \sum_j \left(\sigma_{ge}^j \rho \sigma_{eg}^j - \sigma_{eg}^j \sigma_{ge}^j \rho + \text{h.c.}\right). \tag{2.7}$$

The assumption of individual decay may break in the case of sub-wavelength spacing between the emitters [170], where strongly subradiant states with highly suppressed spontaneous emission emerge. The combination of these states with our protocol opens up an exciting perspective to improve our protocols.

The main element in the protocols is then the choice of the atomic positions and of the external driving fields. For some protocols we split up the chain of emitters into different ensembles, in particular a *source ensemble* (s), a *target ensemble* (t) or a *detector ensemble* (d). Concerning the external drivings, we only require the lasers/microwave fields to act collectively on a given ensemble and not individually on specific emitters. Addressing the

ensembles independently from each other is robust experimentally because the ensembles can be separated by multiples of $2\pi/k_0$ without affecting the dynamics. We then write the driving, which we assume to be on resonance, in full generality as

$$H_{\text{ext}} = \frac{1}{2}\Omega^{(\text{x})}_{\alpha\beta} S^{(\text{x})}_{\alpha\beta} + \text{h.c.}, \tag{2.8}$$

where $\Omega^{(\text{x})}_{\alpha\beta}$ is the Rabi coupling between the states α and β of the ensemble (x).

In all cases, the fidelity and heralding probability can be studied by unraveling the master equation (Equation 2.4) into a non-hermitian evolution and collective and individual quantum jumps as in Equation 0.7. For the calculation of the fidelity or heralding probability it turns out that only the effective non-hermitian evolution is relevant and that we can forget about the decayed part as this already reduced the fidelity or is heralded out through some measurement.

2.2 Protocols for the Preparation of Dicke States

With these atom and waveguide QED tools in mind, we now focus on the preparation of Dicke states in a specific metastable state s in an ensemble of quantum emitters, which we call the target ensemble (t). We take the ensemble to be in the atomic mirror configuration, i.e., with a separation $\phi_{ij} = 0 \pmod{2\pi}$ because this is the setup necessary for the generation of photonic states (see Chapter 1).

In Section 2.2.1, we first focus on adding a single excitation, i.e., preparing the state $|\psi_{m+1}\rangle_{\text{t}}$ from $|\psi_m\rangle_{\text{t}}$. The m excitations can be either directly accumulated in the metastable state s or in additional metastable states s_i to be merged together at a later point. We denote the fidelity of this process as $F_{m\to m+1}$ and the probability of successful heralding in probabilistic protocols as $p_{m\to m+1}$. The definitions of these two quantities are just as in Equation 2.2 and 2.3, respectively.

Once we have analyzed the general step of adding one excitation, we consider in Section 2.2.2 the complete process to prepare an arbitrary Dicke state, $|\psi_0\rangle_{\text{t}} \to |\psi_1\rangle_{\text{t}} \to \cdots \to |\psi_m\rangle_{\text{t}}$. For probabilistic protocols we then calculate the average number of repetitions, R_m, to arrive to $|\psi_m\rangle_{\text{t}}$ and the average fidelity of the process that we denote as F_m. Both R_m and F_m depend on the way the excitations are added and changes with the different protocols.

2.2.1 Summary of the Protocols

Let us start by summarizing the ideas and problems of each protocol shortly here (see also Table 2.1). Details on the protocols are left to Section 2.3, but we note that with all of them, one can add a single collective excitation to an already prepared symmetric Dicke state of m excitations, $|\psi_m\rangle_{\text{t}} \to S^{(\text{t})}_{sg}|\psi_m\rangle_{\text{t}}$.

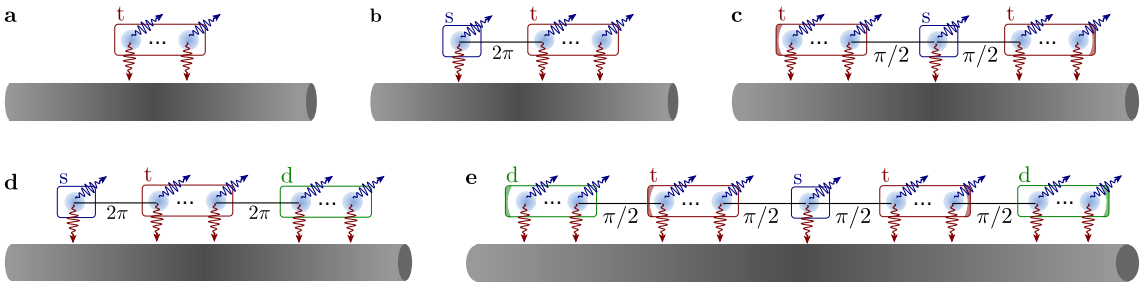

Figure 2.2: Setup for the preparation of a symmetric Dicke state in the target ensemble using emitters coupled to a one-dimensional waveguide. **a** Only the target ensemble (t) is required for the protocol using coherent driving. **b** By coupling a single source emitter (s) to the target ensemble in the atomic mirror configuration, one additional excitation in the target ensemble can be generated deterministically through the joint collective dissipation. **c** The source and target ensemble can alternatively be coupled through coherent flip-flop interactions mediated through the waveguide by placing the source emitter in between the split target ensemble. **d** The protocol using setup b is extended to a probabilistic protocol by adding a detector ensemble (d) in the atomic mirror configuration. **e** Also the protocol using setup c can be extended to a probabilistic protocol by placing a split detector ensemble around the source and target ensembles.

1. Our simplest protocol, which is inspired by Reference [26], is a **probabilistic protocol using coherent driving** of the target ensemble by an external field acting collectively on all emitters to excite the ensemble weakly (see Figure 2.2a). The excited state can then decay collectively to the metastable state s by emitting a photon into the waveguide. If this photon is detected, this measurement heralds the preparation of a symmetric state in the metastable state s. However, this state might contain two excitations instead of only one, lowering the fidelity significantly if the heralding probability is large.

2. This trade-off between the fidelity and the heralding probability can be overcome by designing a **deterministic protocol** with an auxiliary emitter, which we call source emitter (see Figure 2.2b). In this protocol, the source emitter is coupled to the target ensemble through a subradiant state of the joint collective dissipation. The emitter is then excited and the excitation is transferred through this subradiant state to the target ensemble using Quantum Zeno Dynamics [124, 125, 140, 171] as explained in Section 2.3. This process is, however, very slow and therefore leads to significant errors, reducing the fidelity below the one of photon generation. Instead of using the Quantum Zeno Dynamics, one can also use the coherent flip-flop interactions between the source and split target ensemble, acting as atomic mirrors (see Figure 2.2c) [37].

3. In order to increase the fidelity, one can design a **probabilistic protocol using collective dissipation**, in which we use a heralding measurement to exclude the cases in which the target ensemble has undergone decay processes, either collectively or individually. For this purpose, one adds a third ensemble of emitters, on which an appropriate heralding measurement can be performed, a detector ensemble (see Figure 2.2d). In addition to transferring the excitation from the source to the target ensemble, the state of the detector ensemble is then changed by appropriately designing the dynamics. This protocol thus effectively switches the decrease in fidelity

Protocol	$p_{m\to m+1}$	$1-F_{m\to m+1}$	Requirements
Coherent Driving [3]	ηx^2	$(1-\eta)x$	$x=\Omega_{ge}^{(\mathrm{t})}\sqrt{N_m}T/2\ll 1$
Deterministic [1]	1	$1/\sqrt{P_{1\mathrm{d}}}$	$P_{1\mathrm{d}}\gg 1$
Probabilistic (QZD) [3, 5]	$1-\sqrt{N_m/P_{1\mathrm{d}}}$	0	$P_{1\mathrm{d}}\gg 1$
Probabilistic (Coh.) [4]	$1-\sqrt{(m+1)/N_m}$	$(m/N)^{1.9}$	$N\gg 1$

Table 2.1: Scaling of the heralding probability $p_{m\to m+1}$ and fidelity $F_{m\to m+1}$ achieved in the different protocols for the preparation of symmetric Dicke states. We only give the scaling to highest order in $P_{1\mathrm{d}}$ and $N_m=N-m$ and leave out proportionality constants at that order.

of the deterministic protocol over to a decrease of the heralding probability.

4. The previous protocol still requires a large Purcell factor $P_{1\mathrm{d}}$, but by designing a **probabilistic protocol using coherent flip-flop interactions** one can achieve a scaling that depends on the number of emitters N instead of the Purcell factor. One still requires three ensembles, but to achieve a high heralding probability and fidelity, one chooses a concatenated setup in which the source and target ensemble are placed in the middle of the split detector ensemble (see Figure 2.2e). The heralding probability then depends only weakly on the Purcell factor and can be increased by increasing the number of atoms in the target and detector ensemble.

2.2.2 Adding Excitations

The protocols above generate a single collective excitation in the metastable state s of the target ensemble. In three-level systems this adds one excitation directly on top of m collective excitations in s. However, if many metastable states $\{s_i\}$ are available, the already generated m excitations can be stored in these metastable states and one can merge these excitations together at the end of the full protocol. This approach can lower the mean number of steps to reach a specific Dicke state in probabilistic protocols, which is exponential in m when the excitations are added directly. In this section we consider the full process $|\psi_0\rangle_{\mathrm{t}}\to|\psi_1\rangle_{\mathrm{t}}\to\cdots\to|\psi_m\rangle_{\mathrm{t}}$ for different ways of merging the excitations.

When the excitations are **directly added** (see Figure 2.3a), the mean number of steps R_m to reach the state $|\psi_m\rangle$ is exponential, because it is the inverse of the products of the heralding probabilities $p_{j\to j+1}$. In particular,

$$R_m=\prod_{j=0}^{m-1}\frac{1}{p_{j\to j+1}}\geq p^{-m},\qquad F_m\approx 1-\sum_{j=0}^{m-1}(1-F_{j\to j+1}),\tag{2.9}$$

where $p=\max_j p_{j\to j+1}$.

If the excitations have been stored in additional metastable states s_i, one can **merge the excitations** of different metastable states s_i and s_j by using collective microwave or laser drivings (see Figure 2.3b). Because only two metastable states are relevant for

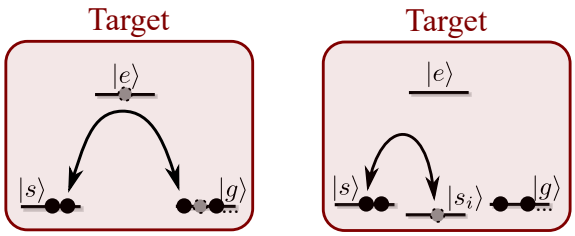

Figure 2.3: The excitations can be added either **a** directly in the metastable states s or **b** stored in additional metastable states s_i to be merged later.

this, we denote a state with n_i (n_j) collective excitations in the metastable state $s_{i(j)}$ by $|n_i, n_j\rangle_{s_i,s_j}$. The necessary operations on the metastable states are i) displacement operators, which can be obtained by weak external driving fields between the state of interest and the ground state g and ii) beamsplitter-like transformations between two metastable states, which can be obtained by directly applying, e.g., two photon Raman processes between the metastable states of interest. Furthermore, one can detect the population in a metastable state very efficiently by pumping to an excited state that emits a collective photon through the waveguide in a cyclic transition (see Section 0.2.4). With this, one can verify that a mode is empty, effectively acting as a projection operator $\mathbb{P}_{0_j}$ on mode s_j. Thus, these tools provide a similar set of tools as the ones used in linear optics protocols with the advantage of having the excitations stored in the metastable states s_i acting as a quantum memory. The excitations can then be combined in various ways. There are two limiting cases of interest:

- If only one additional metastable state is available, one can merge the m excitations in the state s_1 and the newly generated excitation in s by applying a beamsplitter like transformation and heralding on detecting no excitations in the state s (see Figure 2.4a). This leads to the transformation $|k,1\rangle_{s_1,s} \rightarrow |k+1,0\rangle_{s_1,s}$ with a probability $q_k = \left(\frac{k}{k+1}\right)^k \geq \frac{1}{\mathrm{e}}$. If the heralding fails, one has to start from the beginning, such that the mean number of steps to reach m excitations in the state s_1, is calculated recursively through $R_m = q_m^{-1}(1 + R_{m-1})$. We obtain

$$R_m \sim \frac{1}{p}\mathrm{e}^m, \qquad F_m \gtrsim 1 - R_m \max_j (1 - F_{j\rightarrow j+1}), \tag{2.10}$$

  where $p = \max_j p_{j\rightarrow j+1}$ is the maximal number of times one needs to try to successfully generate a single excitation on average.

- If more metastable states are available, in particular $\log_2 m$, one can double the excitations at every step (see Figure 2.4b). This structure is useful because one doesn't need to start from the beginning if the heralding has failed. In particular, one combines k excitations in state s_i and s_j by a 50:50 beamsplitter like transformation and heralds on detecting no excitations in the state s_j. This leads to the transformation $|k,k\rangle_{s_i,s_j} \rightarrow |2k,0\rangle_{s_i,s_j}$ with a probability $q_k = \frac{(2k)!}{2^{2k}(k!)^2}$. Using Stirling's approximation, we see that $q_k \sim 1/\sqrt{\pi k} \rightarrow 0$ vanishes for large excitation numbers. The

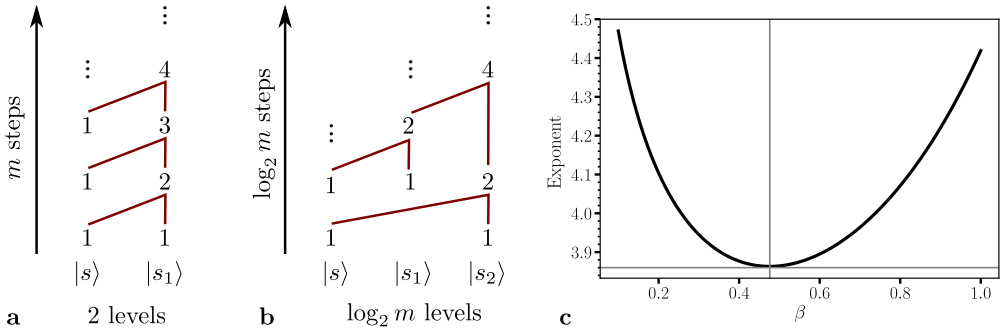

Figure 2.4: **a** The excitations in the metastable states can be merged one by one. This only requires one additional metastable state, but the mean number of steps scales exponentially in the excitation number m to be reached. **b** Alternatively, the excitations in the metastable states can be doubled at each step. This requires additional metastable states, but the mean number of steps scales subexponentially in m. **c** By using number resolving measurements, one can reach a polynomial scaling. The exponent can be minimized by varying the fraction β of excitations that are "lost" after each beamsplitter-like transformation. The horizontal and vertical gray line represent the minimal value of the exponent $\log_{2-\beta}(2/s_\beta)$.

mean number of operations to arrive to a state with m excitations can be calculated recursively through $R_m = q_{m/2}^{-1}\left(1 + 2R_{m/2}\right)$, which scales as

$$R_m \sim \frac{1}{p}\sqrt{m}^{\log_2 m}, \qquad F_m \gtrsim 1 - R_m \max_j \left(1 - F_{j\to j+1}\right). \tag{2.11}$$

Hence, the combination of a logarithmic number of levels with the polynomial decrease of probability leads to a superpolynomial, but subexponential, scaling of R_m with the number of excitations m. It can be shown [172] that by combining the doubling steps with single-mode coherent displacement operations, one can also prepare arbitrary superpositions of single-mode states. Even though the mean number of steps can be reduced a lot by this method, it will also decrease the fidelity because one needs to apply a repumping protocol whenever adding a single excitation fails [3]. We note, that the fidelity can be kept above the fidelity for the photon mapping if one uses the collective decay for the repumping procedure.

If in addition to the linear optics tools, **number resolved detection** in a metastable state is available, one can even reach a polynomial scaling in the mean number of steps. The idea is to try to double the excitations, but to broaden the range of states one keeps. In particular, a state is kept if the excitations in s_j are below a certain fraction β of the original number of excitations k. In that case, one knows that there are at least $(2-\beta)k$ excitations in the other mode. The price to pay is that the number of steps in the tree scales in a less favorable way, $\log_{2-\beta} m$ instead of $\log_2 m$. However, the probability of detecting β excitations, which is given by $s_\beta \approx \int_0^{\beta k/2} \mathrm{d}j \frac{1}{\pi\sqrt{j(k-j)}}$ when the excitation number is large, can be made independent of k, e.g., by choosing $\beta = 1/2$ this probability is $s_{1/2} \approx 1/3$. Combining these features, the average number of steps scales as

$$R_m \sim m^{\log_{2-\beta}(2/s_\beta)}, \tag{2.12}$$

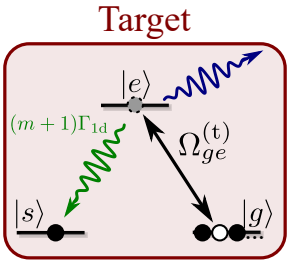

Figure 2.5: For the protocol using coherent driving as described here we require a single guided mode coupling to the $s-e$ transition and a coherent driving on the $g-e$ transition with strength $\Omega_{ge}^{(t)}$.

which is minimized for $\beta \approx 0.476$, leading to a scaling as $R_m \sim m^{3.86}$ (see Figure 2.4c). Thus, by using number resolved detection one can obtain a polynomial scaling in the mean number of operations (see also Reference [173]), which is a big improvement if one wants to scale the protocol to very large excitation numbers.

2.3 Protocols in Detail

Having summarized the main ideas, we devote this section to introducing the main concepts of each protocol. We discuss here only one variant of each protocol and emphasize that by modifying the protocols one can adapt them to much wider parameter ranges and further improve the scalings. These modifications are specific to every protocol and not discussed further here, and we refer the interested reader to References [1, 3, 4].

2.3.1 Probabilistic Protocol using Coherent Driving

Our simplest protocol is inspired by a method originally devised to create long-distant entangled states in atomic ensembles by weakly exciting the atoms and heralding on the detection of a photon emitted when decaying to a metastable state [26]. The emitters are placed in the atomic mirror configuration along the waveguide (see Figure 2.2a) and excited collectively during a short time $T \ll 1/(N_m\Gamma_{1d})$ by an external (or waveguide) field of strength $\Omega_{ge}^{(t)}$ (see Figure 2.5). We assume the state of the target ensemble to already be in a Dicke state $|\psi_m\rangle_t$, either in the metastable state s, which is coupled to the waveguide, or in s_i, which are decoupled, for which then we effectively have $m = 0$ while N_m is unchanged.

We denote the excitation probability from weak driving as $x = \Omega_{ge}^{(t)}\sqrt{N_m}T/2$, so that the state after the pulse is

$$|\psi\rangle_t \propto \left(1 + x\frac{S_{eg}^{(t)}}{\sqrt{N_m}} + x^2\left(\frac{S_{eg}^{(t)}}{\sqrt{N_m}}\right)^2 + \mathcal{O}(x)^3\right)|\psi_m\rangle_t, \tag{2.13}$$

where we have written the normalization $\sqrt{N_m}$ with the operator $S_{eg}^{(t)}$.

After the pulse, we leave the system free to evolve under the interaction with the waveguide for a time $T \gg 1/\Gamma^*$ so that the population of the excited state can be assumed to have completely decayed. The wavefunction of the emitter and the photonic modes (in the waveguide and in free space) at that time is then given by

$$\begin{aligned}|\Psi\rangle_{\mathrm{t}} \propto & |\psi_m\rangle_{\mathrm{t}}|0\rangle_{\mathrm{ph}} + x(1-\delta)|\psi_{m+1}\rangle_{\mathrm{t}}|1\rangle_{\mathrm{ph}} + x\delta|\psi_m^*\rangle_{\mathrm{t}}|1^*\rangle_{\mathrm{ph}} \\ & + x^2(1-2\delta-\delta^2)|\psi_{m+2}\rangle_{\mathrm{t}}|2\rangle_{\mathrm{ph}} + 2x^2\delta|\psi_{m+1}^*\rangle_{\mathrm{t}}|1,1^*\rangle_{\mathrm{ph}} + x^2\delta^2|\psi_m^{**}\rangle_{\mathrm{t}}|2^*\rangle_{\mathrm{ph}},\end{aligned} \tag{2.14}$$

where * in the target ensemble denotes that an incoherent quantum jump to one of the metastable states has happened and for the photonic mode it denotes an occupation of a mode in free space. The spontaneous emission processes occur with a lower probability, $\delta \approx \frac{1}{(m+1)P_{1\mathrm{d}}}$ when the excitations are added directly or $\delta \approx \frac{1}{P_{1\mathrm{d}}}$ when they are stored in an additional metastable state s_i. We remark that there are some small factors related to normalization, that have been left out for the sake of clarity in the expressions. Nevertheless, the conclusions about the scaling of the heralding probability and fidelity hold.

By detecting a photon in the waveguide, we aim to herald on the desired part of the state, the second term, $|\psi_m\rangle_{\mathrm{t}}$. However, due to detecting a photon emitted from states with higher excitations, the heralded state also contains the fourth and the fifth term, which contain one excitation more in the target ensemble. We assume that we can neglect the latter as the probability for this is reduced by $\delta \propto P_{1\mathrm{d}}^{-1}$, that is, the state after heralding is approximately

$$|\psi_{\mathrm{her}}\rangle \approx \frac{1}{\mathcal{N}}\left(|\psi_{m+1}\rangle_{\mathrm{t}} + (1-\eta)x|\psi_{m+2}\rangle\right)\mathrm{t}\right). \tag{2.15}$$

The heralding probability of the heralding measurement (with a photon detector with detection efficiency η) and the fidelity of the heralded state are then given by

$$p_{m\to m+1} \approx \eta x^2 \tag{2.16a}$$

$$1 - F_{m\to m+1} \approx (1-\eta)x \tag{2.16b}$$

As in Reference [26], the error can be made arbitrarily small at the expense of decreasing the heralding probability. If a high fidelity is required the method is practicable only for very few excitations. Apart from the finite detection efficiency $\eta < 1$, the double excitations have turned out to be the main problem of this protocol.

2.3.2 Deterministic Protocol

Instead of exciting the target ensemble by a coherent driving, it is favorable to deterministically add a single excitation to the ensemble. A single emitter naturally acts as a source of a single excitation. When coupled to the waveguide, one can play with the distance of this source emitter to the target ensemble to change the type of interaction between

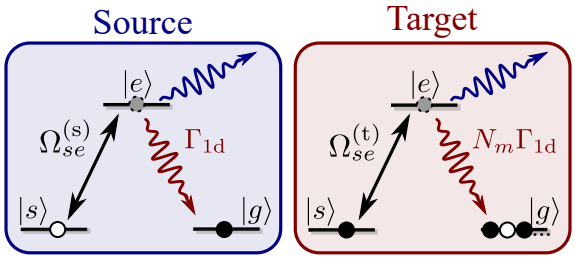

Figure 2.6: In the deterministic protocol, we use a source emitter, which is coupled to the target ensemble either through the collective dissipation or through the coherent flip-flop interaction on the $g-e$ transition. In both ensembles we require a coherent driving on the $s-e$ transition, but with different driving strengths $\Omega_{se}^{(\mathrm{s})}$ and $\Omega_{se}^{(\mathrm{t})}$.

them. As the target ensemble is assumed to be in the atomic mirror configuration, the phase ϕ_{ij} between the source emitter and each emitter in the target ensemble is the same. We focus here on a phase difference of $\phi_{\mathrm{s-t}} = 0 \pmod{2\pi}$ between the source and target ensemble (see Figure 2.2b), i.e., an extension of the atomic mirror configuration. One may as well take $\phi_{\mathrm{s-t}} = \pi \pmod{2\pi}$, which just leads to a slightly different subradiant state but very similar dynamics. At the end of this section we shortly discuss a modification using $\phi_{\mathrm{s-t}} = \pi/2 \pmod{2\pi}$, which is depicted in Figure 2.2c.

In this atomic mirror configuration, the collective dissipation of the source and target ensemble, $S_- = S_{ge}^{(\mathrm{s})} + S_{ge}^{(\mathrm{t})}$, which we assume to be on the transition $g-e$ for this protocol, creates a subspace of subradiant states [124, 125]. This subspace contains all states $|\Psi\rangle$ that are dark with respect to the collective dissipation, i.e., $S_-|\Psi\rangle = 0$. Apart from the states with only population in the metastable states, this subspace contains N_m excited states for every Dicke state with m excitations. As we assume the drivings of the ensembles to be collective, i.e., symmetric in each ensemble, there is only one relevant excited subradiant state, satisfying the symmetry conditions, namely

$$|\Psi_m^{\mathrm{subr}}\rangle = \left(\sqrt{\frac{N_m}{N_m+1}}S_{eg}^{(\mathrm{s})} - \frac{1}{\sqrt{N_m+1}}\frac{S_{eg}^{(\mathrm{t})}}{\sqrt{N_m}}\right)|g\rangle_{\mathrm{s}}|\psi_m\rangle_{\mathrm{t}}. \tag{2.17}$$

This state can be thought of as a generalized singlet state – an antisymmetric combination of either an excitation in the source emitter or the target ensemble with weights depending on the effective number of atoms N_m.

This state can be coupled to the initial state $|\Psi_m^{\mathrm{i}}\rangle = |s\rangle_{\mathrm{s}}|\psi_m\rangle_{\mathrm{t}}$ by an external laser field of strength $\Omega_{se}^{(\mathrm{s})}$ and to the final state $|\Psi_m^{\mathrm{f}}\rangle = |g\rangle_{\mathrm{s}}|\psi_{m+1}\rangle_{\mathrm{t}}$ by an external driving of strength $\Omega_{se}^{(\mathrm{t})}$ (see Figure 2.6). Thus, the full non-hermitian Hamiltonian is given by

$$\begin{aligned} H_{\mathrm{nh}} =& \frac{\Omega_{se}^{(\mathrm{s})}}{2}\left(S_{se}^{(\mathrm{s})} + S_{es}^{(\mathrm{s})}\right) + \frac{\Omega_{se}^{(\mathrm{t})}}{2}\left(S_{se}^{(\mathrm{t})} + S_{es}^{(\mathrm{t})}\right) - \mathrm{i}\frac{\Gamma^*}{2}\left(S_{ee}^{(\mathrm{s})} + S_{ee}^{(\mathrm{t})}\right) \\ & - \mathrm{i}\frac{\Gamma_{1\mathrm{d}}}{2}\left(S_{eg}^{(\mathrm{s})} + S_{eg}^{(\mathrm{t})}\right)\left(S_{ge}^{(\mathrm{s})} + S_{ge}^{(\mathrm{t})}\right) \end{aligned} \tag{2.18}$$

The strong collective decay restricts the evolution to the subspace of subradiant states, the so-called Quantum Zeno Dynamics [140, 171], which leads to an effective three-level

system,

$$|\Psi_m^{\mathrm{i}}\rangle \xleftrightarrow{\sqrt{\frac{N_m}{N_m+1}}\Omega_{se}^{(\mathrm{s})}} |\Psi_m^{\mathrm{subr}}\rangle \xleftrightarrow{-\sqrt{\frac{m+1}{N_m+1}}\Omega_{se}^{(\mathrm{t})}} |\Psi_m^{\mathrm{f}}\rangle. \tag{2.19}$$

To achieve a full population transfer and low errors, one should choose the two effective couplings to be the same $\Omega_m \equiv \sqrt{\frac{N_m}{N_m+1}}\Omega_{se}^{(\mathrm{s})} = -\sqrt{\frac{m+1}{N_m+1}}\Omega_{se}^{(\mathrm{t})}$ so that the excitation is fully transferred at time $T = \pi\sqrt{2}/\Omega_m$. The fidelity of the transfer is not perfect due to two reasons:

- Spontaneous emission at rate Γ^* when populating the excited subradiant state, which leads to an error $\epsilon_* = \frac{T}{4}\frac{\Gamma^*}{2}$, where the factor $\frac{T}{4}$ comes from the integrated population in the excited subradiant state;
- Small population of the superradiant state (that is the symmetric state over the source and target ensemble), to which the initial and final state couple, which leads to an error $\epsilon_{\mathrm{SR}} = \frac{3T}{8}\left(N_m + \frac{N_m+1}{N_m^2}\right)\frac{\Omega_m^2/2}{(N_m+1)\Gamma_{1\mathrm{d}}+\Gamma^*}$, where the factor $\frac{3T}{8}$ comes from the integrated population in the initial and final state.

The coupling strengths and the time of the pulse then have to be chosen such that fidelity is maximal. For this, the couplings have to be chosen large enough so that the subradiant state is populated only during a short time, but at the same time low enough such that the superradiant state is not significantly populated. We are mostly interested in the low excitation limit, so that we continue to work in the limit $N_m \gg m$. By optimizing the driving strength (see Appendix 2.A), we find that for $\Omega_m \approx \sqrt{2\Gamma^*\Gamma_{1\mathrm{d}}/3}$ one can reach the maximal fidelity of (see Figure 2.7)

$$F_{m\to m+1} = \left|\langle\psi_m^{\mathrm{f}}|\mathrm{e}^{-\mathrm{i}H_{\mathrm{nh}}T}|\psi_m^{\mathrm{i}}\rangle\right| \approx \exp\left[-\frac{\pi\sqrt{2}}{4}\frac{1}{\sqrt{\frac{2}{3}P_{1\mathrm{d}}}}\right] \approx 1 - \frac{\pi\sqrt{3}}{4}P_{1\mathrm{d}}^{-1/2}. \tag{2.20}$$

Arbitrary higher excitations can be reached by resetting the source emitter to the metastable state s and transferring the next excitation to the symmetric Dicke state of the target ensemble and repeating this process. Furthermore, one can also prepare any arbitrary superposition of symmetric Dicke states, by alternating between exciting the emitter and transferring the excitation to the target ensemble with an appropriate pulse sequence, as was shown for cavity fields [174]. The appropriate pulse sequence can be found by studying the inverse process, that is, starting from the final state and removing excitations, until one reaches the ground state.

Instead of using the Quantum Zeno Dynamics, one can use coherent flip-flop interactions between the source and target ensemble. To reduce the errors, the source emitter is placed in the middle of the target ensemble, with a phase $\phi_{\mathrm{s-t}} = \pi/2 \pmod{2\pi}$ between the source and target (see Figure 2.2c). This model [37] can be mapped to a cavity

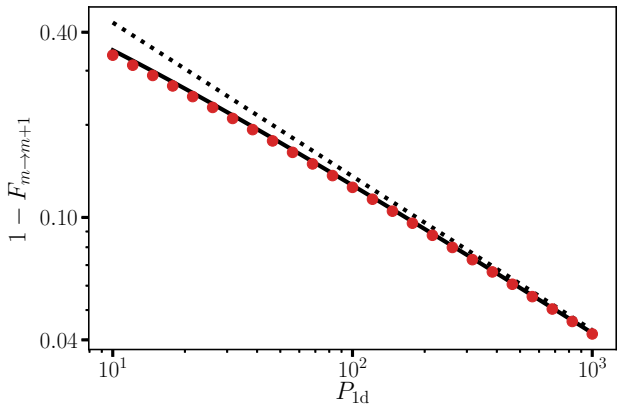

Figure 2.7: The fidelity of the state can be obtained by evolving the initial state with the non-hermitian Hamiltonian of the system for the optimal parameters for different Purcell factors P_{1d} (red dots). The black (black dashed) line shows that the first (and second) approximation in Equation 2.20 works well. We have used the parameters $N_m = 50$ and $m = 0$.

QED configuration, where the source atom plays the role of the TLS with effective decay $\gamma = \Gamma_{1d} + \Gamma^*$ which couples coherently to an effective cavity defined by $\frac{1}{\sqrt{N_m}} S^{(t)}_{eg,+}$, with rate $g = \sqrt{N_m}\Gamma_{1d}$. The cavity mode $S^{(t)}_{eg,+}$ is the symmetric combination between both parts of the split ensemble. The cavity modes are subradiant states, so that the cavity loss is given by $\kappa = \Gamma^*$. This is no longer true when many excitations are stored in the ensemble and is another source of errors. It is known [174] that within the strong nonlinear coupling regime, e.g., when $g \gg \kappa, \gamma$, this model can deterministically generate any arbitrary superposition of the cavity-like mode up to m photons with a fidelity of $F_{m\to m+1} \approx 1 - \frac{m(\kappa+\gamma)}{g} \approx 1 - \frac{m}{\sqrt{N_m}}$.

Even though both these protocols don't suffer from the double excitation problem of the first protocol and no measurement is necessary, they don't reach the desired scaling of the fidelity, $1 - F_{em} \propto m/(NP_{1d})$.

2.3.3 Probabilistic Protocol using Collective Dissipation

To improve the fidelity, one can design a probabilistic protocol, in which a heralding measurement rules out any individual or collective quantum jumps. For this purpose, we introduce a third ensemble in the atomic mirror configuration on which this heralding measurement can be performed, a detector ensemble with N_d emitters (see Figure 2.2d). The heralding measurement checks for population in one of the metastable states, in our case g. Using a cyclic transition, this measurement can be repeated multiple times so that one can assume this measurement to have perfect detection efficiency and to not suffer from dark counts (see Section 0.2.4). We assume here only one detector atom, $N_d = 1$, but in principle all our considerations can be extended to an arbitrary number of emitters

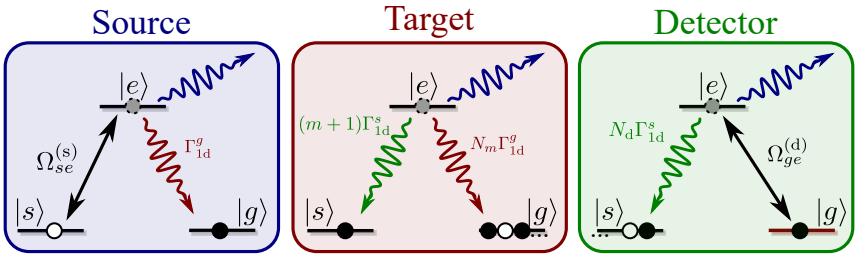

Figure 2.8: For the probabilistic protocols using the Quantum Zeno Dynamics and the coherent flip-flop interactions as described here, we require two guided modes, one on the $s-e$, the other on the $g-e$ transition. Furthermore, we assume that in the source and detector ensemble one of these transitions can be moved out of resonance. A coherent driving on the $s-e$ transition of the source ensemble generates the excitation, that is moved through the target ensemble to the detector ensemble, where a coherent driving on the $g-e$ transition deexcites the emitters. Finally, a heralding measurement is performed on the g state of the emitters in the detector ensemble.

in the detector ensemble.

The idea is to design the interactions in such a way that a transfer of an excitation from the source to the target ensemble also induces a change in the state of the detector ensemble, on which we can herald. This is accomplished, e.g., by using two orthogonal guided modes on the transition $g-e$ ($s-e$) with rates $\Gamma_{1d}^{g(s)}$, as depicted in Figure 2.8, where one of the guided modes in the source and detector ensemble can be decoupled from the guided mode by shifting the levels out of resonance to avoid any undesired transitions. This leads to the emergence of a single subradiant state of both collective dissipation terms, which also satisfies the symmetry conditions in the target ensemble,

$$|\Psi_m^{\text{subr}}\rangle = \frac{1}{\sqrt{N_m+m+2}}\left(\sqrt{N_m}S_{eg}^{(\text{s})} - \frac{S_{eg}^{(\text{t})}}{\sqrt{N_m}} + \sqrt{m+1}S_{es}^{(\text{d})}\right)|g\rangle_{\text{s}}|\psi_m\rangle_{\text{t}}|s\rangle_{\text{d}}. \quad (2.21)$$

This subradiant state is independent of the ratio of decay rates $\Gamma_{1d}^{g/s}$, in contrast to the two orthogonal superradiant states. In addition, the source atom (and the detector ensemble) are driven by external fields on the $s-e$ ($g-e$) transition with strength $\Omega_{se}^{(\text{s})}$ ($\Omega_{ge}^{(\text{d})}$). The full non-hermitian Hamiltonian then reads,

$$\begin{aligned} H_{\text{nh}} =& \frac{\Omega_{se}^{(\text{s})}}{2}\left(S_{se}^{(\text{s})}+S_{es}^{(\text{s})}\right) + \frac{\Omega_{ge}^{(\text{d})}}{2}\left(S_{ge}^{(\text{d})}+S_{eg}^{(\text{d})}\right) - \text{i}\frac{\Gamma^*}{2}\left(S_{ee}^{(\text{s})}+S_{ee}^{(\text{t})}+S_{ee}^{(\text{d})}\right) \\ & - \text{i}\frac{\Gamma_{1d}^{g}}{2}\left(S_{eg}^{(\text{s})}+S_{eg}^{(\text{t})}\right)\left(S_{ge}^{(\text{s})}+S_{ge}^{(\text{t})}\right) - \text{i}\frac{\Gamma_{1d}^{s}}{2}\left(S_{es}^{(\text{t})}+S_{es}^{(\text{d})}\right)\left(S_{se}^{(\text{t})}+S_{se}^{(\text{d})}\right). \end{aligned} \quad (2.22)$$

Analogously to the deterministic case, this leads for weak driving to an effective three-level system

$$|\Psi_m^{\text{i}}\rangle \xleftrightarrow{\sqrt{\frac{N_m}{N_m+2}}\Omega_{se}^{(\text{s})}} |\Psi_m^{\text{subr}}\rangle \xleftrightarrow{-\sqrt{\frac{m+1}{N_m+2}}\Omega_{ge}^{(\text{d})}} |\Psi_m^{\text{f}}\rangle, \quad (2.23)$$

which can transfer an excitation from the initial state $|\Psi_m^{\text{i}}\rangle = |s\rangle_{\text{s}}|\psi_m\rangle_{\text{t}}|s\rangle_{\text{d}}$ to the final state $|\Psi_m^{\text{f}}\rangle = |g\rangle_{\text{s}}|\psi_{m+1}\rangle_{\text{t}}|g\rangle_{\text{d}}$. A full population transfer is achieved for $\sqrt{\frac{N_m}{N_m+2}}\Omega_{se}^{(\text{s})} = -\sqrt{\frac{m+1}{N_m+2}}\Omega_{ge}^{(\text{d})} \equiv \Omega_m$ after a time $T = \pi\sqrt{2}/\Omega_m$.

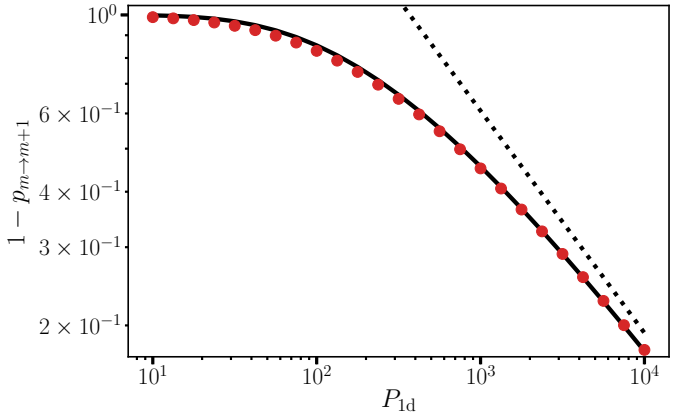

Figure 2.9: The heralding probability of the final state can be obtained by evolving the initial state with the non-hermitian Hamiltonian of Equation 2.22 for the optimal parameters and for different Purcell factors P_{1d} (red dots). The black (black dashed) line shows that the first (and second) approximation in Equation 2.24 works well. We have used the parameters $N_m = 50$ and $m = 0$.

The heralding probability of the heralding measurement on state g of the detector ensemble is reduced by spontaneous emission processes from the subradiant state and populating the superradiant states like for the fidelity in the deterministic protocol (see Section 2.3.2). To reduce the population in the superradiant states, one can in principle optimize the ratio of the decay rates, $\Gamma^s_{1d}/\Gamma^g_{1d}$, but for simplicity we choose here $\Gamma^s_{1d} = \Gamma^g_{1d} \equiv \Gamma_{1d}$. Through a similar optimization as in the previous protocol, one can then find the optimal value of the driving to be $\Omega_m \approx \sqrt{\Gamma^* \Gamma_{1d} \frac{2(m+1)}{3N_m}}$, which leads to a maximal heralding probability of

$$p_{m\to m+1} = |\langle \Psi^f_m | e^{-iH_{nh}T} | \Psi^i_m \rangle|^2 \approx e^{-\frac{\pi\sqrt{3}}{2\sqrt{m+1}}\sqrt{\frac{N_m\Gamma^*}{\Gamma_{1d}}}} \approx 1 - \frac{\pi\sqrt{3}}{2\sqrt{m+1}} (P_{1d}/N_m)^{-1/2} . \quad (2.24)$$

A comparison between the full non-hermitian evolution and this approximation is plotted in Figure 2.9. As this heralding measurement rules out any quantum jumps, the fidelity of the final state will in fact be perfect, i.e. $F_{m\to m+1} = 1$.

Instead of using two orthogonal guided modes, one can replace the single step protocol with two guided modes as described here by a two step protocol using a single guided mode and an additional metastable state as described in References [3, 5]. The results for the scaling of the heralding probability can then be improved to scale as $1 - p_{m\to m+1} \propto P_{1d}^{-1/2}$.

With this probabilistic protocol we are able to exploit the strong collective dissipation in the atomic mirror configuration for the heralded addition of an excitation to an existing symmetric Dicke state. By designing a probabilistic protocol, the large decrease of the fidelity in the deterministic case was transferred to a reduction in the heralding probability. Therefore, one may have to repeat the protocol several times to reach the desired state, but when successful, knows that the state has a high fidelity.

2.3.4 Probabilistic Protocol using Coherent flip-flop Interactions

Recall, that in the deterministic protocol we can replace the Quantum Zeno Dynamics by coherent couplings when the Purcell factor $P_{1\mathrm{d}}$ is not very large. Analogously to this, we can also design a probabilistic protocol, which depends more strongly on the number of emitters N and N_d than on $P_{1\mathrm{d}}$. Inspired by the deterministic protocol in which the source emitter is placed in the middle of the target ensemble (see Figure 2.2c), we concatenate this with the detector ensemble with N_d emitters, that is the source and target are placed in the middle of the split detector ensemble as in Figure 2.2e. Each part of the target (detector) ensemble then contains $N/2$ ($N_\mathrm{d}/2$) emitters.

Analogously to the probabilistic protocol using Quantum Zeno Dynamics, we require two orthogonal guided modes on the transition $g-e$ and $s-e$ with decay rates $\Gamma_{1\mathrm{d}}^{g/s}$, from which the source and detector ensemble can be decoupled (see Figure 2.8). The concatenated configuration induces the coherent couplings

$$H_\mathrm{coll} = \frac{\Gamma_{1\mathrm{d}}^g}{2} S_{ge}^{(\mathrm{s})} S_{eg,+}^{(\mathrm{t})} + \frac{\Gamma_{1\mathrm{d}}^s}{2} S_{se,-}^{(\mathrm{t})} S_{es,-}^{(\mathrm{d})} + \mathrm{h.c.}, \tag{2.25}$$

where the additional indices $\pm$ denote the symmetric (antisymmetric) combination of the parts of the split ensembles. In addition, within each ensemble there are still decay terms, leading to a full non-hermitian Hamiltonian of the form

$$\begin{aligned} H_\mathrm{nh} =& H_\mathrm{coll} + \frac{\Omega_{se}^{(\mathrm{s})}}{2}\left(S_{se}^{(\mathrm{s})} + S_{es}^{(\mathrm{s})}\right) + \frac{\Omega_{ge}^{(\mathrm{d})}}{2}\left(S_{ge}^{(\mathrm{d})} + S_{eg}^{(\mathrm{d})}\right) - \mathrm{i}\frac{\Gamma^*}{2}\left(S_{ee}^{(\mathrm{s})} + S_{ee,+}^{(\mathrm{t})} + S_{ee,+}^{(\mathrm{d})}\right) \\ & - \mathrm{i}\frac{\Gamma_{1\mathrm{d}}^g}{2}\left(S_{eg}^{(\mathrm{s})} S_{ge}^{(\mathrm{s})} + S_{eg,-}^{(\mathrm{t})} S_{ge,-}^{(\mathrm{t})}\right) - \mathrm{i}\frac{\Gamma_{1\mathrm{d}}^s}{2}\left(S_{es,-}^{(\mathrm{t})} S_{se,-}^{(\mathrm{t})} + S_{es,+}^{(\mathrm{d})} S_{se,+}^{(\mathrm{d})}\right). \end{aligned} \tag{2.26}$$

It is more instructive, to consider the states coupled through this Hamiltonian in the low excitation regime, that is

$$\begin{aligned} |\Psi_m^\mathrm{i}\rangle \xleftrightarrow{\Omega_{se}^{(\mathrm{s})}} S_{es}^{(\mathrm{s})}|\Psi_m^\mathrm{i}\rangle \xleftrightarrow{\sqrt{N_m}\Gamma_{1\mathrm{d}}^g} S_{gs}^{(\mathrm{s})}\frac{S_{eg,+}^{(\mathrm{t})}}{\sqrt{N_m}}|\Psi_m^\mathrm{i}\rangle \\ \xleftrightarrow{\sqrt{(m+1)N_\mathrm{d}}\Gamma_{1\mathrm{d}}^s} S_{gs}^{(\mathrm{s})}\frac{S_{eg,+}^{(\mathrm{t})}}{\sqrt{(m+1)N_m}}\frac{S_{eg,-}^{(\mathrm{d})}}{\sqrt{N_\mathrm{d}}}|\Psi_m^\mathrm{i}\rangle \xleftrightarrow{\Omega_{ge}^{(\mathrm{d})}} |\Psi_m^\mathrm{f}\rangle, \end{aligned} \tag{2.27}$$

where the initial and, respectively, final state is defined as $|\Psi_m^\mathrm{i}\rangle = |s\rangle_\mathrm{s}|\psi_m\rangle_\mathrm{t}|s\rangle_\mathrm{d}^{\otimes N_\mathrm{d}}$ and $|\Psi_m^\mathrm{f}\rangle = |g\rangle_\mathrm{s}|\psi_{m+1}\rangle_\mathrm{t}\frac{S_{gs}^{(\mathrm{d})}}{\sqrt{N_\mathrm{d}}}|s\rangle_\mathrm{d}^{\otimes N_\mathrm{d}}$. Note, that we have used here the encoding $|\psi_m\rangle \propto S_{sg,-}^{(\mathrm{t})m}|g\rangle^{\otimes N}$.

A maximal population transfer of the excitation from the source to the detector ensemble via the target ensemble is obtained for tunable decay rates $\Gamma_{1\mathrm{d}}^s = \sqrt{\frac{N_m}{(m+1)N_\mathrm{d}}}\Gamma_{1\mathrm{d}}^g$ and coherent drivings satisfying $\Omega_{se}^{(\mathrm{s})} = \Omega_{se}^{(\mathrm{s})} = \sqrt{2N_m/3}\Gamma_{1\mathrm{d}}^g \equiv \Omega_m$. Note that the ratio of decay rates is of order one when the number of atoms in the target and detector ensemble are comparable, $N_m \approx N_\mathrm{d}$. A tunable decay rate of this order can be easily achieved by

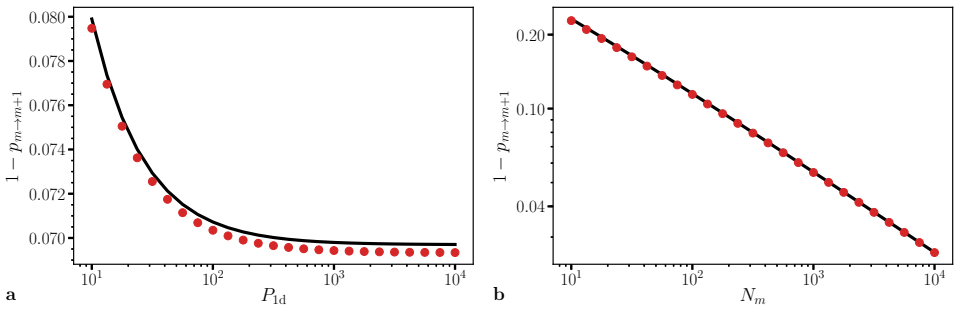

Figure 2.10: The heralding probability of the final state can be obtained by evolving the initial state with the non-hermitian Hamiltonian of the system (red dots) for the optimal parameters for $m = 0$, $N_\mathrm{d} = N_m$ and for **a** different Purcell factors P_1d with $N_m = 10^3$ or **b** different effective emitter numbers N_m with $P_\mathrm{1d} = 10$. The black line shows that the approximation in Equation 2.28 works well. The heralding probability still depends on the Purcell factor, but the dependence on N_m is much more relevant.

off-resonant drivings, that renormalize the decay rates (see Section 0.3.3). After a time of evolution $T = 2\pi/\Omega_m$ the population is transferred completely from the initial to the final state. The probability of the successful heralding measurement is then

$$p_{m\to m+1} \approx \exp\left[-\frac{\sqrt{3}\pi}{32\sqrt{2N_m}}\left(10 + 9\sqrt{\frac{N_m(m+1)}{N_\mathrm{d}}} + 29P_\mathrm{1d}^{-1}\right)\right], \tag{2.28}$$

where $P_\mathrm{1d} = \Gamma_\mathrm{1d}^g/\Gamma^*$. The scaling originates from the fact that the process is very fast, $T \propto N_m^{-1/2}$, and that the non-hermitian terms, which lead to the reduction of the heralding probability, scale with Γ_1d^g and $(m+1)\Gamma_\mathrm{1d}^s = \sqrt{\frac{N_m(m+1)}{N_\mathrm{d}}}\Gamma_\mathrm{1d}^g$. The prefactors in the exponential in front of each term arise from the population of the specific states which are subject to the respective quantum jumps. The above expression is a good approximation of the real heralding probability, which can be obtained through evolution under the non-hermitian Hamiltonian as shown in Figure 2.10. Other choices for the parameters, in particular the ones allowing for $\Gamma_\mathrm{1d}^g = \Gamma_\mathrm{1d}^s$, may also lead to a sufficiently high heralding probability and fidelity. These variations are discussed in Reference [4].

The fidelity for adding the first excitation is perfect, $F_{0\to1} = 1$ but for higher excitations the non-hermitian Hamiltonian couples to more states than just the ones of Equation 2.27. We investigated these deviations from the approximation numerically and found that they reduce the total fidelity by

$$1 - F_m \approx 0.045\left(\frac{m}{N}\right)^{1.9}. \tag{2.29}$$

Notably, the fidelity is independent of the Purcell factor because transitions to unwanted states happen through the excited states which are exposed to individual decay in the same manner.

With this protocol we are able to obtain high fidelities in systems with a low Purcell

factor P_{1d} by a more complex setup and larger number of emitters in the target and detector ensemble.

2.4 Discussion of Required Resources

The different protocols are useful for different experimental platforms, that is, for different resources in the waveguide QED system. We summarize here the conditions and figures of merit for each protocol and identify the best ones contingent upon the available resources (see Section 0.2.2).

- The first protocol discussed here [3] requires $NP_{1d} \gg 1$ and the use of an external single photon detector. The protocol heralds the transfer of single collective excitations with probability $p_{m\to m+1}$, which has a trade-off with the fidelity, which scales as $1 - F_{m\to m+1} \propto \sqrt{p_{m\to m+1}}$. This protocol is especially suited for generating low excitation numbers in systems with either a large Purcell factor P_{1d} or systems with low Purcell factor $P_{1d} < 1$ and large atom number N like current experimental setups for optical fibers.

- In the second protocol [1] we introduced a deterministic protocol ($p_{m\to m+1} = 1$) which also requires a large Purcell factor $P_{1d} \gg 1$ and has a fidelity of $F_{m\to m+1} \approx 1 - 1/\sqrt{P_{1d}} + \mathcal{O}(P_{1d}^{-1})$. This protocols is well suited for engineered dielectrics or, in general, any system with large Purcell factor $P_{1d} \gg 1$. They can also be extended to low mode cavity QED systems if the same conditions hold, i.e., if one works in the bad-cavity limit and has an auxiliary atom which can be addressed independently from the target ensemble.

- The third protocol [3, 5], also exploits the long-range dissipative coupling for equally spaced atoms and requires a large Purcell factor $P_{1d} \gg 1$. The advantage is that the probability of heralding a single collective excitation $p_{m\to m+1} \propto e^{-\alpha/\sqrt{P_{1d}}}$ can be made close to 1 for systems with a Purcell factor $P_{1d} \gg 1$. Moreover, the infidelity of accumulating m excitations is strictly $F_{m\to m+1} = 1$. This is certainly the best suited method in terms of fidelities but to obtain high probabilities we require systems with $P_{1d} \gg 1$.

- The last protocol [4] allows one to overcome the limitations of the probabilities for systems with low Purcell factor P_{1d}, by using a more elaborate configuration of emitter positions. The heralding probability of a single collective excitation is mostly dependent on the number of atoms N, i.e., $p_{m\to m+1} \propto e^{-\alpha\sqrt{m/N}}$ and the average fidelity to accumulate m excitations, though not being 1, is still quite large, $1 - F_m \propto (m/N)^{1.9}$. This is probably the best method for optical fiber setups.

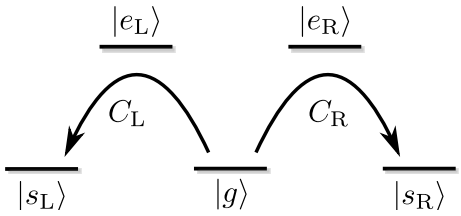

Figure 2.11: For the preparation of symmetric Dicke states over two modes, we require a more elaborate level scheme. For two modes, we can simply mirror the three-level system to obtain an inverted W-type level system. The effect of the protocols on the target ensemble for generating a single excitation in $s_{\mathrm{L/R}}$ are denoted by $C_{\mathrm{L/R}}$.

2.5 Preparation of Multi-Mode Dicke States

Up to now we have developed different methods to prepare a collective excitation in the target ensemble in one specific metastable state that can be triggered to emit the desired photonic state in a single mode. An exciting prospect consists of extending these protocols to generate entangled states of several atomic excitations that can afterwards be triggered to emit, e.g., into orthogonal polarization modes of the waveguide (see Section 1.2). This will enlarge the set of photonic states that can be prepared.

The goal of this section is to extend our protocols for adding a single excitation $|\psi\rangle_\mathrm{t} \rightarrow S_{sg}^{(\mathrm{t})}|\psi\rangle_\mathrm{t}$ to adding a single excitation over two modes in a heralded way, i.e.

$$|\psi\rangle_\mathrm{t} \rightarrow (c_\mathrm{L} S_{s_\mathrm{L}g}^{(\mathrm{t})} + c_\mathrm{R} S_{s_\mathrm{R}g}^{(\mathrm{t})})|\psi\rangle_\mathrm{t} \tag{2.30}$$

with $|c_\mathrm{L}|^2 + |c_\mathrm{R}|^2 = 1$. The index L/R denotes, e.g., the transition coupled to left/right circularly polarized photons. Clearly, this requires a more elaborate level structure, which we now assume to form an inverted W-system (see Figure 2.11). We show how to extend the previous protocols for the heralded generation of a single collective excitation in one metastable state to the case of adding a superposition to two metastable states. Furthermore, we show how this extension works on the example of three photonic states known to be of metrological interest.

2.5.1 Generalization of Protocols

As discussed in Section 2.4, the "best" protocol for adding a single excitation to one metastable state depends on the given experimental waveguide QED resources. The choice of protocol used, however, is irrelevant for the extension that we perform here. We just note, that we focus on directly adding an excitation to the two metastable states, that is we don't require any additional states. For simplicity of notation, we assume that we work in the low excitation regime, in which the Holstein-Primakoff Approximation [132] can be applied, and we approximate the collective spin operators by bosonic operators, i.e., $b_{\mathrm{L/R}}^\dagger \approx S_{s_{\mathrm{L/R}}g}^{(\mathrm{t})}/\sqrt{N}$. We have shown that one can transfer a single excitation from the source atom collectively to the $s_{\mathrm{L/R}}$ state in the target ensemble while inducing a change

in the detector ensemble, from $s_{\mathrm{L/R}}$ to g. We denote this operation as

$$\hat{C}_{\mathrm{L/R}} : |s_{\mathrm{L/R}}\rangle_{\mathrm{s}}|\psi\rangle_{\mathrm{t}}|s_{\mathrm{L/R}}\rangle_{\mathrm{d}} \rightarrow |g\rangle_{\mathrm{s}} b^{\dagger}_{\mathrm{L/R}}|\psi\rangle_{\mathrm{t}}|g\rangle_{\mathrm{d}} + \ldots |s_{\mathrm{L/R}}\rangle_{\mathrm{d}}, \tag{2.31}$$

where we are not writing explicitly the state of the source and target ensemble if some error occurs in the heralding step. For notational simplicity, we write the state of the detector ensemble as if it only contained one emitter, whereas it can actually contain N_{d} emitters. All other possible initial states during the protocol will not change under $\hat{C}_{\mathrm{L/R}}$. It is important to emphasize that the measurement is not performed after each $\hat{C}_{\mathrm{L/R}}$ but just after both operations have been applied as otherwise the superposition would be destroyed.

The protocol starts by preparing a superposition state in the source atom, i.e., $c_{\mathrm{L}}|s_{\mathrm{L}}\rangle_{\mathrm{s}} + c_{\mathrm{R}}|s_{\mathrm{R}}\rangle_{\mathrm{s}}$. The states in the target ensemble are assumed to be in a given state, $|\psi\rangle_{\mathrm{t}}$, which may already contain excitations in the metastable state $s_{\mathrm{L/R}}$. The steps of the protocol can be summarized as follows:

i) We start by transferring one of the states, e.g., s_{L}. For that, we prepare the detector atoms in s_{L} as well, and apply $\hat{C}_{\mathrm{L}}$ such that

$$\begin{aligned} &\left(c_{\mathrm{L}}|s_{\mathrm{L}}\rangle_{\mathrm{s}} + c_{\mathrm{R}}|s_{\mathrm{R}}\rangle_{\mathrm{s}}\right)|\psi\rangle_{\mathrm{t}}|s_{\mathrm{L}}\rangle_{\mathrm{d}} \\ &\xrightarrow{\hat{C}_{\mathrm{L}}} c_{\mathrm{L}}|g\rangle_{\mathrm{s}} b^{\dagger}_{\mathrm{L}}|\psi\rangle_{\mathrm{t}}|g\rangle_{\mathrm{d}} + c_{\mathrm{R}}|s_{\mathrm{R}}\rangle_{\mathrm{s}}|\psi\rangle_{\mathrm{t}}|s_{\mathrm{L}}\rangle_{\mathrm{d}} + \ldots |s_{\mathrm{L}}\rangle_{\mathrm{d}} \end{aligned} \tag{2.32}$$

ii) For the orthogonal mode, we need to transfer the excitation in s_{L} to s_{R} in the detector ensemble to be able to herald the excitation in g at the end. Furthermore, the excitations in g should be transferred to s_{L} so that they don't influence the dynamics. The state after these transformations is then

$$\rightarrow c_{\mathrm{L}}|g\rangle_{\mathrm{s}} b^{\dagger}_{\mathrm{L}}|\psi\rangle_{\mathrm{t}}|s_{\mathrm{L}}\rangle_{\mathrm{d}} + c_{\mathrm{R}}|s_{\mathrm{R}}\rangle_{\mathrm{s}}|\psi\rangle_{\mathrm{t}}|s_{\mathrm{R}}\rangle_{\mathrm{d}} + \ldots |s_{\mathrm{R}}\rangle_{\mathrm{d}}. \tag{2.33}$$

iii) Now, one can apply $\hat{C}_{\mathrm{R}}$ which results in

$$\xrightarrow{\hat{C}_{\mathrm{R}}} c_{\mathrm{L}}|g\rangle_{\mathrm{s}} b^{\dagger}_{\mathrm{L}}|\psi\rangle_{\mathrm{t}}|s_{\mathrm{L}}\rangle_{\mathrm{d}} + c_{\mathrm{R}}|g\rangle_{\mathrm{s}} b^{\dagger}_{\mathrm{R}}|\psi\rangle_{\mathrm{t}}|g\rangle_{\mathrm{d}} + \ldots |s_{\mathrm{R}}\rangle_{\mathrm{d}}. \tag{2.34}$$

iv) Now the excitations have been added but each of them are associated to two different metastable states in the detector atoms. In order to be able to herald them at the same time, one needs to apply a 50:50 beamsplitter-like transformation between the states s_{L} and g states of the detector such that

$$\rightarrow |g\rangle_{\mathrm{s}} \frac{1}{\sqrt{2}} \left(c_{\mathrm{L}} b^{\dagger}_{\mathrm{L}} + c_{\mathrm{R}} b^{\dagger}_{\mathrm{R}}\right)|\psi\rangle_{\mathrm{t}}|g\rangle_{\mathrm{d}} + \ldots |s_{\mathrm{L}}/s_{\mathrm{R}}\rangle_{\mathrm{d}}. \tag{2.35}$$

After the last operation, one can herald the transfer of excitation by measuring the state g of the detector atoms as desired.

We emphasize here again that the measurement has to be performed after both operations to avoid destroying the superpositions between the metastable states. Furthermore, we point out that in case no excitation has been detected in g, one can still measure the state s_{L} of the detector ensemble, and if this heralding is successful one would have generated the state $\frac{1}{\sqrt{2}}\left(c_{\mathrm{L}}b_{\mathrm{L}}^{\dagger}-c_{\mathrm{R}}b_{\mathrm{R}}^{\dagger}\right)|\psi\rangle_{\mathrm{t}}$. Depending on the goal state, this state can still be useful and one would avoid a reduction in the probability by a factor of 2. The heralding probability scales in the same way as for the single-mode preparation, as the operation is only applied twice compared to once for single-mode states with a factor of $\frac{1}{2}$ for some states.

2.5.2 Examples of Metrological Interest

One of the main motivations to obtain two-mode multiphoton states of light is the possibility of measuring phases, φ, beyond the classical limits of light. It is well known that classical sources can only achieve the so-called Standard Quantum Limit , i.e., $\Delta\varphi \propto \frac{1}{\sqrt{M}}$ with M being the number of photons. However, certain two-mode states of light can show a higher precision, and even reach the Heisenberg limit, that is, $\Delta\varphi \propto \frac{1}{M}$. In this Section, we see how one can obtain some of these states of metrological interests using our protocols.

The simplest states to obtain are the so-called Holland-Burnett states [175, 152, 92], which are obtained by applying a beamsplitter transformation on a dual Fock state $|\psi_{\mathrm{HB}}\rangle = U_{\mathrm{BS}}|m,m\rangle$, i.e. $M = 2m$, which can be shown to achieve a precision given by $\Delta\varphi = \frac{1}{\sqrt{M(1+M/2)}}$. As dual Fock states are separable states we can obtain them by simply applying our protocols in the two metastable states $s_{\mathrm{L/R}}$ separately or, even simpler, from two different ensembles (see also Section 1.3).

Another class of non-classical states with improved precision are Yurke states, i.e., $|\psi_{\mathrm{Yurke}}\rangle = \left(|m,m-1\rangle + |m-1,m\rangle\right)/\sqrt{2}$, where $M = 2m-1$. This states do not reach the Heisenberg limit, but scale in the same way, i.e., $\Delta\varphi = \frac{2}{M}$ [176] (at least when $\varphi \approx 0$). We note, that the Yurke state can be written as

$$|\psi_{\mathrm{Yurke}}\rangle = \frac{1}{\sqrt{2}(n-1)!}(b_{\mathrm{L}}^{\dagger}+b_{\mathrm{R}}^{\dagger})b_{\mathrm{L}}^{\dagger n-1}b_{\mathrm{R}}^{\dagger n-1}|0,0\rangle_{s_{\mathrm{L}},s_{\mathrm{R}}}. \tag{2.36}$$

We note here, that the factor of 2 we mentioned for the general protocol can be avoided here because the state $|m,m-1\rangle - |m-1,m\rangle$ can be transformed to the Yurke state by a simple phase shift operator $\exp(-\mathrm{i}\pi b_{\mathrm{L}}^{\dagger}b_{\mathrm{L}})$. As the dual Fock states can be generated efficiently with our protocols, one only needs to add one single excitation over the two metastable states at the end. Other proposals for the generation of Yurke states using linear optical setups, e.g., by photon subtraction [177], can also be implemented by using the transitions between metastable states.

Finally, NOON states $|\psi_{\mathrm{NOON}}\rangle = |m::0\rangle = \left(|m,0\rangle + |0,m\rangle\right)/\sqrt{2}$, that is $M = m$, are the only ones that reach the Heisenberg limit of $\Delta\varphi = \frac{1}{M}$. Using the fundamental theorem

of algebra they can be written as

$$|n::0\rangle = \frac{1}{\sqrt{2n!}}(b_{\mathrm{L}}^{\dagger n} + b_{\mathrm{R}}^{\dagger n})|0,0\rangle_{s_{\mathrm{L}},s_{\mathrm{R}}} = \prod_{j=1}^{n}(b_{\mathrm{L}}^{\dagger} + \mathrm{e}^{\mathrm{i}\varphi_j} b_{\mathrm{R}}^{\dagger})|0,0\rangle_{s_{\mathrm{L}},s_{\mathrm{R}}} \tag{2.37}$$

with $\varphi_j = 2\pi j/n$. Thus by adding excitations one-by-one over two modes with the appropriate phase, one can generate these states using the extension of our protocol in an exponential number of steps. In Reference [178], it is shown, that one can "double" a NOON-state, that is joining two states of the form $|m::0\rangle$ to obtain $|2m-2::0\rangle$ by heralding on a twofold detector coincidence measurement. By using this method together with the metastable states acting as quantum memories, one can obtain NOON-states in a super-polynomial, but subexponential, mean number of steps. This is very similar to the single-mode scheme, where the probability of joining the two states is $\frac{2}{16\cdot 4^{n-1}}\binom{2n-2}{n-1} \approx \frac{1}{8\sqrt{\pi(n-1)}}$. As the phases when adding or doubling states to obtain a NOON-states are very important, the single-mode scheme for a polynomial scaling of the mean number of steps cannot easily be extended to two modes.

2.6 Conclusion and Outlook

Dicke states of ensembles are highly entangled states, robust to particle loss, and when coupled to a one-dimensional waveguide in the atomic mirror configuration, also valuable for the generation of photonic states (see Chapter 1). However, large ensembles behave like a linear system, making the preparation of symmetric Dicke states with a specified excitation number difficult. We have put forward several state preparation protocols, deterministic as well as probabilistic ones, which exploit the tools available in waveguide QED systems. We required the fidelity of the prepared state to scale at least as good as the fidelity of the subsequent photon generation. This led to several variants of the protocols, which have their advantages and disadvantages for a given experimental setup. Furthermore, these protocols were extended to prepare symmetric Dicke states over multiple metastable levels, which can be used for the direct generation of entangled two-mode photonic states.

The first protocol we introduced only required one ensemble in the atomic mirror configuration, which is driven and thus excited weakly by a laser field. The required trapping of atoms in the atomic mirror configuration close to optical nanofibers and photonic crystal waveguides is already possible [59, 179]. Furthermore, the simplicity of the setup makes the first protocol the most viable near-future candidate for the implementation of our methods for the generation of multiphoton states. On the other hand, it is limited to few excitation numbers, which can be overcome by protocols using one or many auxiliary quantum emitters as a source and detector for collective excitations in the target ensemble. Because of the simple trapping conditions, the protocols based on the atomic mirror configuration, are conceptually simple extensions of the first protocol. Satisfying the trapping conditions for coherent flip-flop interactions between ensembles appears to be more challenging, and also requires significantly more quantum emitters. We emphasize,

that the probabilistic protocols studied here only demonstrate the basic principles and the scalings can be improved by modifying the protocols as we propose in References [3, 4, 5].

Further improvements of the protocols can be achieved by finding simpler or more robust protocols for merging excitations in the metastable levels. This problem is very similar to merging photonic states with beamsplitters and heralding on no detection events [85], but the "photons" are the collective excitations in a metastable state, which act as a quantum memory. In principle, one could also use flip-flop interactions if the target ensemble wouldn't be in the atomic mirror configuration. This has not been investigated yet, but could lead to dynamics that are useful for state preparation.

Coming back to our atomic mirror setup, one can think of preparing collective states of the ensemble other than superpositions of symmetric Dicke states and investigate their usefulness for quantum applications. As an example, take the spin squeezed states, which can enhance the sensitivity of atomic interferometers [161]. These symmetric states have a reduced uncertainty in the excitation number (basically S_z) in exchange for a higher uncertainty in S_y. The squeezing of the collective spin state can be implemented by first exciting the ensemble collectively to the desired mean number of excitations and subsequently performing a quantum non-demolition measurement of the excitation number of the ensemble [180, 64]. We emphasize, that such a spin squeezed state does not emit a squeezed coherent photonic state, because the reduced uncertainty is not in one of the quadratures, but in the photon number. Future applications of these states need to be investigated.

Appendix

2.A Optimization Procedure in Detail

For most protocols of Section 2.3 we required an optimization procedure for maximizing the fidelity or the heralding probability. We show here the main steps of this procedure on the example of the deterministic protocol.

We first check the conditions on the ratio of coupling strengths $\Omega_{se}^{(\mathrm{s})}$ and $\Omega_{se}^{(\mathrm{t})}$ and optimal time of interaction T for a full population transfer from the initial to the final state when the decay terms can be neglected. We find that the coupling strengths in the effective three level system should be equal , $\Omega_m \equiv \sqrt{\frac{N_m}{N_m+1}}\Omega_{se}^{(\mathrm{s})} = -\sqrt{\frac{m+1}{N_m+1}}\Omega_{se}^{(\mathrm{t})}$, such that after a time $T = \pi\sqrt{2}/\Omega_m$ the excitation is transferred (see Figure 2.12a). The reduction in fidelity then comes from two factors:

- Spontaneous emission at rate Γ^* when populating the excited subradiant state, which leads to an error $\epsilon_* = \frac{T}{4}\frac{\Gamma^*}{2}$, where the integrated population in the excited subradiant state, $\frac{T}{4}$, is multiplied by the rate of spontaneous emission processes;
- Populating the superradiant states, to which the initial and final state couple, leads to an error of

$$\begin{aligned}\epsilon_{\mathrm{SR}} &\approx \frac{3T}{8}\frac{1}{(N_m+1)\Gamma_{1\mathrm{d}}+\Gamma^*}\frac{1}{2}\left(\frac{1}{N_m}\Omega_{se}^{(\mathrm{s})2}+\frac{N_m(m+1)}{N_m+1}\Omega_{se}^{(\mathrm{t})2}\right)\\ &\approx \frac{3T}{16}\frac{N_m\Omega_m^2}{(N_m+1)\Gamma_{1\mathrm{d}}+\Gamma^*},\end{aligned} \tag{2.38}$$

  where the factor $\frac{3T}{8}$ comes from the integrated population in the initial and final state and the prefactors in front of the Rabi couplings from the coupling to the superradiant state.

The fidelity of the state at time T can thus be approximated by

$$F_{m\to m+1} \approx \exp\left[-(\epsilon_* + \epsilon_{\mathrm{SR}})\right] = \exp\left[-\frac{\pi\sqrt{2}}{8\Omega_m}\left(\Gamma^* + \frac{3}{2}\frac{N_m\Omega_m^2}{(N_m+1)\Gamma_{1\mathrm{d}}+\Gamma^*}\right)\right], \tag{2.39}$$

which is plotted in Figure 2.12b. To maximize the fidelity, we choose the effective coupling $\Omega_m^{\mathrm{opt}} \approx \sqrt{2\Gamma^*\Gamma_{1\mathrm{d}}/3}$, where we have assumed to work in the low excitation regime $N_m \gg m$.

At this optimal driving, we find a fidelity of

$$F_{m\to m+1} \approx \exp\left[-\frac{\pi\sqrt{2}}{4}\frac{1}{\sqrt{\frac{2}{3}P_{1\mathrm{d}}}}\right] \approx 1 - \frac{\pi\sqrt{3}}{4}P_{1\mathrm{d}}^{-1/2}. \tag{2.40}$$

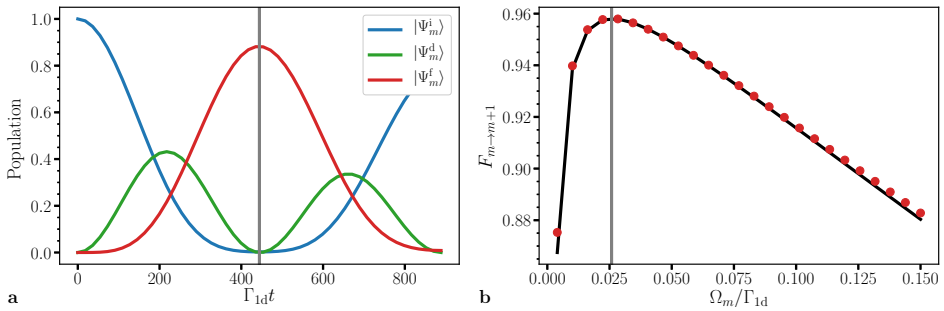

Figure 2.12: **a** The population in the target state $|\Psi_m^{\mathrm{f}}\rangle$ (red line) builds up from the initial state $|\Psi_m^{\mathrm{i}}\rangle$ (blue line) over the subradiant state $|\Psi_m^{\mathrm{d}}\rangle$ (green line) and is maximal after the time $T = \pi\sqrt{2}/\Omega_m$ (gray line). We plotted the time evolution for the parameters $N_m = 100$, $m = 0$, $P_{1\mathrm{d}} = 10^3$ and $\Omega_m = 0.01$. **b** At the time T the fidelity (red dots) is well approximated by the expression of Equation 2.39 (black line) and is maximal when the coupling satisfies $\Omega_m = \Omega_m^{\mathrm{opt}}$ (gray line). We have used the same parameters as for the time evolution, evaluated the state at $T = \pi\sqrt{2}/\Omega_m$, and only varied the coupling strength Ω_m.

Photon Scattering in the Ultrastrong Coupling Regime

3

Abstract

In the ultrastrong coupling regime the coupling strength between the emitter and the photons is comparable to the transition energy, $g \sim \Delta$. In this regime, new features in the light-matter interaction emerge and lead to new applications using, e.g., large nonlinearities induced by the emitter [45] and the generation of non-classical states of light [181, 182]. However, the theoretical description of phenomena in this regime is limited because many tools used in the regime $g \ll \Delta$ – like the Rotating Wave Approximation – can no longer be applied.

One of the theoretical tools available is a polaron transformation with a subsequent minimization of the ground state energy. This transformation is useful because it removes most of the qubit-photon entanglement in the ground state for moderate coupling strengths. The polaron transformation has proven to be useful, both for numerical simulations with matrix product states [42] and for analytical predictions of the single photon scattering amplitude [120]. Our contribution is the extension to the two photon scattering amplitude, which is essential to understand the photon-photon interactions induced by the emitter. We provide tools for the calculation of the scattering amplitude for arbitrary couplings and energy dispersion relations and, more importantly, when additional photon interaction terms coming from the polaron transformation are present. We show that this approach yields good qualitative and quantitative results for moderate coupling strengths.

In the following, we first motivate the importance of understanding scattering processes and introduce the basic concepts (Section 3.1). Then, we introduce the polaron transformation and find a set of self-consistent equations for the variational parameters (Section 3.2). Next, we derive the scattering amplitude for one and two photons on a single quantum emitter (Section 3.3) and compare these predictions to results obtained numerically in the polaron frame (Section 3.4). Finally, we summarize and discuss future perspectives (Section 3.5).

This chapter is based on and uses parts of Reference

- [6]: V. Paulisch, T. Shi, and J. J. García-Ripoll. "Multiphoton Scattering in the Ultrastrong coupling regime" *In preparation.* (2018).

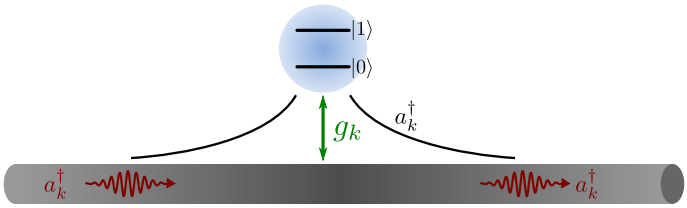

Figure 3.1: A single emitter is coupled to waveguide modes with strength g_k. The ground state of the ultrastrongly coupled system, is a qubit-photon dressed state localized in space around the emitter. The ground state far away from the emitter contains no photons.

3.1 Motivation and Basic Concepts

Up to this point, we have treated waveguide QED systems in a regime, where the light-matter coupling strength exceeds the rate of decoherence processes but is much smaller than the transition energies of the emitters. In this regime, the Rotating Wave Approximation (RWA) [28] can be applied because the exchange of interactions between light and matter dominates over pair creation and annihilation processes. Under this approximation, the counterrotating terms $\sigma_+^j a_k^\dagger + \sigma_-^j a_k$ in Equation 0.1 are dropped and in addition to the energy, the excitation number $\hat{N} = \sum_j \sigma_{ee}^j + \sum_k a_k^\dagger a_k$ is conserved. These two conserved quantities make the theoretical description much easier as one can solve each excitation sector independently.

On the other hand, the desire to reduce interaction times and increase nonlinearities [43, 44, 45] has lead to higher and higher coupling strengths up to a point where the RWA, and theoretical methods based on it, break down [41, 42]. This so-called ultrastrong coupling regime was first observed in superconducting resonator systems [32, 33] and recently even in superconducting waveguide QED systems [83]. For the ultrastrong coupling regime in resonators a generalized RWA was proposed [183] and one can find the spectrum analytically [184]. For waveguide QED systems on the other hand, there are only few theoretical tools available yet, so that one has mostly relied on numerical simulations, e.g., with matrix product states [42, 185] or the renormalization group [186].

Furthermore, we need to relate theoretical predictions to experimental results to check how far the they are valid. Scattering processes are a way to bridge the gap between experiment and theory as they are typically easy to prepare and measure. In addition, one can reconstruct system properties, like the scattering matrix, from the scattering of coherent states [141]. In the regime where $g \ll \Delta$ the scattering of photons is well understood and analytical results have been found with various techniques – using the wavefunctions directly [187, 188], input-output-theory [189, 190], path integral formalism [191, 144] or diagrammatic approaches [192, 193, 194]. In the ultrastrong coupling regime it has proven useful to combine a polaron transformation with scattering theory to predict the reflection and transmission coefficients for the scattering of a single photon on a single quantum emitter at moderate coupling strength [120].

Because analyzing processes in the ultrastrong coupling regime is already difficult

enough, we restrict our discussion here to a single quantum emitter coupled only to the one-dimensional photonic environment, that is without any decay into other modes (see Figure 3.1). The light-matter Hamiltonian (compare to Equation 0.1) is then given by

$$H = \frac{\Delta}{2}\sigma_z + \sum_k \omega_k a_k^\dagger a_k + \sum_k g_k \sigma_x \left(a_k^\dagger + a_k\right), \tag{3.1}$$

where Δ is the qubit energy, ω_k the dispersion relation, a_k the annihilation operator of a photonic mode in the waveguide and g_k the coupling strength between them. We use here the Pauli matrices $\sigma_{x/z}$, which relate to the notation in the first chapters as $\sigma_x = \sigma_{eg} + \sigma_{ge}$ and $\sigma_z = \sigma_{ee} - \sigma_{gg}$.

The dispersion relation ω_k and the coupling g_k depend on the underlying microscopic model, and we assume here an approximately linear dispersion around the qubit frequency and an environment with ohmic spectral density, such that $g_k = \sqrt{\pi\alpha\omega_k/2L}$. Recall from Section 0.3.1, that the transition to ultrastrong coupling occurs around $\alpha \sim 0.01$. For the numerical results, we take a modulus sine dispersion relation $\omega_k = \omega_c \left|\sin(k \cdot \delta x/2)\right|$ with a hard ultraviolet cutoff ω_c. This cutoff is related to the discretization δx of the waveguide because we assume linear dispersion around the transition energy $\Delta \ll \omega_c$, where $\omega_k \approx k \cdot \omega_c \delta_x/2$. Because we have set the speed of light in the medium $c \equiv 1$, we require $\omega_c \delta_x/2 = 1$. For the analytical results it is often favorable to work in a continuum model with perfect linear dispersion $\omega_k = |k|$ and a smooth exponential cutoff in the coupling, $g(k) = \sqrt{\pi\alpha\omega/2}\mathrm{e}^{-\omega/2\omega_c}$. We explained how to go from the discrete to the continuum description in Section 0.3.1.

As in Reference [120], we study the scattering between asymptotically free photonic states, from an initial state $|\psi_\mathrm{i}\rangle$ to a final state $|\psi_\mathrm{f}\rangle$. The scattering amplitude between these two asymptotically free states is defined as

$$S_{\mathrm{f;i}} = \lim_{t_{\mathrm{f,i}} \to \pm\infty} \mathrm{e}^{\mathrm{i}E_\mathrm{f} t_\mathrm{f}} \langle\psi_\mathrm{f}| \mathrm{e}^{-\mathrm{i}H(t_\mathrm{f} - t_\mathrm{i})} |\psi_\mathrm{i}\rangle \mathrm{e}^{-\mathrm{i}E_\mathrm{i} t_\mathrm{i}}, \tag{3.2}$$

where the energies $E_{\mathrm{f/i}}$ are the respective eigenenergies far away from the emitter, i.e., $E_{\mathrm{f/i}}|\psi_{\mathrm{f/i}}\rangle = H_0|\psi_{\mathrm{f/i}}\rangle$. For finding an analytical expression, the scattering amplitude is typically expressed in the interaction picture with respect to H_0, i.e.,

$$S_{\mathrm{f;i}} = \langle\psi_\mathrm{f}|\mathcal{T} \exp\left[-\mathrm{i}\int_{-\infty}^{\infty} \mathrm{d}t\ V(t)\right] |\psi_\mathrm{i}\rangle, \tag{3.3}$$

where the interaction term $V = H - H_0$ is taken in the interaction picture, that is, $V(t) = \mathrm{e}^{\mathrm{i}H_0 t} V \mathrm{e}^{-\mathrm{i}H_0 t}$ and $\mathcal{T}$ is the time ordering operator.[8]

3.2 Polaron Transformation

The polaron transformation is a transformation based on the Lang-Firsov transformation [195], which displaces the electromagnetic field depending on the state of the emitter. The

[8] The time ordered product of two commuting operators is defined as $\mathcal{T}O(s_1)O(s_2) = \Theta(s_1 - s_2)O(s_1)O(s_2) + \Theta(s_2 - s_1)O(s_2)O(s_1)$ with Θ the Heaviside step function.

variational polaron transformation [196, 197] was originally used to study the ground state of the spin-boson model [198, 199]. Interestingly, this transformation removes most of the qubit-photon entanglement in the ground state of the polaron transformed Hamiltonian for moderate coupling strengths $\alpha \lesssim 0.25$ [185, 120].

Before we introduce the polaron transformation, let us simplify the Hamiltonian by assuming a symmetric dispersion, $\omega_{-k} = \omega_k$, and bidirectional coupling, $g_{-k} = g_k$. In this case, we can work with the orthogonal even and odd modes, $A_k = \frac{1}{\sqrt{2}}(a_k + a_{-k})$ and $B_k = \frac{1}{\sqrt{2}}(a_k - a_{-k})$ respectively. While both modes evolve under the free Hamiltonian

$$H_0 = \frac{\Delta}{2}\sigma_z + \sum_k \omega_k A_k^\dagger A_k + \sum_k \omega_k B_k^\dagger B_k, \tag{3.4}$$

only the even modes couple to the emitter with a coupling of $\sqrt{2}g_k$. For simplicity, we continue to write g_k and use $g_k = \sqrt{\pi\alpha\omega_k/L}$ in the calculations, so that the Hamiltonian reads

$$H = \frac{\Delta}{2}\sigma_z + \sum_{k>0} \omega_k A_k^\dagger A_k + \sum_{k>0} g_k \sigma_x \left(A_k^\dagger + A_k\right), \tag{3.5}$$

The dynamics of the original operators a_k can be directly recovered by using the relation $a_{\pm k} = \frac{1}{\sqrt{2}}(A_k \pm B_k)$.

For low coupling strengths ($\alpha \lesssim 0.01$) and low excitations, one typically applies the rotating-wave approximation [28] in which the counterrotating terms $\sigma_- a_k + \sigma_+ a_k^\dagger$ are neglected. In this case, the number of excitations in the system is conserved and one can treat the evolution in each excitation sector separately. However, for larger coupling strengths the RWA breaks down and ultrastrong coupling effects become relevant [41, 42]. To obtain analytical predictions in this regime, it was shown to be useful [120] to transform the Hamiltonian, such that the ground state of the new Hamiltonian $H_\mathrm{P} = U_\mathrm{P}^\dagger H U_\mathrm{P}$ is close to the disentangled state $|\mathrm{vac}\rangle \approx |0\rangle_\mathrm{TLS}|0\rangle_\mathrm{ph}$. The transformation used is a polaron transformation U_P with variational parameters f_k,

$$U_\mathrm{P} = \exp\left[\sigma_x \sum_{k>0}\left(f_k A_k - f_k^* A_k^\dagger\right)\right]. \tag{3.6}$$

The action of the polaron transformation on the photonic and spin operators can be calculated by using the relation $\mathrm{e}^X Y \mathrm{e}^{-X} = \sum_m \frac{1}{m!}[X,Y]_m$ with $[X,Y]_m = \big[X,[X,Y]_{m-1}\big]$ and $[X,Y]_0 = Y$, which is intimately related to the Baker–Campbell–Hausdorff formula. The operators transform as

$$U_P^\dagger A_k^\dagger U_P = A_k^\dagger - f_k\sigma_x, \tag{3.7a}$$

$$U_P^\dagger \sigma_x U_P = \sigma_x, \tag{3.7b}$$

$$U_P^\dagger \sigma_z U_P = \sigma_z \mathrm{e}^{2\sigma_x \sum_{k>0}\left(f_k A_k - f_k^* A_k^\dagger\right)} = \frac{\tilde{\Delta}}{\Delta}\sigma_z O_{-\mathbf{f}}^\dagger O_{\mathbf{f}}, \tag{3.7c}$$

with the operators $O_{\mathbf{f}} = \exp\left[2\sigma_x \sum_{k>0} f_k A_k\right]$ and $\tilde{\Delta} = \Delta \mathrm{e}^{-2\sum_{k>0}|f_k|^2}$. The Hamiltonian in the polaron frame is then given by

$$H_P = U_P^\dagger H U_P = \frac{\tilde{\Delta}}{2}\sigma_z O_{-\mathbf{f}}^\dagger O_{\mathbf{f}} + \sum_{k>0}\omega_k A_k^\dagger A_k + \sum_{k>0}\sigma_x\left(G_k A_k + G_k^* A_k^\dagger\right) + E_0 \tag{3.8}$$

with $G_k = g_k - \omega_k f_k$ and an energy shift $E_0 = \sum_{k>0}\omega_k |f_k|^2 - g_k(f_k + f_k^*)$. We now aim to find the variational parameters f_k that minimize the ground state energy of this Hamiltonian. Note, that when $\Delta = 0$, the polaron Hamiltonian is diagonalized for $f_k = g_k/\omega_k$ and when $g_k = 0$, the original Hamiltonian is already diagonal (i.e., H_P is diagonal for the variational parameter $f_k = 0$). Thus, we expect the optimal parameters to lie somewhere in between.

The ground state energy, which we aim to minimize, is $-\tilde{\Delta}/2 + E_0$, assuming the ground state contains no photons. This yields a set of self-consistent equations for the variational parameters f_k [196, 185],

$$f_k^{\mathrm{opt}} = \frac{g_k}{\omega_k + \tilde{\Delta}}, \qquad \text{with } \tilde{\Delta} = \Delta \exp\left[-2\sum_{k>0}|f_k^{\mathrm{opt}}|^2\right]. \tag{3.9}$$

The renormalized energy for both the linear and modulus sine dispersion relation show a scaling as $\tilde{\Delta} = \Delta\left(p\Delta/\omega_c\right)^{\alpha/(1-\alpha)}$ for large ultraviolet cutoffs ω_c as predicted for the spin-boson model [119]. The scaling parameter p depends on the microscopic model used. Note, that this expression is not well-defined for $\alpha = 1$ because of the phase transition of the ohmic model at this point. As we are working in the parameter regime $\alpha \leq 0.5$, we do not discuss this further and refer the interested reader to Reference [119]. For these optimized parameters, the polaron Hamiltonian reads up to a constant energy shift (and where we write $f_k = f_k^{\mathrm{opt}}$)

$$H_P = \frac{\tilde{\Delta}}{2}\sigma_z O_{-\mathbf{f}}^\dagger O_{\mathbf{f}} + \sum_{k>0}\omega_k A_k^\dagger A_k + \tilde{\Delta}\sum_{k>0} f_k \sigma_x (A_k^\dagger + A_k). \tag{3.10}$$

At first glance, this might not seem like an improvement over the original Hamiltonian as the counterrotating terms still appear, and only the coupling strength is renormalized to $f_k = \frac{g_k}{\omega_k + \tilde{\Delta}}$. However, when expanding the polaron Hamiltonian in orders of f_k, or equivalently $\sqrt{\alpha}$, the counterrotating terms vanish in first order [120]. To see this, we introduce the operator $F = \sum_{k>0} f_k A_k$ and expand

$$O_{\mathbf{f}} = 1 + 2\sigma_x F + 2FF + \mathcal{O}(\alpha^{3/2}). \tag{3.11}$$

Then, the resulting Hamiltonian, expanded up to the second excitation subspace, is

$$\begin{aligned} H_P^{(2)} =& H_0 + \delta_0\left(F^\dagger\sigma_- + \sigma_+ F\right) - \delta_0\sigma_z F^\dagger F + \delta_0\sigma_z(FF + \text{h.c.}) \\ &- \delta_0(\sigma_z\sigma_x F^\dagger FF + \text{h.c.}) + \delta_0\sigma_z F^\dagger F^\dagger FF, \end{aligned} \tag{3.12}$$

where we have introduced $\delta_0 = 2\tilde{\Delta}$. For a slightly simplified notation in the later sections, we shift the energy, such that the free Hamiltonian for the even mode is now given by

$$H_0 = \tilde{\Delta}\frac{1}{2}(\sigma_z + 1) + \sum_{k>0} \omega_k A_k^\dagger A_k. \tag{3.13}$$

From the expanded polaron Hamiltonian, it is clear that the Hamiltonian in the single excitation subspace,

$$H_P^{(1)} = H_0 + \delta_0 \left(F^\dagger \sigma_- + \sigma_+ F\right) + \delta_0 F^\dagger F, \tag{3.14}$$

already conserves the number of excitations. For the higher order counterrotating terms one can apply the RWA, so that the terms $\sigma_z FF$ and $\sigma_- F^\dagger FF$ vanish. In the polaron frame this approximation is justified for larger couplings α than in the original Hamiltonian because the effective coupling strength in the counterrotating terms scales with α instead of $\sqrt{\alpha}$.

This is closely tied to the rate at which transitions out of a specific subspace with a given excitation number occur, which we sketch shortly here. Because the parity is conserved, these transitions to first order are either proportional to $\tilde{\Delta} f_{k_1} f_{k_2}$ (i.e., the creation or annihilation of two photons) or to $\tilde{\Delta} f_k$ (i.e., the creation or annihilation of an excitation in the TLS and a photon). These rates have to be compared to the energy difference between the state inside and outside of this subspace, that is $\omega_{k_1} + \omega_{k_2}$ and $\tilde{\Delta} + \omega_k$, respectively. The limiting transitions are the generation of two photons at low energies because the ratio $f_{k_1} f_{k_2}/(\omega_{k_1} + \omega_{k_2}) \sim \alpha$ does not vanish for small ω_k. We therefore expect the polaron transformation to be limited to moderate coupling strengths $\alpha \lesssim 0.25$.

As a final point, note that because the interaction is localized in space and the initial state is a wavepacket localized far away from the emitter, we can replace the scattering under the original Hamiltonian by the scattering under the polaron Hamiltonian H_P. This is valid, because the polaron transformation leaves the ground state of the system far away from the emitter invariant [185].

3.3 Analytical Results for Scattering Amplitudes

In the regime where the RWA is valid the photon-qubit scattering has been thoroughly studied in recent years for waveguides with linear dispersion [200, 191, 189, 192, 201, 190, 193, 144] and also for dispersive waveguides [191, 202, 203, 194]. Unfortunately, these results can only be partly generalized to the Hamiltonian in the polaron frame due to the form of the coupling $\delta_0 f_k$ and the additional terms like $\delta_0 F^\dagger F$.

The single photon scattering in the polaron frame was studied theoretically and numerically in Reference [120] and we extended the results to the scattering of two photons in the ultrastrong coupling regime. As the two photon scattering amplitude can be derived

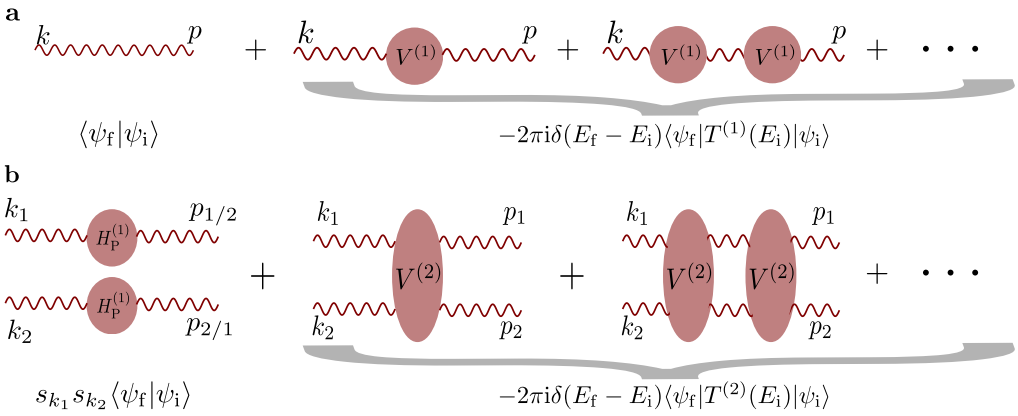

Figure 3.2: The scattering amplitude splits up into an independent part and a part described by the T-operator. (a) For the scattering of a single photon, it splits into a noninteracting part and a scattered part. (b) For the scattering of two photons, it splits up into independent scattering and a correlated scattering part.

from expressions in the single excitation subspace, we first summarize the main ideas in the single excitation subspace in Section 3.3.1. Having laid this foundation, in Section 3.3.2, we calculate the scattering matrix of two photons by expressing it in terms of the Green's functions $G^{(1)}$ of the one excitation subspace, which can be obtained analytically. We emphasize that our results are valid for any original coupling strength g_k and dispersion relation ω_k.

3.3.1 Single Excitation Regime

For calculating the scattering amplitude between two asymptotically free states of a single excitation, we need to calculate

$$S_{\mathrm{f;i}} = \langle\psi_{\mathrm{f}}|\mathcal{T}\exp\left[-\mathrm{i}\int_{-\infty}^{\infty}\mathrm{d}t\; V^{(1)}(t)\right]|\psi_{\mathrm{i}}\rangle, \tag{3.15}$$

where $V^{(1)}$ is taken in the interaction picture with respect to the free Hamiltonian H_0. This interaction term can be written in form of a vector of operators, $\vec{O}_1 = (b, F)$, and an interaction matrix, $\mathbf{u}_1 = (0, \delta_0; \delta_0, \delta_0)$, as

$$V^{(1)} = H_P^{(1)} - H_0 = \vec{O}_1^{\dagger}\mathbf{u}_1\vec{O}_1. \tag{3.16}$$

The time dependence of the potential in the interaction picture only appears in the vector of operators $\vec{O}_1$, whereas the interaction matrix $\mathbf{u}_1$ is time-independent. Furthermore, we note that the vector of operators $\vec{O}_1$ annihilates all excitations of $|\psi_{\mathrm{f/i}}\rangle$ such that one can project onto the ground state in between the creation and annihilation operators in the interaction term, i.e., $V^{(1)} = \vec{O}_1^{\dagger}|\mathrm{vac}\rangle\mathbf{u}_1\langle\mathrm{vac}|\vec{O}_1$ for our purposes.

By expanding the scattering amplitude in a Dyson series and summing all orders of this expansion, we find that the scattering amplitude splits up into a noninteracting and

scattered part, which can also be seen from the diagrammatic approach in Figure 3.2a. In particular,

$$\begin{aligned}
S_{\mathrm{f;i}} =&\langle\psi_\mathrm{f}|1-\mathrm{i}\int_{-\infty}^{\infty}\mathrm{d}t_1\ V^{(1)}(t)+(-\mathrm{i})^2\int_{-\infty}^{\infty}\mathrm{d}t\int_{-\infty}^{t}\mathrm{d}t_2\ V^{(1)}(t_1)V^{(1)}(t_2)+\ldots|\psi_\mathrm{i}\rangle\\
=&\langle\psi_\mathrm{f}|\psi_\mathrm{i}\rangle-\mathrm{i}\int_{-\infty}^{\infty}\mathrm{d}t\ \mathrm{e}^{\mathrm{i}(E_\mathrm{f}-E_\mathrm{i})t}\vec{v}_\mathrm{f}^{\dagger}\mathbf{u}_1\vec{v}_\mathrm{i}\\
&+(-\mathrm{i})^2\int_{-\infty}^{\infty}\mathrm{d}t\int_{0}^{\infty}\mathrm{d}\tau\ \mathrm{e}^{\mathrm{i}(E_\mathrm{f}-E_\mathrm{i})t}\vec{v}_\mathrm{f}^{\dagger}\mathbf{u}_1\langle 0|\vec{O}_1(\tau)\vec{0}_1^{\dagger}|0\rangle\mathrm{e}^{\mathrm{i}E_\mathrm{i}\tau}\mathbf{u}_1\vec{v}_\mathrm{i}+\ldots\\
=&\langle\psi_\mathrm{f}|\psi_\mathrm{i}\rangle-2\pi\mathrm{i}\delta(E_\mathrm{f}-E_\mathrm{i})\vec{v}_\mathrm{f}^{\dagger}\left[\mathbf{u}_1+\mathbf{u}_1\mathbf{\Pi}^{(1)}(E_\mathrm{i})\mathbf{u}_1+\ldots\right]\vec{v}_\mathrm{i}\\
=&\langle\psi_\mathrm{f}|\psi_\mathrm{i}\rangle-2\pi\mathrm{i}\delta(E_\mathrm{f}-E_\mathrm{i})\vec{v}_\mathrm{f}^{\dagger}\underbrace{\left[\mathbf{u}_1^{-1}-\mathbf{\Pi}^{(1)}(E_\mathrm{i})\right]^{-1}}_{\equiv\mathbf{T}^{(1)}(E_\mathrm{i})}\vec{v}_\mathrm{i},
\end{aligned}\tag{3.17}$$

where we have used the fact that the integrals factorize[9] such that we can define the so-called self-energy bubble $\mathbf{\Pi}^{(1)}(z)\equiv\int_0^\infty\mathrm{d}\tau\langle 0|\vec{O}_1(\tau)\vec{0}_1^{\dagger}|0\rangle\mathrm{e}^{\mathrm{i}z\tau}$. The initial and final vectors are $\vec{v}_{\mathrm{f/i}}=\langle\mathrm{vac}|\vec{O}_1|\psi_{\mathrm{f/i}}\rangle$. The infinite sum $\mathbf{u_1}\sum_n\left(\mathbf{\Pi}^{(1)}\mathbf{u}_1\right)^n$ converges to the finite two-by-two matrix

$$\mathbf{T}^{(1)}=\mathbf{u}_1+\mathbf{u}_1\mathbf{\Pi}^{(1)}\mathbf{T}^{(1)}=\left[\mathbf{u}_1^{-1}-\mathbf{\Pi}^{(1)}(E_\mathrm{i})\right]^{-1}.\tag{3.18}$$

Note, that the scattering amplitude splits into a noninteracting part $\langle\psi_\mathrm{i}|\psi_\mathrm{f}\rangle$ and a scattered part, that is described by the T operator, $-2\pi\mathrm{i}\delta(E_\mathrm{f}-E_\mathrm{i})\langle\psi_\mathrm{f}|T^{(1)}(E_\mathrm{i})|\psi_\mathrm{i}\rangle$ with $T^{(1)}(z)=\vec{O}_1^{\dagger}\mathbf{T}^{(1)}(z)\vec{O}_1$. The bold-type variables denote two-by-two matrices and we refer to their (i,j)-elements by writing for example $\mathbf{T}_{ij}^{(1)}$. On the other hand, the T operator and also the Green's Functions $G^{(0)}$ and $G^{(1)}$, which are introduced below, are operators, and if they have an index, it should be understood as $G^{(0)}_{O_1O_2}=\langle\mathrm{vac}|O_1G^{(0)}O_2^{\dagger}|\mathrm{vac}\rangle$.

The self-energy bubble can be calculated from the Green's function of the free Hamiltonian $G^{(0)}(z)=(z-H_0)^{-1}$ as

$$\mathbf{\Pi}^{(1)}(z)=-\mathrm{i}\int_0^\infty\mathrm{d}t\langle\mathrm{vac}|\vec{O}_1(t)\vec{O}_1^{\dagger}|\mathrm{vac}\rangle\mathrm{e}^{\mathrm{i}zt}=\mathrm{diag}\left(G^{(0)}_{bb}(z),G^{(0)}_{FF}(z)\right),\tag{3.19}$$

where the elements of the diagonal self-energy bubble are $G^{(0)}_{bb}(z)=(z-\tilde{\Delta})^{-1}$ and $G^{(0)}_{FF}(z)=\Sigma(z)/(4\tilde{\Delta}^2)$. The self-energy $\Sigma(\omega)$ is given by

$$\Sigma(\omega^+)=4\tilde{\Delta}^2\sum_{k>0}\frac{|f_k|^2}{\omega-\omega_k+\mathrm{i}\eta}\equiv\delta_L(\omega)-\mathrm{i}\Gamma(\omega)/2,\tag{3.20}$$

where $\omega^+=\omega+\mathrm{i}\eta$ with an infinitesimal $\eta>0$. The self-energy contains a renormalization of the energy, the so-called Lamb shift δ_L, and a decay rate Γ, which determine the

[9] As an example take the expression at second order, which factorizes after a change of variables from t_2 to $\tau=t-t_2$.

scattering characteristics. This expression can be evaluated in the continuum regime by applying the Sokhotski–Plemelj theorem $\lim_{\eta\to 0}\frac{1}{\omega\pm \mathrm{i}\eta} = \mp \mathrm{i}\pi\delta(\omega) + \mathcal{P}\frac{1}{\omega}$, where $\mathcal{P}$ denotes the Cauchy principal value. Recall, that $f_k = \frac{1}{\sqrt{L}} f(k)$, so that we obtain

$$\delta_L(\omega) = \delta_0^2\, \mathcal{P}\int_0^\infty \frac{\mathrm{d}k}{2\pi}\frac{|f(k)|^2}{\omega-\omega(k)}, \tag{3.21a}$$

$$\Gamma(\omega_k) = \delta_0^2 |f(k)|^2/\omega'(\omega_k), \tag{3.21b}$$

where the derivative $\omega'(z) = \partial_k\omega_k\big|_{\omega_k=z}$. For the linear dispersion relation with exponential cutoff in the coupling strength, one can actually find the self-energy (for $\omega > 0$) analytically for a large cutoff ω_c to be

$$\Sigma(\omega) = \frac{2\alpha\tilde{\Delta}^2}{(\omega+\tilde{\Delta})^2}\left(\omega\ln\frac{\omega}{\tilde{\Delta}} - \omega - \tilde{\Delta} - \mathrm{i}\pi\omega\right). \tag{3.22}$$

Note, that although this expression seems to be independent of the cutoff ω_c, the dependence is hidden in the renormalized transition energy $\tilde{\Delta}$.

By straightforwardly inverting the two-by-two matrices, we can calculate the $\mathbf{T}^{(1)}(z)$-matrix to be

$$\mathbf{T}^{(1)}(z) \equiv \left[\mathbf{u}_1^{-1} - \mathbf{\Pi}^{(1)}(z)\right]^{-1} = \frac{1}{h(z)}\begin{pmatrix} (z-\tilde{\Delta})\Sigma(z) & \delta_0(z-\tilde{\Delta}) \\ \delta_0(z-\tilde{\Delta}) & \delta_0^2\chi(z)\end{pmatrix}, \tag{3.23}$$

where we have defined the denominator $h(z) \equiv z - \tilde{\Delta} - \chi(z)\Sigma(z)$ and $\chi(z) \equiv \frac{z+\tilde{\Delta}}{2\tilde{\Delta}}$.

For the scattering of a single photon, the only relevant contribution comes from $\mathbf{T}^{(1)}_{22}(z)$. Due to the energy conservation term in the scattering amplitude, an initial photonic state $|\psi_\mathrm{i}\rangle = A_k^\dagger|\mathrm{vac}\rangle$ can only scatter to a final state of the form $|\psi_\mathrm{f}\rangle = s_k A_k^\dagger|\mathrm{vac}\rangle$, where the chiral phase shift s_k is given by

$$s_k = 1 - \mathrm{i}\frac{f_k^2}{\omega'(k)}\mathbf{T}^{(1)}_{22}(\omega_k) = 1 - \mathrm{i}\frac{\chi(\omega_k)\Gamma(\omega_k)}{(\omega_k-\tilde{\Delta}) - \chi(\omega_k)\Sigma(\omega_k)} = \frac{h(\omega_k)^*}{h(\omega_k)}, \tag{3.24}$$

where we used the relation of Equation 3.21b. From the chiral phase shift, which has its name because $|s_k| = 1$, one can calculate the transmission and reflection coefficients as $t_k = \frac{1}{2}(s_k+1)$ and $r_k = \frac{1}{2}(s_k-1)$. These expressions can be obtained by noting that a right-moving photonic state scatters as

$$a_k^\dagger|\mathrm{vac}\rangle = \frac{1}{\sqrt{2}}\left(A_k^\dagger + B_k^\dagger\right)|\mathrm{vac}\rangle \longrightarrow \frac{1}{\sqrt{2}}\left(s_k A_k^\dagger + B_k^\dagger\right)|\mathrm{vac}\rangle = \left(t_k a_k^\dagger + r_k a_{-k}^\dagger\right)|\mathrm{vac}\rangle. \tag{3.25}$$

We have plotted the reflectivity in Figure 3.3 to show, that when the coupling strength α is increased, the dependence on the frequency moves away from the Lorentzian predicted within the RWA to a much wider and asymmetric distribution.

Let us shortly compare these results with the well known results from the standard rotating wave regime, where the effective photon-photon interaction term $F^\dagger F$ can be

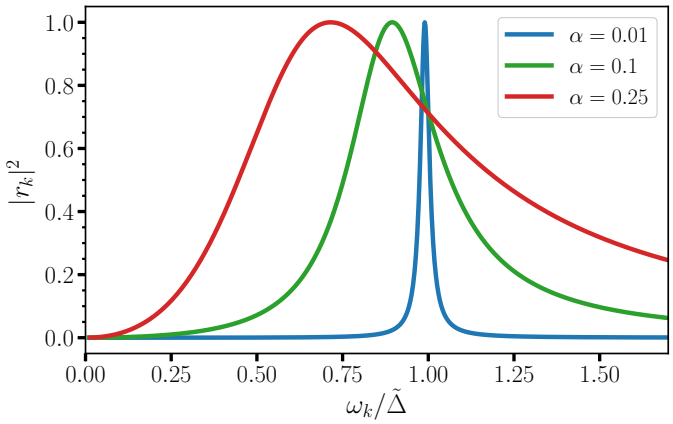

Figure 3.3: The reflectivity $|r_k|^2$ changes its dependence on the frequency when α is increased. For small α the reflectivity is well described by a Lorentzian, but for larger α it shifts and is no longer symmetric.

neglected and we find $\chi(z) = 1$. Furthermore, the Lamb shift typically vanishes $\delta_L \sim 0$ and the decay rate is uniform $\Gamma(\omega) \sim \Gamma$, we then recover the standard result [189]

$$r_k \approx \frac{-\mathrm{i}\Gamma/2}{(\omega_k - \tilde{\Delta}) + \mathrm{i}\Gamma/2}. \tag{3.26}$$

For extending the results to the two-photon regime, the Green's functions $G^{(1)} = \left(z - H_{\mathrm{P}}^{(1)}\right)^{-1}$ are more relevant than the $T^{(1)}$-operator. Fortunately, they can be expressed in terms of each other by the relation [204]

$$G^{(1)} = G^{(0)} + G^{(0)} T^{(1)} G^{(0)}. \tag{3.27}$$

In particular, we calculated the elements of the Green's function to be (see Appendix 3.A)

$$G_{bb}^{(1)}(\omega) = \frac{1 - \Sigma(\omega)/\delta_0}{h(\omega)}, \tag{3.28a}$$

$$G_{bA_k}^{(1)}(\omega) = \frac{1}{h(\omega)} \frac{\delta_0 f_k}{\omega - \omega_k} = G_{A_k b}^{(1)}(\omega), \tag{3.28b}$$

$$G_{A_p A_k}^{(1)}(\omega) = \frac{\delta_{pk}}{\omega - \omega_k} + \frac{\delta_0 f_p}{\omega - \omega_p} \frac{\chi(\omega)}{h(\omega)} \frac{\delta_0 f_k}{\omega - \omega_k}. \tag{3.28c}$$

3.3.2 Two Excitation Regime

We now focus on finding an analytical expression for the two photon scattering amplitude in the polaron frame. We solve the two photon scattering by using the hardcore boson representation [205] with annihilation (creation) operators b ($b^\dagger$). In this representation, the TLS operators are replaced by bosonic operators, $\sigma_z \to 2b^\dagger b - 1$ and $\sigma_- \to b$. To

recover the results for a two level system, one has to introduce an energy penalty for double excitations, $u_0 b^\dagger b^\dagger bb$, which has to be taken to the limit $u_0 \to \infty$ at the end of the calculations. Under these considerations, the Hamiltonian we aim to approximate is

$$H_{\mathrm{P}}^{(2)} = H_{\mathrm{P}}^{(1)} - 2\delta_0 b^\dagger F^\dagger bF - \delta_0(b^\dagger F^\dagger FF + \mathrm{h.c.}) - \delta_0 F^\dagger F^\dagger FF + u_0 b^\dagger b^\dagger bb. \tag{3.29}$$

The scattering matrix between two asymptotically free states, from $|\psi_{\mathrm{i}}\rangle$ to $|\psi_{\mathrm{f}}\rangle$, with eigenenergies $H_0|\psi_{\mathrm{f/i}}\rangle = E_{\mathrm{f/i}}|\psi_{\mathrm{f/i}}\rangle$ is given by Equation 3.2 where the Hamiltonian this time is $H = H_{\mathrm{P}}^{(2)}$. Instead of transforming to the interaction picture with respect to the free Hamiltonian H_0, we use a frame rotating with the single excitation Hamiltonian $H_{\mathrm{P}}^{(1)}$. This transformation allows us to relate the two photon scattering amplitude to expressions obtained in the single excitation subspace, which we just solved analytically. The scattering amplitude can then be calculated using a Dyson expansion of

$$S_{\mathrm{f;i}} = \lim_{t_{\mathrm{f/i}} \to \pm\infty} \mathrm{e}^{\mathrm{i}E_{\mathrm{f}}t_{\mathrm{f}}} \langle \psi_{\mathrm{f}}(t_{\mathrm{f}})| \mathcal{T} \exp\left[-\mathrm{i}\int_{t_{\mathrm{i}}}^{t_{\mathrm{f}}} \mathrm{d}t\ V^{(2)}(t)\right] |\psi_{\mathrm{i}}(t_{\mathrm{i}})\rangle \mathrm{e}^{-\mathrm{i}E_{\mathrm{i}}t_{\mathrm{i}}}, \tag{3.30}$$

where $|\psi_{\mathrm{f/i}}(t_{\mathrm{f/i}})\rangle = \exp\left[\mathrm{i}H_{\mathrm{P}}^{(1)}t_{\mathrm{f/i}}\right]|\psi_{\mathrm{f/i}}\rangle$. Similarly to the expression in the single excitation regime, the interaction term can be written as a product of vectors and matrices,

$$V^{(2)} = H_P^{(2)} - H_P^{(1)} = \vec{O}_2^\dagger \mathbf{u}_2 \vec{O}_2, \tag{3.31}$$

where the interaction matrix $\mathbf{u}_2 = (u_0, 0, 0; 0, -2\delta_0, -\delta_0; 0, -\delta_0, -\delta_0)$ is now a three-by-three matrix and the vector of operators $\vec{O}_2 = (bb, bF, FF)$ now has to be taken in the interaction picture rotating with $H_{\mathrm{P}}^{(1)}$. As the initial state contains two excitations, which are completely annihilated by $\vec{O}_2$, we can project onto the vacuum in between the vectors of the two creation and annihilation operators, that is, we can write $V^{(2)} = \vec{O}_2^\dagger |\mathrm{vac}\rangle \mathbf{u}_2 \langle \mathrm{vac}| \vec{O}_2$.

As for the single photon case, the scattering matrix splits up into two parts (see Figure 3.2b) when performing the Dyson expansion, i.e.,

$$S_{\mathrm{f;i}} = S_{\mathrm{f;i}}^{\mathrm{unco}} - 2\pi i \delta(E_{\mathrm{f}} - E_{\mathrm{i}}) \vec{w}_{\mathrm{f}}^\dagger \mathbf{T}^{(2)}(E_{\mathrm{i}}) \vec{w}_{\mathrm{i}}, \tag{3.32}$$

where the uncorrelated part for an initial state $|\psi_{\mathrm{i}}\rangle = A_{k_1}^\dagger A_{k_1}^\dagger |\mathrm{vac}\rangle$ to a final state $|\psi_{\mathrm{f}}\rangle = A_{p_1}^\dagger A_{p_1}^\dagger |\mathrm{vac}\rangle$ is given by

$$S_{\mathrm{f;i}}^{\mathrm{unco}} = s_{k_1} s_{k_2} \left(\delta_{p_1 k_1}\delta_{p_2 k_2} + \delta_{p_2 k_1}\delta_{p_1 k_2}\right). \tag{3.33}$$

This part of the scattering amplitude is the only relevant one if the two photons don't overlap in momentum or position space or have a too narrow or wide bandwidth.

The more interesting case is when the photonic modes overlap, and correlations are induced. The correlated part of the scattering is encoded in the $\mathbf{T}^{(2)}$-matrix. Just as for the single photon case, it can be obtained from an infinite sum, which converges to

$$\mathbf{T}^{(2)}(z) = \mathbf{u}_2 + \mathbf{u}_2 \mathbf{\Pi}^{(2)}(z) \mathbf{T}^{(2)}(z) = \left[\mathbf{u}_2^{-1} - \mathbf{\Pi}^{(2)}(z)\right]^{-1}. \tag{3.34}$$

The self-energy bubble $\mathbf{\Pi}^{(2)}(z)$ contains correlators of the four operators appearing in every combination of (bb, bF, FF) as

$$\mathbf{\Pi}^{(2)}(z) = -\mathrm{i}\int_0^\infty \mathrm{d}t\langle\mathrm{vac}|\vec{O}_2(t)\vec{O}_2^\dagger|\mathrm{vac}\rangle \mathrm{e}^{\mathrm{i}zt}. \tag{3.35}$$

By applying Wick's theorem [151] one can reduce the four-point correlators to two two-point correlators, which can be expressed in terms of the Green's function $G^{(1)}$ in the single excitation subspace. In fact, one needs to calculate convolutions over these Green's Functions, for example, for the element $\mathbf{\Pi}_{11}^{(2)}(z)$ we find (see Appendix 3.B)

$$\mathbf{\Pi}_{11}^{(2)}(z) = 2\mathrm{i}\int_{-\infty}^\infty \frac{\mathrm{d}\omega}{2\pi} G_{bb}^{(1)}(\omega)G_{bb}^{(1)}(z-\omega). \tag{3.36}$$

For the model with linear dispersion, the convolution can be calculated easily, at least numerically, because $G_{bb}^{(1)}(z) = \langle\mathrm{vac}|bG^{(1)}b^\dagger|\mathrm{vac}\rangle$ is known analytically (see Section 3.3.1) and doesn't have any poles along the real axis for $\alpha < 0.5$ (see Appendix 3.A).

For the final step, we note that the energy conservation for the scattering of a photonic initial state $|\psi_\mathrm{i}\rangle = A_{k_1}^\dagger A_{k_2}^\dagger|\mathrm{vac}\rangle$ (and similarly for the final state) originates from the time dependence of

$$\langle\mathrm{vac}|\vec{O}(t)|\psi_\mathrm{i}(t_\mathrm{i})\rangle \mathrm{e}^{\mathrm{i}E_\mathrm{i}t_\mathrm{i}} = \vec{w}_\mathrm{i}\mathrm{e}^{-\mathrm{i}(\omega_{k_1}+\omega_{k_2})t} = \vec{v}_\mathrm{i}\frac{\delta_0 f_{k_1}}{h(\omega_{k_1})}\frac{\delta_0 f_{k_2}}{h(\omega_{k_2})}\mathrm{e}^{-\mathrm{i}(\omega_{k_1}+\omega_{k_2})t}, \tag{3.37}$$

which at the same time defines the prefactor $\vec{v}_{\mathrm{f/i}}$ (see Appendix 3.C). This relation can be shown by applying Wick's theorem and expressing the two two-point correlators in terms of the Green's Function $G^{(1)}$. The vector in terms of the total energy $E = E_\mathrm{f} = E_\mathrm{i}$ and the difference energies $\epsilon_\mathrm{i} = \omega_{k_1} - \omega_{k_2}$, $\epsilon_\mathrm{f} = \omega_{p_1} - \omega_{p_2}$ is given by

$$\vec{v}_{\mathrm{f/i}} = \begin{pmatrix} 2 \\ (E-2\tilde{\Delta})/\delta_0 \\ \frac{1}{2\delta_0^2}(E-2\tilde{\Delta})^2 - \frac{1}{2\delta_0^2}\epsilon_{\mathrm{f/i}}^2 \end{pmatrix} \tag{3.38}$$

By combining the above results, we obtain the correlated part of the scattering amplitude to be

$$S_{p_1p_2;k_1k_2}^\mathrm{corr} = -2\pi\mathrm{i}\delta(E_\mathrm{f}-E_\mathrm{i})\frac{\delta_0 f_{p_1}}{h(\omega_{p_1})}\frac{\delta_0 f_{p_2}}{h(\omega_{p_2})}\vec{v}_\mathrm{f}^{\,\dagger}\mathbf{T}^{(2)}(E_\mathrm{i})\vec{v}_\mathrm{i}\frac{\delta_0 f_{k_1}}{h(\omega_{k_1})}\frac{\delta_0 f_{k_2}}{h(\omega_{k_2})}, \tag{3.39}$$

where $E_\mathrm{i} = \omega_{k_1} + \omega_{k_2}$ and $E_\mathrm{f} = \omega_{p_1} + \omega_{p_2}$. We have verified these results using the path integral formalism [2].

For the standard result, where interaction terms containing more than one photon operator can be neglected, the only relevant term in the $\mathbf{\Pi}^{(2)}$-matrix is the element $\mathbf{\Pi}_{11}^{(2)}(z)$, which is typically the largest of all matrix elements anyways (see Appendix 3.B). For $\delta_L \sim 0$ and $\Gamma(\omega) \sim \Gamma$ we find $\frac{\delta_0 f_k}{h(\omega_k)} = \tau_k = \frac{\sqrt{\Gamma}}{\omega_k - \tilde{\Delta} + \mathrm{i}\Gamma/2}$. Moreover, the middle part is given by $\vec{v}_\mathrm{f}^{\,\dagger}\mathbf{T}^{(2)}(E_\mathrm{i})\vec{v}_\mathrm{i} = 4\left(E_\mathrm{i} - 2\tilde{\Delta} + \mathrm{i}\Gamma\right)$ so that we recover the standard result [189]

$$S_{p_1p_2;k_1k_2}^\mathrm{corr} \approx -8\pi\mathrm{i}\delta(E_\mathrm{i}-E_\mathrm{f})\tau_{p_1}\tau_{p_2}\left(E_\mathrm{i} - 2\tilde{\Delta} + \mathrm{i}\Gamma\right)\tau_{k_1}\tau_{k_2}. \tag{3.40}$$

3.4 Numerical Simulation of Two-Photon Scattering

To check the analytical expression of the scattering amplitude of Equation 3.39, we can compare it to numerical results for the scattering of two photons under the specific Hamiltonians we have encountered, that is

1. the polaron Hamiltonian $H_{\mathrm{P}}^{(2)}$ expanded up to second order and under the rotating wave approximation from Equation 3.12;[10]
2. the full polaron Hamiltonian H_{P} of Equation 3.10;
3. the original Hamiltonian H of Equation 3.5.

The numerical evolution under the original and the full polaron Hamiltonian requires advanced numerical tools and can be achieved by the method of Matrix Product States. This comparison showed that in single excitations subspace the analytical predictions are valid for moderate coupling strengths $\alpha \lesssim 0.25$ [120]. Similar calculations in the two-photon subspace are being carried out currently. We concentrate in the following on the comparison with the approximated polaron Hamiltonian $H_{\mathrm{P}}^{(2)}$ and point out the main characteristics.

For the numerical results, one discretizes the waveguide of length L into $2n+1$ parts of width δx so that the wavevectors are discretized into

$$k_n \in \frac{\pi}{(2n+1)\delta x} \cdot \{0, \pm 1, \dots \pm n\} \tag{3.41}$$

and takes a dispersion relation $\omega_k = \omega_c |\sin(k\delta x/2)|$. This dispersion relation is linear for small frequencies and has a hard ultraviolet cutoff $\omega_c = 2c/\delta x$. Last but not least, for an ohmic spectral function, we take the light matter coupling is of the form $g_k = \sqrt{\pi\alpha\omega_k/L}$ such that the spectral function is ohmic.

We take as initial states gaussian wavepackets centered at positions far away from the emitter $|\psi_{\mathrm{i}}\rangle = \sum_{k_1,k_2} \phi_{k_1,k_2} A_{k_1}^\dagger A_{k_2}^\dagger |\mathrm{vac}\rangle$. In particular, we use gaussian wavepackets,

$$\phi_{k_1,k_2} = \frac{1}{2\mathcal{N}} \left(\mathrm{e}^{-\frac{(\omega_1-\mu_1)^2}{2s} - \mathrm{i}\omega_1 x_1} \mathrm{e}^{-\frac{(\omega_2-\mu_2)^2}{2s} - \mathrm{i}\omega_2 x_2} + \omega_1 \leftrightarrow \omega_2 \right), \tag{3.42}$$

where $\omega_j = \omega_{k_j}$. The normalization can be expressed in terms of the parameters s, μ_j, and x_j (see Appendix 3.D). We then let the wavepacket evolve for a sufficiently long time T such that the wavepacket has interacted with the two level system and it had time to fully decay back to the ground state, but not too long so that the wavepacket doesn't reach the end of the waveguide, i.e., $T \leq L/c$. The form of the scattering amplitude predicts that

[10] These results should agree exactly in the limit of large cutoff ω_c.

the final state splits up into an uncorrelated and a correlated part, such that the outgoing wavepacket $|\psi_\mathrm{f}\rangle = \sum_{p_1,p_2} \psi_{p_1,p_2} A^\dagger_{p_1} A^\dagger_{p_2} |\mathrm{vac}\rangle$ has the form

$$\psi_{p_1,p_2} = s_{p_1} s_{p_2} \mathrm{e}^{-\mathrm{i}(\omega_1+\omega_2)T} \left(\phi_{p_1,p_2} + \phi_{p_2,p_1}\right) + \mathrm{e}^{-\mathrm{i}(\omega_1+\omega_2)T} \psi^\mathrm{corr}_{p_1,p_2}, \tag{3.43}$$

where the correlated part is given by $\psi^\mathrm{corr}_{p_1,p_2} = \sum_{k_1,k_2} S^\mathrm{corr}_{p_1 p_2;k_1 k_2} \phi_{k_1,k_2}$. There are some simplifications for the analytical approximation of this sum, which we summarize in Appendix 3.D.

In Figure 3.4 we show the close to perfect agreement between the numerical and analytical results. The slight deviations come from the finite cutoff and only approximately linear dispersion. We would like to make a few remarks on our results and their physical relevance:

- We are only interested in the correlated part here because the uncorrelated part is well understood and it was shown that the analytical predictions from the polaron transformation work well [120]. Therefore, we take the correlated part from the difference

  $$\mathrm{e}^{-\mathrm{i}(\omega_1+\omega_2)T} \psi^\mathrm{corr}_{p_1,p_2} = \psi_{p_1,p_2} - s_{p_1} s_{p_2} \mathrm{e}^{-\mathrm{i}(\omega_1+\omega_2)T} \left(\phi_{p_1,p_2} + \phi_{p_2,p_1}\right) \tag{3.44}$$

  and compare it to the analytical predictions. With this approach we are able to focus on the most interesting and new features of the two photon scattering.[11] For this purpose, we plot the modulus of the wavefunction $|\psi^\mathrm{corr}_{p_1,p_2}|^2$ and the spectrum $\langle N_k \rangle = \langle A^\dagger_k A_k \rangle$. We have checked, that the correlated part vanishes when the wavepackets don't overlap in momentum or positions space.

- Within the RWA, one expects a narrow peak around the resonance frequency for the correlated part, which we recover for small coupling strength α as shown in Figure 3.4a. When the coupling strength is increased (see Figure 3.4b-c), the shape widens in momentum space and the region of correlated interaction can stretch over the whole wavepacket. Furthermore, the shape of the wavepacket of the full scattered state ψ_{p_1,p_2} deviates from the gaussian shape of the initial state ϕ_{k_1,k_2}.

- The last thing we point out is the dependence of the correlated part on the width s of the initial gaussian wavepackets. In principle, the significance of the correlated part depends on this width because when the initial state is too narrow or to wide, the correlated part will vanish. For example, if the wavepacket is spread out over a large space region, the probability of two photons close to the emitter at the same time, and therefore the probability for correlations, is very low. A simulation of this limit would require the use of many modes, so that we only show the difference between $s = 0.1$ (Figure 3.4b) and $s = 0.01$ (Figure 3.4d). By comparing these figures, one can see that the ratio of the correlated part of the scattering and the initial state decreases when it becomes narrower in momentum space.

[11] On the other hand we skip over some results form the interplay between the uncorrelated and correlated part [206], like the reemergence of the resonance frequency in the spectrum of the reflected photons when the correlated part is present.

There are many more important phenomena and applications of our analysis, that one could look at, but we close here the discussion on the simulation within the polaron frame.

3.5 Conclusion and Outlook

Light-matter interactions are well understood when the coupling strength is much smaller than the transition energies of the atom-like systems, $g \ll \Delta$. When the coupling strength is increased to $g \sim \Delta$, typically used methods and approximations break down. We have presented here a method for studying the dynamics of a photon confined to a waveguide, which interacts with a single TLS in this ultrastrong coupling regime. In particular, we focused on the scattering of multiphoton states, because the results for the scattering matrix are experimentally accessible through the scattering of coherent states on the quantum emitter [141]. Understanding how processes in the ultrastrong coupling regime can be approximated is essential for finding and developing new approaches for inducing strong photon-photon nonlinearities via quantum emitters or decreasing interaction times between the TLSs and the photons.

Our proposed method relies on a polaron transformation with a subsequent minimization of the ground state energy. This correctly predicts the renormalization of the TLS transition energy, as studied for the spin-boson model [119]. Furthermore, the counter-rotating terms vanish to first order in the polaron transformed picture and thus similar techniques, as when the RWA is valid, can be applied. However, as the polaron transformation introduces photon-photon interaction and higher order terms in the Hamiltonian, the known methods need to be refined. We have derived explicitly the scattering amplitude of one and two photons by expansion in a Dyson series and subsequent summation of the terms, which can be expressed as products of low-dimensional matrices. Furthermore, we have shown how to recover the standard results under the RWA.

These approximated analytical results can be compared against other analytical or numerical approaches, e.g., to results from numerical evolution of a two photon wavepacket under the polaron transformed Hamiltonian in the subspace of two excitations. Furthermore, our analytical results should be compared with simulations based on other numerical methods able to evolve the two-photon wavepacket under the full polaron Hamiltonian. Numerical simulations using Matrix Product States are currently being carried out. Apart from numerical simulations, there is at least one more way of checking our results against other (exact) analytical results, e.g., at the Toulouse point ($\alpha = 0.5$). Even though this coupling strength is above the point until which we expect good results ($\alpha \lesssim 0.25$), it can give a rough idea on the validity of the approximations. In the single excitation subspace there is a qualitative agreement between the two results [120], and this result extends to the two excitation subspace at low energies.

Motivated by the results for the ultrastrong coupling of a single quantum emitter to the waveguide, one can extend the methods to the coupling of two and even more emitters. In this case, one first has to find the variational parameters that minimize the ground

state energy. This is possible analytically for up to two emitters, but for more than two this is only possible numerically. Even though this limits the applications, it can already give insight into collective decay processes and interactions between quantum emitters mediated through the waveguide.

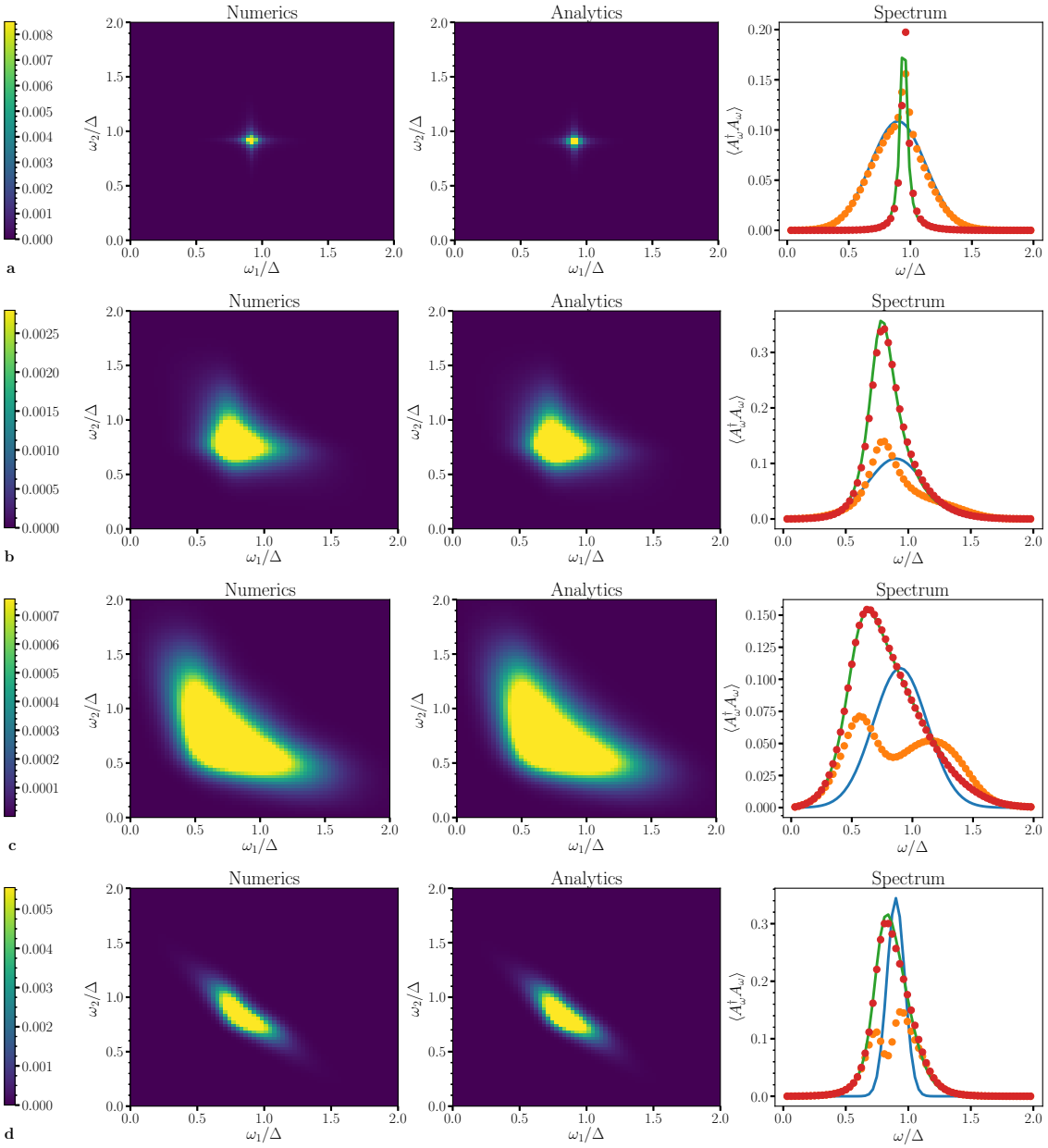

Figure 3.4: The left and middle panel compare the numerical and analytical results for the correlated part of the scattering, $|\psi^{\text{corr}}_{k_1,k_2}|^2$. In the right panel we compare the results for the spectrum $\langle N_k \rangle$. The blue line denotes the distribution of the initial state, the orange dots are for the full scattered result ψ_{k_1,k_2} and the red and green line show only the correlated part $\psi^{\text{corr}}_{k_1,k_2}$ and the good agreement between the numerics (red) and the analytical prediction (green). The first three plots are for the same gaussian distribution $s = 0.1$, $\mu_1 = \mu_2 = 0.9\Delta$, $x_1, x_2 = -0.2L$ for different coupling strengths **a** $\alpha = 0.02$, **b** $\alpha = 0.1$, and **c** $\alpha = 0.2$. **d** In the last plot we have used the same parameters as in (b) but with a smaller width $s = 0.01$.

Appendix

3.A Remarks on the Single Excitation Green's Function

We have calculated the Green's function for one excitation from the T-matrix by using the relation [204]

$$G^{(1)} = G^{(0)} + G^{(0)}T^{(1)}G^{(0)}, \tag{3.45}$$

which yields for the elements $G^{(1)}_{O_1O_2} = \langle \mathrm{vac}|O_1 G^{(1)} O_2^\dagger|\mathrm{vac}\rangle$ the functions

$$G^{(1)}_{bb}(\omega) = \frac{1-\Sigma(\omega)/\delta_0}{h(\omega)}, \tag{3.46a}$$

$$G^{(1)}_{bA_k}(\omega) = \frac{1}{h(\omega)}\frac{\delta_0 f_k}{\omega-\omega_k} = G^{(1)}_{A_k b}(\omega), \tag{3.46b}$$

$$G^{(1)}_{A_pA_k}(\omega) = \frac{\delta_{pk}}{\omega-\omega_k} + \frac{\delta_0 f_p}{\omega-\omega_p}\frac{\chi(\omega)}{h(\omega)}\frac{\delta_0 f_k}{\omega-\omega_k}, \tag{3.46c}$$

$$G^{(1)}_{bF}(\omega) = \frac{\Sigma(\omega)/\delta_0}{h(\omega)} = G^{(1)}_{Fb}(\omega), \tag{3.46d}$$

$$G^{(1)}_{FF}(\omega) = \frac{(\omega-\tilde{\Delta})\Sigma(\omega)/\delta_0^2}{h(\omega)}. \tag{3.46e}$$

These results can also be found by applying the LSZ reduction formula [207].

First of all, we note that for using the Green's Functions for the two photon scattering, one needs an extension to negative momenta. For this, one calculates the self-energy $\Sigma(\omega)$ in that regime. Both for the linear dispersion relation in the continuum and the modulus sine dispersion relation, we find for large cutoffs ω_c

$$\Sigma(\omega) = \frac{2\alpha\tilde{\Delta}^2}{(\omega+\tilde{\Delta})^2}\left(\omega\ln\frac{\omega}{\tilde{\Delta}} - \omega - \tilde{\Delta} - \mathrm{i}\pi\omega\right), \text{for } \omega > 0, \tag{3.47a}$$

$$\Sigma(\omega) = \frac{2\alpha\tilde{\Delta}^2}{(\omega+\tilde{\Delta})^2}\left(\omega\ln\frac{-\omega}{\tilde{\Delta}} - \omega - \tilde{\Delta}\right), \text{for } \omega < 0, \tag{3.47b}$$

with $\Sigma(0) = -2\alpha\tilde{\Delta}$ and $\Sigma(-\tilde{\Delta}) = -\alpha\tilde{\Delta}$.

Furthermore, we note that the Green's functions don't have a pole along the real axis for $\alpha < 0.5$. Along the positive real axis (or in general within the band if we consider a hard

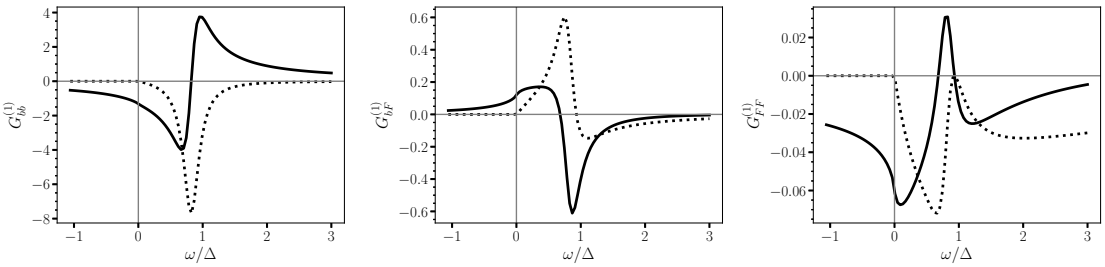

Figure 3.5: Plot of the relevant Green's functions $G^{(1)}_{bb}$, $G^{(1)}_{bF}$, and $G^{(1)}_{FF}$ for $\alpha = 0.2$ in the continuum model with linear dispersion. The solid line depicts the real part and the dotted line the imaginary part, which vanishes outside the band, that is for $\omega < 0$ for our continuum case.

ultraviolet cutoff ω_c) this is obvious because the self-energy has a non-zero imaginary part. To prove this statement outside of the band, one can use general results for the Green's function, i.e. it is monotonically increasing with ω and furthermore $G(\omega \to \pm\infty) = \pm\infty$. Therefore only the value at the edges of the band matter. In the continuum limit with linear dispersion, we are therefore interested in $G^{(1)}(0)$. The most relevant part to look at is the denominator $h(\omega)$. At the origin it attains the value $h(0) = -(1-\alpha)\tilde{\Delta}$, which is negative for $\alpha < 1$ and therefore $G^{(1)}$ has no pole along the real axis. This behavior is also obvious from plots of these functions as seen in Figure 3.5.

3.B Calculation of the Energy Bubble

This section is concerned with the calculation of the energy bubble, which is given by

$$\mathbf{\Pi}^{(2)}(z) = -\mathrm{i}\int_0^\infty \mathrm{d}t\ \langle \mathrm{vac}|\vec{O}_2(t)\vec{O}_2^\dagger|\mathrm{vac}\rangle \mathrm{e}^{-\mathrm{i}zt}. \tag{3.48}$$

By applying Wick's theorem on the four-point correlators, $\langle \mathrm{vac}|\vec{O}_2^\dagger(t)\vec{O}_2|\mathrm{vac}\rangle$, we obtain the product of two two-point correlators, which can be expressed in terms of the single excitation Green's function. As an example we calculate one element of $\mathbf{\Pi}^{(2)}(z)$, in particular,

$$\begin{aligned}
\mathbf{\Pi}^{(2)}_{11}(z^+) &= -\mathrm{i}\int_0^\infty \mathrm{d}\tau \langle \mathrm{vac}|\mathrm{b}^2(\tau)\mathrm{b}^{\dagger 2}|0\rangle \mathrm{e}^{\mathrm{i}z\tau} \\
&= -2\mathrm{i}\int_0^\infty \mathrm{d}\tau \int_{-\infty}^\infty \frac{\mathrm{d}\omega}{2\pi}\int_{-\infty}^\infty \frac{\mathrm{d}\omega'}{2\pi} \mathrm{i}\mathrm{G}^{(1)}_{\mathrm{bb}}(\omega^+)\mathrm{e}^{-\mathrm{i}\omega\tau}\cdot \mathrm{i}\mathrm{G}^{(1)}_{\mathrm{bb}}(\omega'^+)\mathrm{e}^{-\mathrm{i}\omega'\tau}\cdot \mathrm{e}^{\mathrm{i}z^+\tau} \\
&= 2\mathrm{i}\int_{-\infty}^\infty \frac{\mathrm{d}\omega}{2\pi} G^{(1)}_{bb}(\omega)G^{(1)}_{bb}(z-\omega) = 2\mathrm{i}(G^{(1)}_{bb} * G^{(1)}_{bb})(z),
\end{aligned} \tag{3.49}$$

where we have introduced the convolution $(f*g)(E) = \int_{-\infty}^\infty \frac{\mathrm{d}\omega}{2\pi} f(\omega)g(E-\omega)$. The reduction to the convolution can be obtained by applying the Residue theorem and carefully paying attention to the poles of $h(\omega)$, which are all below the real axis, and of $(z-\omega-\omega'+\mathrm{i}\eta)^{-1}$,

which comes from the time integral. The full self-energy bubble is a three-by-three matrix with the elements

$$\mathbf{\Pi}^{(2)} = \mathrm{i} \begin{pmatrix} 2G^{(1)}_{bb} * G^{(1)}_{bb} & 2G^{(1)}_{bb} * G^{(1)}_{bF} & 2G^{(1)}_{bF} * G^{(1)}_{bF} \\ 2G^{(1)}_{bb} * G^{(1)}_{Fb} & G^{(1)}_{bb} * G^{(1)}_{FF} + G^{(1)}_{bF} * G^{(1)}_{bF} & 2G^{(1)}_{bF} * G^{(1)}_{FF} \\ 2G^{(1)}_{Fb} * G^{(1)}_{Fb} & 2G^{(1)}_{Fb} * G^{(1)}_{FF} & 2G^{(1)}_{FF} * G^{(1)}_{FF} \end{pmatrix}, \tag{3.50}$$

where we have left out the dependence on the frequency for a more compact notation. As these expressions don't give an intuitive picture of the functions, we provide plots of them in Figure 3.6. Note, that the interesting parts of the functions are around the resonance at $E \sim 2\tilde{\Delta}$.

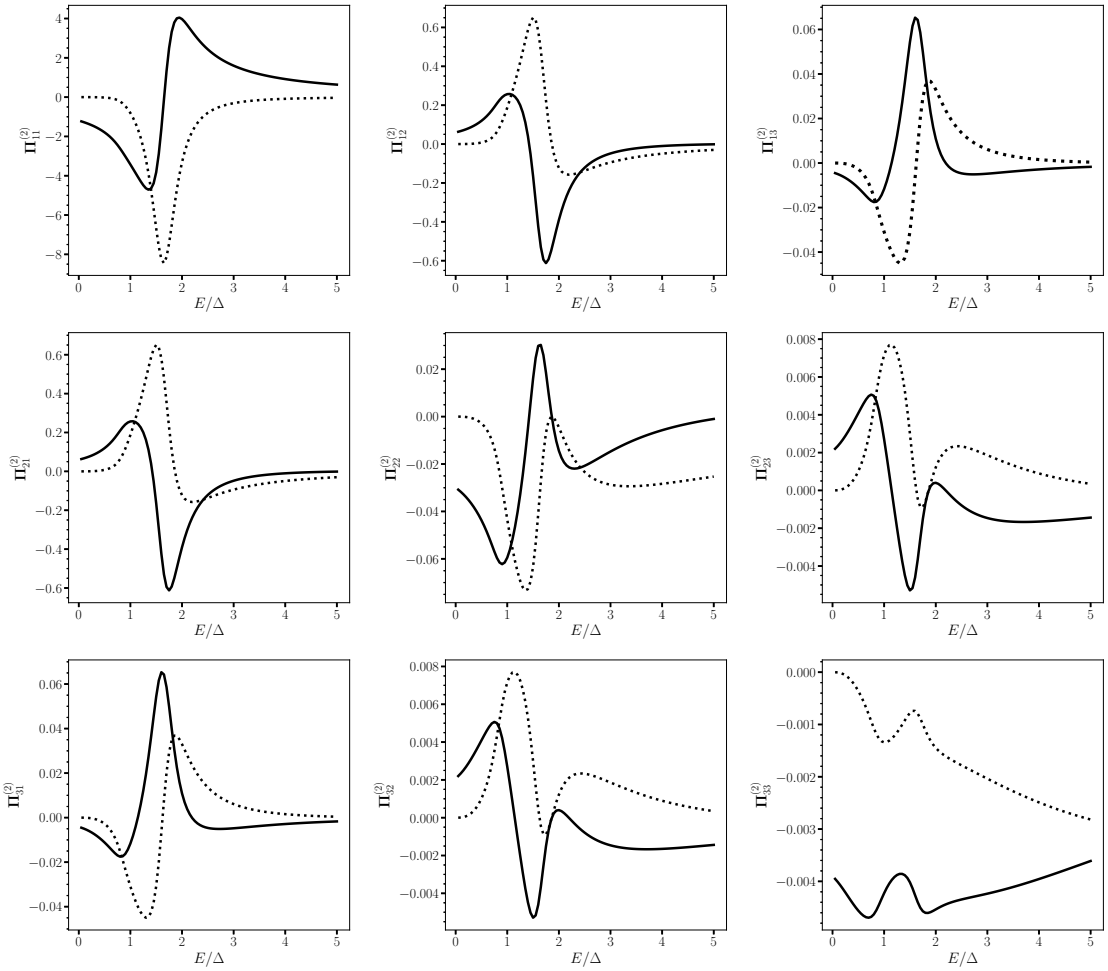

Figure 3.6: Plot of the elements of the self-energy bubble $\mathbf{\Pi}^{(2)}$ for $\alpha = 0.1$ in the continuum model with linear dispersion. The solid line plots the real part and the dotted line the imaginary part. All functions go to zero at large frequencies, outside of the plotted range for some elements.

3.C Energy Conservation

This section is concerned with the energy conservation originating in the time dependence of the relation $\langle \mathrm{vac}|\vec{O}_2(t)|\psi_\mathrm{i}\rangle = \vec{w}_\mathrm{i} \mathrm{e}^{-\mathrm{i}E_\mathrm{i}t}$. To prove this, we first use

$$\langle \mathrm{vac}|b(t)A_k^\dagger|\mathrm{vac}\rangle = \mathrm{i}\int_{-\infty}^{\infty} \frac{\mathrm{d}\omega}{2\pi} G^{(1)}_{bA_k}(\omega^+)\mathrm{e}^{-\mathrm{i}\omega t} = \frac{\delta_0 f_k}{h(\omega_k)}\mathrm{e}^{-\mathrm{i}\omega_k t} \equiv \beta_k \mathrm{e}^{-\mathrm{i}\omega_k t}, \tag{3.51a}$$

$$\langle \mathrm{vac}|F(t)A_k^\dagger|\mathrm{vac}\rangle = \mathrm{i}\int \frac{\mathrm{d}\omega}{2\pi} G^{(1)}_{FA_k}(\omega^+)\mathrm{e}^{-\mathrm{i}\omega t} = \frac{(\omega_k - \tilde{\Delta})f_k}{h(\omega_k)}\mathrm{e}^{-\mathrm{i}\omega_k t} \equiv \alpha_k \mathrm{e}^{-\mathrm{i}\omega_k t}. \tag{3.51b}$$

These results can be found by the same considerations as in Appendix 3.B. The next step is applying Wick's theorem to reduce the correlator of four operators to a product of two correlators, which is possible because $\left[b(t), A_k^\dagger\right] \in \mathbb{C}$. For example for the first element we obtain

$$\begin{aligned}\langle \mathrm{vac}|b(t)b(t)A_{k_1}^\dagger A_{k_2}^\dagger|\mathrm{vac}\rangle &= \langle \mathrm{vac}|\overbrace{b(t)\overbrace{b(t)A_{k_1}^\dagger}A_{k_2}^\dagger}|\mathrm{vac}\rangle + \langle \mathrm{vac}|\overbrace{b(t)\overbrace{b(t)A_{k_1}^\dagger A_{k_2}^\dagger}}|\mathrm{vac}\rangle \\ &= 2\langle \mathrm{vac}|b(t)A_{k_1}^\dagger|\mathrm{vac}\rangle \cdot \langle \mathrm{vac}|b(t)A_{k_2}^\dagger|\mathrm{vac}\rangle = 2\beta_{k_1}\beta_{k_2}\mathrm{e}^{-\mathrm{i}E_\mathrm{i}t}\end{aligned} \tag{3.52}$$

where $E_\mathrm{i} = \omega_{k_1} + \omega_{k_2}$ is the total energy. The other elements follow analogously and we obtain

$$\vec{w}_\mathrm{i} = \begin{pmatrix} 2\beta_{k_1}\beta_{k_2} \\ \alpha_{k_1}\beta_{k_2} + \beta_{k_1}\alpha_{k_2} \\ 2\alpha_{k_1}\alpha_{k_2} \end{pmatrix} = \underbrace{\begin{pmatrix} 2 \\ (E_\mathrm{i} - 2\tilde{\Delta})/\delta_0 \\ \frac{1}{2\delta_0^2}(E_\mathrm{i} - 2\tilde{\Delta})^2 - \frac{1}{2\delta_0^2}\epsilon_\mathrm{i}^2 \end{pmatrix}}_{\equiv \vec{v}_\mathrm{i}} \frac{\delta_0 f_{k_1}}{h(\omega_{k_1})}\frac{\delta_0 f_{k_2}}{h(\omega_{k_2})}, \tag{3.53}$$

where $\epsilon_\mathrm{i} = \omega_{k_1} - \omega_{k_2}$. An analogous result holds for $\vec{w}_\mathrm{f}$.

3.D Remarks on Numerical Methods

Concerning the numerics, we have mixed the discrete case and the continuum case during the calculation and need to pay attention that they always agree with each other. The gaussian wavepacket is given by

$$\phi_{k_1,k_2} = \frac{1}{2\mathcal{N}}\left(\mathrm{e}^{-\frac{(\omega_1-\mu_1)^2}{2s} - \mathrm{i}\omega_1 x_1}\mathrm{e}^{-\frac{(\omega_2-\mu_2)^2}{2s} - \mathrm{i}\omega_2 x_2} + \omega_1 \leftrightarrow \omega_2\right), \tag{3.54}$$

where the normalization in the continuum model with linear dispersion is given by

$$\begin{aligned}\mathcal{N}^2 &= \int \frac{\mathrm{d}\omega_1}{2\pi}\int \frac{\mathrm{d}\omega_2}{2\pi}\frac{1}{4}\left|\mathrm{e}^{-\frac{(\omega_1-\mu_1)^2}{2s} - \mathrm{i}\omega_1 x_1}\mathrm{e}^{-\frac{(\omega_2-\mu_2)^2}{2s} - \mathrm{i}\omega_2 x_2} + \omega_1 \leftrightarrow \omega_2\right|^2 \\ &= \frac{1}{(2\pi)^2}\frac{\pi s}{2}\left(1 + \mathrm{e}^{-\frac{\mu_-^2 + s^2 x_-^2}{2s}}\right),\end{aligned} \tag{3.55}$$

where $\mu_- = \mu_1 - \mu_2$ and $x_- = x_1 - x_2$.

Another simplification is to note that the gaussian wavepackets can be written as a product of the sum $E = \omega_1 + \omega_2$ and difference frequency $\epsilon = \omega_1 - \omega_2$. Note, that then the parameter range needs to be restricted to $\epsilon \in [-E, E]$. A short calculation shows that

$$\phi_{k_1,k_2} = \frac{1}{\mathcal{N}}\phi_+(E)\phi_-(\epsilon) = \frac{1}{\mathcal{N}}\mathrm{e}^{-\frac{(E-\mu_+)^2}{4s} - \mathrm{i}Ex_+/2}\left(\mathrm{e}^{-\frac{(\epsilon-\mu_-)^2}{4s} - \mathrm{i}\epsilon x_-/2} + \epsilon \to -\epsilon\right). \quad (3.56)$$

The last simplification is a separation of the correlated part into different terms. For this, we note, that by writing $\vec{v}_{\mathrm{f/i}} = \vec{\nu} - \frac{\epsilon_{\mathrm{f/i}}^2}{2\delta_0^2}\hat{e}_3$ with $\hat{e}_3 = (0,0,1)$ one can separate

$$\vec{v}_{\mathrm{f}}^{\dagger}\mathbf{T}^{(2)}(E)\vec{v}_{\mathrm{i}} = \left[c_1(E) - \frac{1}{2\delta_0^2}\left(e_{\mathrm{f}}^2 + e_{\mathrm{i}}^2\right)c_2(E) + \frac{1}{4\delta_0^4}e_{\mathrm{f}}^2 e_{\mathrm{i}}^2 c_3(E)\right], \quad (3.57)$$

where the scalars are given by the matrix products $c_1(E) = \vec{\nu}^{\dagger}\mathbf{T}^{(2)}(E)\vec{\nu}$, $c_2(E) = \hat{e}_3\mathbf{T}^{(2)}(E)\vec{\nu}$ and $c_3(E) = \hat{e}_3\mathbf{T}^{(2)}(E)\hat{e}_3$. The correlated part of the state is then given by

$$\begin{aligned}\psi_{p_1,p_2}^{\mathrm{corr}} &= -i\sum_{k_1,k_2} 2\pi\delta(E_{\mathrm{f}} - E_{\mathrm{i}})S_{p_1p_2;k_1k_2}^{\mathrm{corr}}\phi_{k_1,k_2} \\ &= -i\frac{\delta_0 f_{p_1}}{h(\omega_{p_1})}\frac{\delta_0 f_{p_2}}{h(\omega_{p_2})}\frac{1}{\mathcal{N}}\phi_+(E) \\ &\quad \times\left[\left(c_1(E) - \frac{e_{\mathrm{f}}^2}{2\delta_0^2}c_2(E)\right)I_1(E) + \left(\frac{e_{\mathrm{f}}^2}{2\delta_0^2}c_3(E) - c_2(E)\right)I_2(E)\right], \end{aligned} \quad (3.58)$$

where the integrals over the gaussians are given by

$$I_1(E) = 2\int_{-E}^{E}\frac{\mathrm{d}\epsilon}{2\pi}\frac{\delta_0 f(\frac{E+\epsilon}{2})}{h(\frac{E+\epsilon}{2})}\frac{\delta_0 f(\frac{E-\epsilon}{2})}{h(\frac{E-\epsilon}{2})}\phi_-(\epsilon), \quad (3.59a)$$

$$I_2(E) = 2\int_{-E}^{E}\frac{\mathrm{d}\epsilon}{2\pi}\frac{\delta_0 f(\frac{E+\epsilon}{2})}{h(\frac{E+\epsilon}{2})}\frac{\delta_0 f(\frac{E-\epsilon}{2})}{h(\frac{E-\epsilon}{2})}\frac{\epsilon^2}{2\delta_0^2}\phi_-(\epsilon). \quad (3.59b)$$

Bibliography

[1] A. González-Tudela, V. Paulisch, D. E. Chang, H. J. Kimble, and J. I. Cirac. "Deterministic Generation of Arbitrary Photonic States Assisted by Dissipation" *Phys. Rev. Lett.* **115** 163603 (2015).

[2] V. Paulisch, M. Perarnau-Llobet, A. González-Tudela, and J. I. Cirac. "Quantum Metrology with Multimode Photonic States" *In preparation.* (2018).

[3] A. González-Tudela, V. Paulisch, H. J. Kimble, and J. I. Cirac. "Efficient Multiphoton Generation in Waveguide Quantum Electrodynamics" *Phys. Rev. Lett.* **118** 213601 (2017).

[4] V. Paulisch, A. González-Tudela, H. J. Kimble, and J. I. Cirac. "Heralded multiphoton states with coherent spin interactions in waveguide QED" *New J. Phys.* **19** 043004 (2017).

[5] V. Paulisch, H. J. Kimble, J. I. Cirac, and A. González-Tudela. "Generation of single and two-mode multiphoton states in waveguide QED" *arXiv:1802.00210.* (2018).

[6] V. Paulisch, T. Shi, and J. J. García-Ripoll. "Multiphoton Scattering in the Ultrastrong coupling regime" *In preparation.* (2018).

[7] V. Paulisch, H. J. Kimble, and A. González-Tudela. "Universal quantum computation in waveguide QED using decoherence free subspaces" *New J. Phys.* **18** 043041 (2016).

[8] V. Paulisch, H. Rui, H. K. Ng, and B.-G. Englert. "Beyond adiabatic elimination: A hierarchy of approximations for multi-photon processes" *Eur. Phys. J. Plus* **129** 12 (2014).

[9] M. A. Nielsen and I. L. Chuang. "Quantum computation and quantum information" Cambridge University Press, 2000.

[10] N. Gisin and R. Thew. "Quantum communication" *Nat. Photonics* **1** 165–171 (2007).

[11] V. Giovannetti, S. Lloyd, and L. Maccone. "Quantum Metrology" *Phys. Rev. Lett.* **96** 010401 (2006).

[12] I. Georgescu, S. Ashhab, and F. Nori. "Quantum simulation" *Rev. Mod. Phys.* **86** 153–185 (2014).

[13] H. J. Kimble. "The quantum internet" *Nature* **453** 1023–1030 (2008).

[14] D. E. Chang, V. Vuletić, and M. D. Lukin. "Quantum nonlinear optics — photon by photon" *Nat. Photonics* **8** 685–694 (2014).

[15] A. Furusawa. “Quantum States of Light” Springer-Verlag GmbH, 2016.

[16] R. E. Slusher, L. W. Hollberg, B. Yurke, J. C. Mertz, and J. F. Valley. “Observation of Squeezed States Generated by Four-Wave Mixing in an Optical Cavity” *Phys. Rev. Lett.* **55** 2409–2412 (1985).

[17] L.-A. Wu, H. J. Kimble, J. L. Hall, and H. Wu. “Generation of Squeezed States by Parametric Down Conversion” *Phys. Rev. Lett.* **57** 2520–2523 (1986).

[18] J. Miller et al. “Prospects for doubling the range of Advanced LIGO” *Phys. Rev. D* **91** 062005 (2015).

[19] R. Demkowicz-Dobrzański, M. Jarzyna, and J. Kołodyński. “Quantum Limits in Optical Interferometry” *Progress in Optics*. Elsevier, 2015, 345–435.

[20] I. L. Chuang and Y. Yamamoto. “Simple quantum computer” *Phys. Rev. A* **52** 3489–3496 (1995).

[21] Y. Yamamoto, M. Kitagawa, and K. Igeta. “Quantum Mechanical Aspects of Optical Communication and Optical Computing” *Proceedings of the 3rd Asia Pacific Physics Conference*. Ed. by C. N. Y. Y. W. Chan A. F. Leung and K. Young. World Scientific, New Jersey, 1988, 1988, 779–799.

[22] G. J. Milburn. “Quantum optical Fredkin gate” *Phys. Rev. Lett.* **62** 2124–2127 (1989).

[23] E. Knill, R. Laflamme, and G. J. Milburn. “A scheme for efficient quantum computation with linear optics” *Nature* **409** 46–52 (2001).

[24] R. J. Thompson, G. Rempe, and H. J. Kimble. “Observation of normal-mode splitting for an atom in an optical cavity” *Phys. Rev. Lett.* **68** 1132–1135 (1992).

[25] M. Brune et al. “Quantum Rabi Oscillation: A Direct Test of Field Quantization in a Cavity” *Phys. Rev. Lett.* **76** 1800–1803 (1996).

[26] L.-M. Duan, M. D. Lukin, J. I. Cirac, and P. Zoller. “Long-distance quantum communication with atomic ensembles and linear optics” *Nature* **414** 413–418 (2001).

[27] N. Sangouard, C. Simon, H. de Riedmatten, and N. Gisin. “Quantum repeaters based on atomic ensembles and linear optics” *Rev. Mod. Phys.* **83** 33–80 (2011).

[28] C. Cohen-Tannoudji, J. Dupont-Roc, and G. Grynberg. “Atom-Photon Interactions: Basic Processes and Applications” Wiley-VCH, 1998.

[29] J. I. Cirac, P. Zoller, H. J. Kimble, and H. Mabuchi. “Quantum State Transfer and Entanglement Distribution among Distant Nodes in a Quantum Network” *Phys. Rev. Lett.* **78** 3221–3224 (1997).

[30] A. Reiserer and G. Rempe. “Cavity-based quantum networks with single atoms and optical photons” *Rev. Mod. Phys.* **87** 1379–1418 (2015).

[31] S. Ritter et al. “An elementary quantum network of single atoms in optical cavities” *Nature* **484** 195–200 (2012).

[32] T. Niemczyk et al. “Circuit quantum electrodynamics in the ultrastrong-coupling regime” *Nat. Phys.* **6** 772–776 (2010).

[33] P. Forn-Díaz et al. "Observation of the Bloch-Siegert Shift in a Qubit-Oscillator System in the Ultrastrong Coupling Regime" *Phys. Rev. Lett.* **105** 237001 (2010).

[34] P. Solano, P. Barberis-Blostein, F. K. Fatemi, L. A. Orozco, and S. L. Rolston. "Super-radiance reveals infinite-range dipole interactions through a nanofiber" *Nat. Commun.* **8** 1857 (2017).

[35] A. Goban et al. "Superradiance for Atoms Trapped along a Photonic Crystal Waveguide" *Phys. Rev. Lett.* **115** 063601 (2015).

[36] D. E. Chang, A. S. Sørensen, E. A. Demler, and M. D. Lukin. "A single-photon transistor using nanoscale surface plasmons" *Nat. Phys.* **3** 807–812 (2007).

[37] D. E. Chang, L Jiang, A. V. Gorshkov, and H. J. Kimble. "Cavity QED with atomic mirrors" *New J. Phys.* **14** 063003 (2012).

[38] D. E. Chang, J. S. Douglas, A. González-Tudela, C.-L. Hung, and H. J. Kimble. "Quantum Matter Built from Nanoscopic Lattices of Atoms and Photons" *In preparation.* (2018).

[39] J. L. O'Brien, A. Furusawa, and J. Vučković. "Photonic quantum technologies" *Nat. Photonics* **3** 687–695 (2009).

[40] D. Porras and J. I. Cirac. "Collective generation of quantum states of light by entangled atoms" *Phys. Rev. A* **78** 053816 (2008).

[41] J. Bourassa et al. "Ultrastrong coupling regime of cavity QED with phase-biased flux qubits" *Phys. Rev. A* **80** 032109 (2009).

[42] B. Peropadre, D. Zueco, D. Porras, and J. J. García-Ripoll. "Nonequilibrium and Nonperturbative Dynamics of Ultrastrong Coupling in Open Lines" *Physical Review Letters* **111** 243602 (2013).

[43] G. Romero, D. Ballester, Y. M. Wang, V. Scarani, and E. Solano. "Ultrafast Quantum Gates in Circuit QED" *Phys. Rev. Lett.* **108** 120501 (2012).

[44] T. H. Kyaw, D. A. Herrera-Martí, E. Solano, G. Romero, and L.-C. Kwek. "Creation of quantum error correcting codes in the ultrastrong coupling regime" *Phys. Rev. B* **91** 064503 (2015).

[45] E. Sanchez-Burillo, D. Zueco, J. J. Garcia-Ripoll, and L. Martin-Moreno. "Scattering in the Ultrastrong Regime: Nonlinear Optics with One Photon" *Phys. Rev. Lett.* **113** 263604 (2014).

[46] B. C. Sanders and G. J. Milburn. "Quantum limits to all-optical phase shifts in a Kerr nonlinear medium" *Phys. Rev. A* **45** 1919–1923 (1992).

[47] A. Nysteen, D. P. S. McCutcheon, M. Heuck, J. Mørk, and D. R. Englund. "Limitations of two-level emitters as nonlinearities in two-photon controlled-phase gates" *Phys. Rev. A* **95** 062304 (2017).

[48] I. Buluta, S. Ashhab, and F. Nori. "Natural and artificial atoms for quantum computation" *Rep. Prog. Phys.* **74** 104401 (2011).

[49] T. D. Ladd et al. "Quantum computers" *Nature* **464** 45–53 (2010).

[50] R. Blatt and D. Wineland. "Entangled states of trapped atomic ions" *Nature* **453** 1008–1015 (2008).

[51] I. Bloch. "Quantum coherence and entanglement with ultracold atoms in optical lattices" *Nature* **453** 1016–1022 (2008).

[52] R. Hanson and D. D. Awschalom. "Coherent manipulation of single spins in semiconductors" *Nature* **453** 1043–1049 (2008).

[53] M. V. G. Dutt et al. "Quantum Register Based on Individual Electronic and Nuclear Spin Qubits in Diamond" *Science* **316** 1312–1316 (2007).

[54] J. Clarke and F. K. Wilhelm. "Superconducting quantum bits" *Nature* **453** 1031–1042 (2008).

[55] R. J. Schoelkopf and S. M. Girvin. "Wiring up quantum systems" *Nature* **451** 664–669 (2008).

[56] P. Solano et al. "Optical Nanofibers" *Advances In Atomic, Molecular, and Optical Physics*. Elsevier, 2017, 439–505.

[57] P. Lodahl, S. Mahmoodian, and S. Stobbe. "Interfacing single photons and single quantum dots with photonic nanostructures" *Rev. Mod. Phys.* **87** 347–400 (2015).

[58] X. Gu, A. F. Kockum, A. Miranowicz, Y. Liu, and F. Nori. "Microwave photonics with superconducting quantum circuits" *Phys. Rep.* **718-719** 1–102 (2017).

[59] E. Vetsch et al. "Optical Interface Created by Laser-Cooled Atoms Trapped in the Evanescent Field Surrounding an Optical Nanofiber" *Phys. Rev. Lett.* **104** 203603 (2010).

[60] A. Goban et al. "Atom-Light Interactions in Photonic Crystals" *Nat. Commun.* **5** 3808 (2014).

[61] K. P. Nayak et al. "Optical nanofiber as an efficient tool for manipulating and probing atomic Fluorescence" *Opt. Express* **15** 5431 (2007).

[62] K. P. Nayak and K Hakuta. "Single atoms on an optical nanofibre" *New J. Phys.* **10** 053003 (2008).

[63] S. T. Dawkins, R. Mitsch, D. Reitz, E. Vetsch, and A. Rauschenbeutel. "Dispersive Optical Interface Based on Nanofiber-Trapped Atoms" *Phys. Rev. Lett.* **107** 243601 (2011).

[64] J.-B. Béguin et al. "Generation and Detection of a Sub-Poissonian Atom Number Distribution in a One-Dimensional Optical Lattice" *Phys. Rev. Lett.* **113** 263603 (2014).

[65] I. H. Deutsch, R. J. C. Spreeuw, S. L. Rolston, and W. D. Phillips. "Photonic band gaps in optical lattices" *Phys. Rev. A* **52** 1394–1410 (1995).

[66] H. Sørensen et al. "Coherent Backscattering of Light Off One-Dimensional Atomic Strings" *Phys. Rev. Lett.* **117** 133604 (2016).

[67] N. V. Corzo et al. "Large Bragg Reflection from One-Dimensional Chains of Trapped Atoms Near a Nanoscale Waveguide" *Phys. Rev. Lett.* **117** 133603 (2016).

[68] M. Arcari et al. "Near-Unity Coupling Efficiency of a Quantum Emitter to a Photonic Crystal Waveguide" *Phys. Rev. Lett.* **113** 093603 (2014).

[69] T. G. Tiecke et al. "Nanophotonic quantum phase switch with a single atom" *Nature* **508** 241–244 (2014).

[70] A. Javadi et al. "Spin-photon interface and spin-controlled photon switching in a nanobeam waveguide" *arXiv:1709.06369v1.* (2017).

[71] J. D. Hood et al. "Atom–atom interactions around the band edge of a photonic crystal waveguide" *Proceedings of the National Academy of Sciences* **113** 10507–10512 (2016).

[72] B.-H. Liu et al. "Experimental control of the transition from Markovian to non-Markovian dynamics of open quantum systems" *Nat. Phys.* **7** 931–934 (2011).

[73] C. Gonzalez-Ballestero, F. J. García-Vidal, and E. Moreno. "Non-Markovian effects in waveguide-mediated entanglement" *New J. Phys.* **15** 073015 (2013).

[74] M. Endres et al. "Atom-by-atom assembly of defect-free one-dimensional cold atom arrays" *Science* **354** 1024–1027 (2016).

[75] D. Barredo, S. de Léséleuc, V. Lienhard, T. Lahaye, and A. Browaeys. "An atom-by-atom assembler of defect-free arbitrary two-dimensional atomic arrays" *Science* **354** 1021–1023 (2016).

[76] H. Lan and Y. Ding. "Ordering, positioning and uniformity of quantum dot arrays" *Nano Today* **7** 94–123 (2012).

[77] O. Astafiev et al. "Resonance Fluorescence of a Single Artificial Atom" *Science* **327** 840–843 (2010).

[78] I.-C. Hoi et al. "Generation of Nonclassical Microwave States Using an Artificial Atom in 1D Open Space" *Phys. Rev. Lett.* **108** 263601 (2012).

[79] A. F. van Loo et al. "Photon-Mediated Interactions Between Distant Artificial Atoms" *Science* **342** 1494–1496 (2013).

[80] J. A. Mlynek, A. A. Abdumalikov, C. Eichler, and A. Wallraff. "Observation of Dicke superradiance for two artificial atoms in a cavity with high decay rate" *Nat. Commun.* **5** 5186 (2014).

[81] Y. Liu and A. A. Houck. "Quantum electrodynamics near a photonic bandgap" *Nat. Phys.* **13** 48–52 (2016).

[82] P. Forn-Díaz, C. Warren, C. Chang, A. Vadiraj, and C. Wilson. "On-Demand Microwave Generator of Shaped Single Photons" *Phys. Rev. Appl* **8** 054015 (2017).

[83] P. Forn-Díaz et al. "Ultrastrong coupling of a single artificial atom to an electromagnetic continuum in the nonperturbative regime" *Nat. Phys.* **13** 39–43 (2016).

[84] F. Dell'Anno, S. D. Siena, and F. Illuminati. "Multiphoton quantum optics and quantum state engineering" *Phys. Rep.* **428** 53–168 (2006).

[85] O. Steuernagel. "Synthesis of Fock states via beam splitters" *Opt. Commun.* **138** 71–74 (1997).

[86] M. Dakna, J. Clausen, L. Knöll, and D.-G. Welsch. "Generation of arbitrary quantum states of traveling fields" *Phys. Rev. A* **59** 1658–1661 (1999).

[87] M. D. Eisaman, J. Fan, A. Migdall, and S. V. Polyakov. "Invited Review Article: Single-photon sources and detectors" *Rev. Sci. Instrum.* **82** 071101 (2011).

[88] A. Migdall. "Single-Photon Generation and Detection" Academic Press, 2013.

[89] D. C. Burnham and D. L. Weinberg. "Observation of Simultaneity in Parametric Production of Optical Photon Pairs" *Phys. Rev. Lett.* **25** 84–87 (1970).

[90] A. I. Lvovsky and J. Mlynek. "Quantum-Optical Catalysis: Generating Nonclassical States of Light by Means of Linear Optics" *Phys. Rev. Lett.* **88** 250401 (2002).

[91] E. Bimbard, N. Jain, A. MacRae, and A. I. Lvovsky. "Quantum-optical state engineering up to the two-photon level" *Nat. Photonics* **4** 243–247 (2010).

[92] J. J. Cooper, D. W. Hallwood, and J. A. Dunningham. "Entanglement-enhanced atomic gyroscope" *Phys. Rev. A* **81** 043624 (2010).

[93] M. Yukawa et al. "Generating superposition of up-to three photons for continuous variable quantum information processing" *Opt. Express* **21** 5529 (2013).

[94] C. K. Law and H. J. Kimble. "Deterministic generation of a bit-stream of single-photon pulses" *J. Mod. Opt.* **44** 2067–2074 (1997).

[95] M. Keller, B. Lange, K. Hayasaka, W. Lange, and H. Walther. "Continuous generation of single photons with controlled waveform in an ion-trap cavity system" *Nature* **431** 1075–1078 (2004).

[96] J. Beugnon et al. "Quantum interference between two single photons emitted by independently trapped atoms" *Nature* **440** 779–782 (2006).

[97] H. G. Barros et al. "Deterministic single-photon source from a single ion" *New J. Phys.* **11** 103004 (2009).

[98] M. Mücke et al. "Generation of single photons from an atom-cavity system" *Phys. Rev. A* **87** 063805 (2013).

[99] C. Kurtsiefer, S. Mayer, P. Zarda, and H. Weinfurter. "Stable Solid-State Source of Single Photons" *Phys. Rev. Lett.* **85** 290–293 (2000).

[100] V. Zwiller, T. Aichele, W. Seifert, J. Persson, and O. Benson. "Generating visible single photons on demand with single InP quantum dots" *Appl. Phys. Lett.* **82** 1509 (2003).

[101] M. Pechal et al. "Microwave-Controlled Generation of Shaped Single Photons in Circuit Quantum Electrodynamics" *Phys. Rev. X* **4** 041010 (2014).

[102] C. Lang et al. "Correlations, indistinguishability and entanglement in Hong–Ou–Mandel experiments at microwave frequencies" *Nat. Phys.* **9** 345–348 (2013).

[103] Z. H. Peng, S. E. de Graaf, J. S. Tsai, and O. V. Astafiev. "Tuneable on-demand single-photon source in the microwave range" *Nat. Commun.* **7** 12588 (2016).

[104] A. Kuzmich et al. "Generation of nonclassical photon pairs for scalable quantum communication with atomic ensembles" *Nature* **423** 731–734 (2003).

[105] C. W. Chou, S. V. Polyakov, A. Kuzmich, and H. J. Kimble. "Single-Photon Generation from Stored Excitation in an Atomic Ensemble" *Phys. Rev. Lett.* **92** 213601 (2004).

[106] M. D. Eisaman et al. "Shaping Quantum Pulses of Light Via Coherent Atomic Memory" *Phys. Rev. Lett.* **93** 233602 (2004).

[107] T. Chanelière et al. "Storage and retrieval of single photons transmitted between remote quantum memories" *Nature* **438** 833–836 (2005).

[108] J. K. Thompson. "A High-Brightness Source of Narrowband, Identical-Photon Pairs" *Science* **313** 74–77 (2006).

[109] D. Fukuda et al. "Titanium-based transition-edge photon number resolving detector with 98% detection efficiency with index-matched small-gap fiber coupling" *Opt. Express* **19** 870 (2011).

[110] K. P. Seshadreesan, S. Kim, J. P. Dowling, and H. Lee. "Phase estimation at the quantum Cramér-Rao bound via parity detection" *Phys. Rev. A* **87** 043833 (2013).

[111] C. C. Gerry, A. Benmoussa, and R. A. Campos. "Quantum nondemolition measurement of parity and generation of parity eigenstates in optical fields" *Phys. Rev. A* **72** 053818 (2005).

[112] Y. Nakamura and T. Yamamoto. "Breakthroughs in Photonics 2012: Breakthroughs in Microwave Quantum Photonics in Superconducting Circuits" *IEEE Photonics Journal* **5** 0701406–0701406 (2013).

[113] S. R. Sathyamoorthy, T. M. Stace, and G. Johansson. "Detecting itinerant single microwave photons" *C. R. Phys.* **17** 756–765 (2016).

[114] Y.-F. Chen et al. "Microwave Photon Counter Based on Josephson Junctions" *Phys. Rev. Lett.* **107** 217401 (2011).

[115] S. Haroche, M. Brune, and J.-M. Raimond. "Measuring the photon number parity in a cavity: from light quantum jumps to the tomography of non-classical field states" *J. Mod. Opt.* **54** 2101–2114 (2007).

[116] H. T. Dung, L. Knöll, and D.-G. Welsch. "Resonant dipole-dipole interaction in the presence of dispersing and absorbing surroundings" *Phys. Rev. A* **66** 063810 (2002).

[117] M. Wubs, L. G. Suttorp, and A. Lagendijk. "Multiple-scattering approach to interatomic interactions and superradiance in inhomogeneous dielectrics" *Phys. Rev. A* **70** 053823 (2004).

[118] S. Buhmann and D. Welsch. "Dispersion forces in macroscopic quantum electrodynamics" *Prog. Quantum Electron.* **31** 51–130 (2007).

[119] A. J. Leggett et al. "Dynamics of the dissipative two-state system" *Rev. Mod. Phys.* **59** 1–85 (1987).

[120] T. Shi, Y. Chang, and J. J. Garcia-Ripoll. "Ultrastrong coupling few-photon scattering theory" *arXiv:1701.04709.* (2017).

[121] H.-P. Breuer and F. Petruccione. "The Theory of Open Quantum Systems" Oxford University Press, 2002.

[122] A. González-Tudela and D. Porras. "Mesoscopic Entanglement Induced by Spontaneous Emission in Solid-State Quantum Optics" *Phys. Rev. Lett.* **110** 080502 (2013).

[123] W. Fulton and J. Harris. "Representation Theory - A First Course" Springer, 1991.

[124] P. Zanardi and M. Rasetti. "Noiseless Quantum Codes" *Phys. Rev. Lett.* **79** 3306–3309 (1997).

[125] D. A. Lidar, I. L. Chuang, and K. B. Whaley. "Decoherence-Free Subspaces for Quantum Computation" *Phys. Rev. Lett.* **81** 2594–2597 (1998).

[126] D. A. Lidar. "Review of Decoherence Free Subspaces, Noiseless Subsystems, and Dynamical Decoupling" *Quantum Information and Computation for Chemistry.* Advances in Chemical Physics. John Wiley & Sons, Inc., 2014, 295–354.

[127] R. H. Dicke. "Coherence in Spontaneous Radiation Processes" *Phys. Rev.* **93** 99–110 (1954).

[128] A. V. Andreev, V. I. Emel'yanov, and Y. A Il'inskiĭ. "Collective spontaneous emission (Dicke superradiance)" *Soviet Physics Uspekhi* **23** 493–514 (1980).

[129] M. Gross and S. Haroche. "Superradiance: An essay on the theory of collective spontaneous emission" *Phys. Rep.* **93** 301–396 (1982).

[130] R. Friedberg, S. Hartmann, and J. Manassah. "Limited superradiant damping of small samples" *Phys. Lett. A* **40** 365–366 (1972).

[131] C. Greiner, B. Boggs, and T. Mossberg. "Superradiant Emission Dynamics of an Optically Thin Material Sample in a Short-Decay-Time Optical Cavity" *Phys. Rev. Lett.* **85** 3793–3796 (2000).

[132] T. Holstein and H. Primakoff. "Field Dependence of the Intrinsic Domain Magnetization of a Ferromagnet" *Phys. Rev.* **58** 1098–1113 (1940).

[133] C. Kittel. "Quantum Theory of Solids" Wiley, 1987.

[134] E. Ressayre and A. Tallet. "Holstein-Primakoff transformation for the study of cooperative emission of radiation" *Phys. Rev. A* **11** 981–988 (1975).

[135] P Facchi and S Pascazio. "Quantum Zeno dynamics: mathematical and physical aspects" *J. Phys. A: Math. Theor.* **41** 493001 (2008).

[136] B. Misra and E. C. G. Sudarshan. "The Zeno's paradox in quantum theory" *J. Math. Phys.* **18** 756–763 (1977).

[137] W. Itano, D. Heinzen, J. Bollinger, and D. Wineland. "Quantum Zeno effect" *Phys. Rev. A* **41** 2295–2300 (1990).

[138] F. Schäfer et al. "Experimental realization of quantum zeno dynamics" *Nat. Commun.* **5** 3194 (2014).

[139] A. Signoles et al. "Confined quantum Zeno dynamics of a watched atomic arrow" *Nat. Phys.* **10** 715–719 (2014).

[140] A. Beige, D. Braun, B. Tregenna, and P. L. Knight. "Quantum Computing Using Dissipation to Remain in a Decoherence-Free Subspace" *Phys. Rev. Lett.* **85** 1762–1765 (2000).

[141] T. Ramos and J. J. García-Ripoll. "Multiphoton Scattering Tomography with Coherent States" *Phys. Rev. Lett.* **119** 153601 (2017).

[142] N. Gisin, G. Ribordy, W. Tittel, and H. Zbinden. "Quantum cryptography" *Rev. Mod. Phys.* **74** 145–195 (2002).

[143] A. N. Boto et al. "Quantum Interferometric Optical Lithography: Exploiting Entanglement to Beat the Diffraction Limit" *Phys. Rev. Lett.* **85** 2733–2736 (2000).

[144] T. Shi, D. E. Chang, and J. I. Cirac. "Multiphoton-scattering theory and generalized master equations" *Phys. Rev. A* **92** 053834 (2015).

[145] K. M. Gheri, C. Saavedra, P. Törmä, J. I. Cirac, and P. Zoller. "Entanglement engineering of one-photon wave packets using a single-atom source" *Phys. Rev. A* **58** R2627–R2630 (1998).

[146] C. W. Helstrom. "Quantum Detection and Estimation Theory" Elsevier Science, 1976.

[147] A. S. Holevo. "Probabilistic and Statistical Aspects of Quantum Theory (Statistics & Probability) (English and Russian Edition)" Elsevier Science, 1982.

[148] S. L. Braunstein and C. M. Caves. "Statistical distance and the geometry of quantum states" *Phys. Rev. Lett.* **72** (1994).

[149] B. Yurke, S. L. McCall, and J. R. Klauder. "SU(2) and SU(1,1) interferometers" *Phys. Rev. A* **33** 4033–4054 (1986).

[150] H. F. Hofmann. "All path-symmetric pure states achieve their maximal phase sensitivity in conventional two-path interferometry" *Phys. Rev. A* **79** 033822 (2009).

[151] G. C. Wick. "The Evaluation of the Collision Matrix" *Phys. Rev.* **80** 268–272 (1950).

[152] R. A. Campos, C. C. Gerry, and A. Benmoussa. "Optical interferometry at the Heisenberg limit with twin Fock states and parity measurements" *Phys. Rev. A* **68** 023810 (2003).

[153] G. Tóth and I. Apellaniz. "Quantum metrology from a quantum information science perspective" *J. Phys. A: Math. Theor.* **47** 424006 (2014).

[154] M. Lax. "Formal Theory of Quantum Fluctuations from a Driven State" *Phys. Rev.* **129** 2342–2348 (1963).

[155] T. J. Barnea et al. "Nonlocality of W and Dicke states subject to losses" *Phys. Rev. A* **91** 032108 (2015).

[156] G. Tóth. "Detection of multipartite entanglement in the vicinity of symmetric Dicke states" *Journal of the Optical Society of America B* **24** 275 (2007).

[157] S. Campbell, M. S. Tame, and M. Paternostro. "Characterizing multipartite symmetric Dicke states under the effects of noise" *New J. Phys.* **11** 073039 (2009).

[158] M. Huber, P. Erker, H. Schimpf, A. Gabriel, and B. Hiesmayr. "Experimentally feasible set of criteria detecting genuine multipartite entanglement inn-qubit Dicke states and in higher-dimensional systems" *Phys. Rev. A* **83** 040301 (2011).

[159] L.-M. Duan. "Entanglement Detection in the Vicinity of Arbitrary Dicke States" *Phys. Rev. Lett.* **107** 180502 (2011).

[160] A. I. Lvovsky, B. C. Sanders, and W. Tittel. "Optical quantum memory" *Nat. Photonics* **3** 706–714 (2009).

[161] C. Groß. "Spin Squeezing and Non-linear Atom Interferometry with Bose-Einstein Condensates" Springer, 2012.

[162] R. G. Unanyan and M. Fleischhauer. "Decoherence-Free Generation of Many-Particle Entanglement by Adiabatic Ground-State Transitions" *Phys. Rev. Lett.* **90** 133601 (2003).

[163] X. L. Zhang, Y. X. Zhang, and M. Feng. "Generation of symmetric Dicke states of many atomic qubits by adiabatic passage" *Europhys. Lett.* **82** 10004 (2008).

[164] L.-M. Duan and H. J. Kimble. "Efficient Engineering of Multiatom Entanglement through Single-Photon Detections" *Phys. Rev. Lett.* **90** 253601 (2003).

[165] J. K. Stockton, R. van Handel, and H. Mabuchi. "Deterministic Dicke-state preparation with continuous measurement and control" *Phys. Rev. A* **70** 022106 (2004).

[166] C. Thiel, J. von Zanthier, T. Bastin, E. Solano, and G. S. Agarwal. "Generation of Symmetric Dicke States of Remote Qubits with Linear Optics" *Phys. Rev. Lett.* **99** 193602 (2007).

[167] A. Retzker, E. Solano, and B. Reznik. "Tavis-Cummings model and collective multiqubit entanglement in trapped ions" *Phys. Rev. A* **75** 022312 (2007).

[168] C. E. López, J. C. Retamal, and E. Solano. "Selective control of the symmetric Dicke subspace in trapped ions" *Phys. Rev. A* **76** 033413 (2007).

[169] Y.-F. Xiao, X.-B. Zou, and G.-C. Guo. "Generation of atomic entangled states with selective resonant interaction in cavity quantum electrodynamics" *Phys. Rev. A* **75** 012310 (2007).

[170] A. Asenjo-Garcia, M. Moreno-Cardoner, A. Albrecht, H. J. Kimble, and D. E. Chang. "Exponential Improvement in Photon Storage Fidelities Using Subradiance and "Selective Radiance" in Atomic Arrays" *Phys. Rev. X* **7** 031024 (2017).

[171] P. Facchi and S. Pascazio. "Quantum Zeno Subspaces" *Phys. Rev. Lett.* **89** 080401 (2002).

[172] J. Fiurášek. "Conditional generation of N-photon entangled states of light" *Phys. Rev. A* **65** 053818 (2002).

[173] K. R. Motes et al. "Efficient recycling strategies for preparing large Fock states from single-photon sources — Applications to quantum metrology" *Phys. Rev. A* **94** 012344 (2016).

[174] C. K. Law and J. H. Eberly. "Arbitrary Control of a Quantum Electromagnetic Field" *Phys. Rev. Lett.* **76** 1055–1058 (1996).

[175] M. J. Holland and K. Burnett. "Interferometric detection of optical phase shifts at the Heisenberg limit" *Phys. Rev. Lett.* **71** 1355–1358 (1993).

[176] B. Yurke. "Input States for Enhancement of Fermion Interferometer Sensitivity" *Phys. Rev. Lett.* **56** 1515–1517 (1986).

[177] T. Ono, J. S. Chesterking, H. Cable, J. L. O'Brien, and J. C. F. Matthews. "Quantum-enhanced phase estimation using optical spin squeezing" *New J. Phys.* **19** 053005 (2016).

[178] P. Kok, H. Lee, and J. P. Dowling. "Creation of large-photon-number path entanglement conditioned on photodetection" *Phys. Rev. A* **65** 052104 (2002).

[179] C.-L. Hung, S. M. Meenehan, D. E. Chang, O Painter, and H. J. Kimble. "Trapped atoms in one-dimensional photonic crystals" *New J. Phys.* **15** 083026 (2013).

[180] J. Appel et al. "Mesoscopic atomic entanglement for precision measurements beyond the standard quantum limit" *Proceedings of the National Academy of Sciences* **106** 10960–10965 (2009).

[181] C. Ciuti, G. Bastard, and I. Carusotto. "Quantum vacuum properties of the intersubband cavity polariton field" *Phys. Rev. B* **72** 115303 (2005).

[182] A. Ridolfo, S. Savasta, and M. J. Hartmann. "Nonclassical Radiation from Thermal Cavities in the Ultrastrong Coupling Regime" *Phys. Rev. Lett.* **110** 163601 (2013).

[183] E. K. Irish. "Generalized Rotating-Wave Approximation for Arbitrarily Large Coupling" *Phys. Rev. Lett.* **99** 173601 (2007).

[184] D. Braak. "Integrability of the Rabi Model" *Phys. Rev. Lett.* **107** 100401 (2011).

[185] G. Díaz-Camacho, A. Bermudez, and J. J. García-Ripoll. "Dynamical polaronAnsatz: A theoretical tool for the ultrastrong-coupling regime of circuit QED" *Phys. Rev. A* **93** 063828 (2016).

[186] S. Bera, H. U. Baranger, and S. Florens. "Dynamics of a qubit in a high-impedance transmission line from a bath perspective" *Phys. Rev. A* **93** 033847 (2016).

[187] J. T. Shen and S. Fan. "Coherent photon transport from spontaneous emission in one-dimensional waveguides" *Opt. Lett.* **30** 2001 (2005).

[188] J.-T. Shen and S. Fan. "Strongly Correlated Two-Photon Transport in a One-Dimensional Waveguide Coupled to a Two-Level System" *Phys. Rev. Lett.* **98** 153003 (2007).

[189] S. Fan, Ş. E. Kocabaş, and J.-T. Shen. "Input-output formalism for few-photon transport in one-dimensional nanophotonic waveguides coupled to a qubit" *Phys. Rev. A* **82** 063821 (2010).

[190] T. Caneva et al. "Quantum dynamics of propagating photons with strong interactions: a generalized input–output formalism" *New J. Phys.* **17** 113001 (2015).

[191] T. Shi and C. P. Sun. "Lehmann-Symanzik-Zimmermann Reduction Approach to Multi-Photon Scattering in Coupled-Resonator Arrays" *Phys. Rev. B* **79** 205111 (2009).

[192] M. Pletyukhov and V. Gritsev. "Scattering of massless particles in one-dimensional chiral channel" *New J. Phys.* **14** 095028 (2012).

[193] D. L. Hurst and P. Kok. "Analytic Few Photon Scattering in Waveguide QED for Entanglement Generation" *arXiv:1705.07016*. (2017).

[194] Ş. E. Kocabaş. "Effects of modal dispersion on few-photon–qubit scattering in one-dimensional waveguides" *Phys. Rev. A* **93** 033829 (2016).

[195] I. G. Lang and Y. A. Firsov. "Kinetic Theory of Semiconductors with Low Mobility" *J. Exptl. Theoret. Phys. (U.S.S.R.)* **16** 1843 (1963).

[196] R. Silbey and R. A. Harris. "Variational calculation of the dynamics of a two level system interacting with a bath" *The Journal of Chemical Physics* **80** 2615–2617 (1984).

[197] R. A. Harris and R. Silbey. "Variational calculation of the tunneling system interacting with a heat bath. II. Dynamics of an asymmetric tunneling system" *The Journal of Chemical Physics* **83** 1069–1074 (1985).

[198] V. J. Emery and A. Luther. "Low- temperature properties of the Kondo Hamiltonian" *Phys. Rev. B* **9** 215–226 (1974).

[199] W. Zwerger. "Dynamics of a dissipative two level system" *Zeitschrift für Physik B Condensed Matter* **53** 53–62 (1983).

[200] J.-T. Shen and S. Fan. "Strongly correlated multiparticle transport in one dimension through a quantum impurity" *Phys. Rev. A* **76** 062709 (2007).

[201] S. Xu and S. Fan. "Input-output formalism for few-photon transport: A systematic treatment beyond two photons" *Phys. Rev. A* **91** 043845 (2015).

[202] L. Zhou, Z. R. Gong, Y. xi Liu, C. P. Sun, and F. Nori. "Controllable Scattering of a Single Photon inside a One-Dimensional Resonator Waveguide" *Phys. Rev. Lett.* **101** 100501 (2008).

[203] D. Roy. "Correlated few-photon transport in one-dimensional waveguides: Linear and nonlinear dispersions" *Phys. Rev. A* **83** 043823 (2011).

[204] J. R. Taylor. "Scattering Theory: The Quantum Theory of Nonrelativistic Collisions (Dover Books on Engineering)" Dover Publications, 2006.

[205] E. Batyev and L. Braginskii. "Antiferromagnet in a strong magnetic field: analogy with Bose gas" *Sov. Phys. JETP* **60** 781 (1984).

[206] A. Nysteen, P. T. Kristensen, D. P. S. McCutcheon, P. Kaer, and J. Mørk. "Scattering of two photons on a quantum emitter in a one-dimensional waveguide: exact dynamics and induced correlations" *New J. Phys.* **17** 023030 (2015).

[207] M. E. Peskin and D. V. Schroeder. "An Introduction To Quantum Field Theory (Frontiers in Physics)" CRC Press, 1995.

Acknowledgements

First of all, I would like to thank my supervisor Ignacio Cirac for the opportunity of doing research with him. His tremendous knowledge and experience have made every meeting insightful, his intuition and incredible understanding lead him to ask the right questions, and his ingenious ideas have pushed all of our projects to the next level. His way of thinking and approach to solving problems have inspired and influenced me in many ways.

Second, I am deeply grateful to my co-supervisor Alejandro González-Tudela for countless discussions, helpful suggestions, his patience, and in general for guiding me through life in academia. I appreciate to have been able to continuously work and interact with him during the last years and have truly enjoyed it.

I also thank Jan von Delft for kindly agreeing to act as a referee for this thesis.

I would also like to thank all my other collaborators, without whom this thesis would not have been possible in this form. In chronological order, I would like to thank Jeff Kimble for guiding us through the experimental side and sharing his knowledge and experience; Tao Shi for teaching us a part of his tremendous collection of methods and skills; and Juanjo García Ripoll for introducing me to methods in the ultrastrong coupling regime and to numerical techniques.

I have greatly benefitted from the research environment at MPQ, both within the theory group as well as with the experimental divisions. I would like to thank all former and current members of our group for creating such an inspiring, interactive, and cooperative research environment. In particular, I would like to thank my former and current office mates, Juan Bermejo-Vega, Xiaotong Ni, Anna Hackenbroich, Asli Cebe and András Molnar, who have filled the time in the office (and elsewhere) with a lot of fun, interesting discussions and have become close friends. Moreover, I would like to thank Andrea Kluth for all her guidance and support in all administrative matters and beyond.

I would also like to thank the QUINFOG group at the CSIC-IFF in Madrid for their hospitality during my stay in 2017, which allowed me to meet inspiring people and broaden my knowledge. In particular, I would like to thank Tomás Ramos for many fruitful discussions and for introducing me to life in Madrid.

Special thanks go to my Spanish-German tandem group at MPQ for all the fun hours we had in both languages, my fellow PhD representatives for improving the life of PhD candidates at MPQ, Anna Hashagen for many hours of sports and hot chocolate, my

colleagues at the THW for taking over my share of work during my writing phase, and all my friends for bringing balance to my life.

Most importantly, I owe my deepest gratitude to my family for their unconditional love and support. Finally, I thank Maximilian Girlich for his love, support, patience, and cooking, especially during the last phase of my PhD.

Funding from the Max-Planck-Institute of Quantum Optics, Nanosystems Initiative Munich, and DAAD is gratefully acknowledged.